HOLUB, Robert Ph.D., Chemistry

Charge Dispersion in the Fission of ^{232}Th by Protons

CHARGE DISPERSION IN THE FISSION OF ^{232}Th BY 28 - 83 MeV PROTONS

by

Robert Holub

A thesis submitted to the Faculty of
Graduate Studies and Research in partial fulfilment
of the requirements for the degree of
Doctor of Philosophy

Chemistry Department
McGill University,
Montreal, Canada

July, 1970

Ph. D. Chemistry

Robert Holub

Charge Dispersion in Fission of ^{232}Th by 28 - 83 MeV Protons

Abstract

The independent cross sections of ^{139}Ba, ^{140}La, ^{141}La, ^{141}Ce, ^{143}Ce, ^{139}Ce, and the cumulative cross sections of ^{139}Cs, ^{140}Ba, ^{141}Ba, ^{143}La, ^{141}Ce, and ^{144}Ce produced in the proton-induced fission of ^{232}Th at energies 28 - 83 MeV have been measured radiochemically. The shapes of the excitation functions whose maxima gave a curve when plotted vs the neutron-to-proton ratios of the products, the most probable charges, the full-widths of the charge dispersion curves at half-maxima, together with their changes with energy, were explained by increasing neutron evaporation with increasing energy as well as by increased contributions from symmetric fission. A prescription for applying a charge dispersion correction when the $N/Z_p(A)$ function is not constant with mass has been presented. It has been suggested that the variations of the $Z_p(A)$ function with mass are a liquid-drop model feature perturbed primarily by single-particle effects following Brandt and Kelson (8) theory and secondarily by spherical shell effects. The phenomenological rules as suggested by Brandt and Kelson (8) have been shown to hold true for most of the asymmetrically fissioning nuclei. Calculations of the most probable charges using various hypotheses have been performed.

Acknowledgments

I wish to express my sincere gratitude to Professor L. Yaffe, not only for suggesting the problem for this thesis and guidance during the work, but also for his generosity and understanding which enabled me to spend the happiest years of my life at McGill University.

I am equally grateful to the National Research Council of Canada for an award of a Scholarship (1967-1970) and to the Chemistry Department for Demonstratorship (1966-1967).

I am very much indebted to all my colleagues for the many things I have learned from them.

I thank sincerely Miss Hana Glaser for the conscientious typing and the friendly help she has given me.

I wish also to thank Professor R. E. Bell for permission to use the McGill Cyclotron and Mr. R. Mills for his assistance in carrying out the irradiations.

TABLE OF CONTENTS

A. INTRODUCTION

1. Historical and General Introduction

Fission was discovered by Hahn and Strassman (1) in 1939. Not long after this discovery Bohr and Wheeler's (2) Liquid Drop Model, which is still more or less the basis of all theories of nuclear fission, was developed. With the advent of the Shell Model theory, the asymmetry of the mass distribution in low-energy fission was considered to be basically a shell effect. However, deviations from the relatively simple picture given by the liquid-drop model and shell model soon appeared. The peculiar character of fission as statistical and collective, and as a single-particle process was becoming more and more apparent. The availability of computers enabled theoreticians to calculate in more detail the potential-energy surfaces for deformations leading to fission, and the saddle-point shapes were established, mostly by Swiatecki (3). Even though many features of fission were thus understood - as reviewed in Wilets (4), Hyde (5), Fraser & Milton (6) and Huizenga & Gindler (7) - some resisted all attempts at understanding (like asymmetry at low energies). Major contributions were made in the late sixties, especially at the Conference of Physics and Chemistry of Fission in Vienna in 1969 where the details of the single-particle theory of fission were presented. In this respect Brandt & Kelson (8) made the most recent and thorough contribution at the end of 1969. Another very useful approach is based on a double-humped fission barrier. However, this hypothesis cannot as yet offer any explanation of the

asymmetry of fission except by postulating a third hump in the fission barrier (Strutinski (9)).

It seems though that the ultimate goal of complete understanding of nuclear fission may be within reach.

2. Topical Introduction

This introduction is based on the following sources: Nuclear Chemistry, Volumes 1 and 2, edited by Leo Yaffe (10); Physics of the Nucleus, M. A. Preston (11); Theoretical Nuclear Physics, Blatt & Weisskopf (12); Quantum Mechanics, A. Messiah (13); Nuclear and Radiochemistry, Friedlander, Kennedy & Miller (14).

2a. Main Properties of Nuclear Matter

In order to understand a phenomenon as complicated as fission, many nuclear models and basic concepts must be employed at various stages. A brief outline of some of the features is given below.

(i) Fermi Gas Model

This concept of nuclear matter, as a first approximation, underlies all considerations in nuclear fission. It is proposed that the nucleus consists of nucleons moving in a potential well ($\approx$ 39 MeV deep for neutrons and $\approx$31 MeV for protons), subject to the Pauli principle, and for a nucleus like ^{232}Th, having a total kinetic energy of the order of 1200 MeV. In the ground-state the available states are filled up to the Fermi energy, E_F, which depends on the nuclear density only and equals

$$E_F = \frac{\hbar^2}{2m}\left(3\pi^2\rho\right)^{2/3} \qquad (1)$$

where m = mass of nucleon and ρ = density of nucleons.

The energy states in the potential well can be - using Myers & Swiatecki's (15) term - "bunched" in degeneracies as described by shell-model states (2 states for the first closed shell, 6 states for the second, etc.) or "unbunched" in varying degrees - according to the non-sphericity of the ground-state nucleus - up to the smooth completely unbunched level spectrum corresponding to the ideal Fermi gas. The idea behind this, the more bunching the more stable the nucleus, is also used by Vandenbosch (16) and Strutinski (9) to explain dips in the fission barriers. It also expresses the fact that non-sphericity disturbs the simple shell structure and removes the shell degeneracies. The density, g_o, of the states around the Fermi energy equals simply

$$g_o = \frac{3}{2}\frac{A}{E_F} \qquad (2)$$

which for ^{232}Th + n is approximately 10 MeV^{-1}.

As shown by Ericson (17) the available states $\rho(E^*)$ at higher excitation energy, E*, are

$$\rho(E^*) = \exp\left[2\left(\frac{\pi^2}{6} g_o E^*\right)^{\frac{1}{2}} / \left(48 E^*\right)^{\frac{1}{2}}\right] \qquad (3)$$

These relationships reflect very important properties of nuclear matter showing the exponential increase of possibilities of arrangements of A particles at an excitation energy corresponding to the raising of a certain number of indistinguishable particles to higher states. Essentially the same considerations concerning bunching and unbunching hold for excited states up to the energy of the order of 50 to 100 MeV, the region where statistical behavior (compound nucleus) prevails. It should be

kept in mind that the properties outlined above represent a first approximation only and any applicability to fission theory is only a qualitative feature underlying more elaborate ideas.

(ii) Semiempirical Mass Formula

To a great degree nuclear matter can be considered to be a charged liquid drop having surface tension. An additional feature, not found in a classical charged drop, is the so-called symmetry energy (also called Wigner term) reflecting the tendency of nuclear matter to possess an equal number of neutrons and protons. One very useful formula, as given by Green (18), is written

$$E_B = -a_1 A + a_2 A^{2/3} + a_3 Z(Z-1)A^{-1/3} + .25\, a_4 (A-2Z)^2 A^{-1} \pm \delta A^{-1} \qquad (4)$$

where E_B = nuclear binding energy δ = pairing energy constant

$a_1 = 15.83$ $a_2 = 17.97$

$a_3 = .718$ $a_4 = 94.07$

Since the terms in the above equation play such an important role in fission in the mass and charge distribution and charge dispersion, it is useful to realize their magnitude - i. e. the magnitude of the potential energy terms involved in fission - for a typical situation encountered in this work. In Table 1. the individual terms are listed (neglecting even-odd effects).

From equation (4), if mass A is kept constant, the behavior along an isobaric chain can be determined. The equation

used in this case (taken from (14)) is

$$\Delta M = k(Z - Z_A)^2 \qquad (5)$$

where $k = 0.718 \times A^{-1/3} + 94.07A^{-1} = k_{Coulomb} + k_{symmetry}$ and Z_A = most stable charge (taken from Coryell (19)).

In Table 2 the values calculated from equation (5) using masses pertinent to this work are given. The most probable charge of a fragment, Z_p, was calculated using the Unchanged Charge Distribution hypothesis, which assumes that the fragments have the same charge density as the fissioning nucleus (UCD hypothesis). As an average fissioning nucleus ^{232}Pa was taken. This is an approximation based on the calculations of Croall & Cuninghame (20).

In the last two rows the Coulomb and symmetry components of the constant k, $k_{Coul.}$, and $k_{sym.}$ are given. If one takes the equation (5) as a potential energy term of a harmonic oscillator, the constant k, and its components $k_{Coul.}$ and $k_{sym.}$ correspond to "stiffness" coefficients. The values show that $k_{sym.} > k_{Coul.}$ in all cases. McHugh & Michel (21) point out that if one assumes the above stiffness coefficients as describing the restoring force of nuclear matter then the statistical and quantum fluctuations will result in the observed charge dispersions.

From Tables 1 and 2 it can be seen that the energies involved are quite large in comparison with fission barriers ($B_f \approx 5$ to 8 MeV) in the heavy mass region, especially in cases further away from the beta-stability line.

In conclusion it should be pointed out that even the recent calculations of Myers & Swiatecki (15), which go "one step beyond the liquid-drop theory of nuclear matter", introduce three additional adjustable parameters.

TABLE 1

The Individual Terms of Green's Mass Formula

	A = 230	A = 141
E_{volume}	+3641 MeV	+2233 MeV
$E_{surface}$	-675 MeV	-486 MeV
$E_{Coulomb}$	-938 MeV	-425 MeV
$E_{symmetry}$	-225 MeV	-140 MeV

TABLE 2

The Individual Terms and Constants of Mass Parabola

	A = 141	A = 91	A = 230
k	0.817	1.21	
$Z_{A\ Cor}$	58.55	35.7	
Z_p(UCD)	55.3	40.1	
$E_{Z_A - Z_P}$*	8.6 MeV	23.4 MeV	
$k_{Coulomb}$	0.15	0.165	0.125
$k_{symmetry}$	0.667	1.045	0.41

* Energy associated with the most probable charges, Z_p, given by UCD hypothesis, with respect to the most stable charge Z_A as given by Coryell (19).

(iii). Shell Model

The shell model has had a great deal of success in the description of many properties of various nuclei. The model is based on the assumption that an effective average potential is obtained as a result of all the nuclear forces for a given number of nucleons. In spite of the very high density the Pauli exclusion principle ensures that there is not continuous scattering of one particle from another and so it is meaningful to talk about an average nuclear potential. Using some form of average potential the single-particle states are calculated and quantum numbers N, n, l and m are assigned, where N is the principal quantum number (corresponding to number of "phonons"), n is the number of nodes of the radial wave function (including that in the origin), and l and m are the angular momentum magnitude and its direction with respect to the z axis respectively. As mentioned earlier the bunching, as in the spherical nucleus of closed shells, is a convenient extrapolation only and one is free to include perturbation terms to modify the potential to get better agreement with experiment. For instance, the degenerate l shells are split into $l + \frac{1}{2}$ and $l - \frac{1}{2}$ shells by $\vec{l}.\vec{s}$ coupling. These finally give the "magic" numbers. In addition to the above, s - the spin quantum number - is used to complete the description.

A more elaborate approach is the Hartree-Fock self-consistent potential method which takes the approach of a variational problem where an interparticle potential is found which will give the best agreement with experiment. In the case of the single-particle theory of fission however, it is solved by iteration (in fact by guesswork in the case of Brandt & Kelson (8))

because of mathematical difficulties connected with the infinitely repulsive core, etc.

It is important to bear in mind that all nucleons are indistinguishable and all the calculations are performed using Slater determinants, products of single-particle wave functions of the nucleus, properly antisymmetrized to satisfy the Pauli principle (i. e. when two particles of different quantum numbers are exchanged the total wave function must give an amplitude of opposite sign). The Hartree-Fock matrix can be written (as given on page 19 in reference (10)) for any single-particle eigenfunction ψ_k as

$$\sum_{\ell}\left[T_{\ell k}+\sum_{t=1}^{A}\left(V_{\ell tkt}-V_{\ell ttk}\right)\right]\psi_{\ell}=\lambda_k\psi_k \qquad (6)$$

where T_{lk} and V_{ltkt} = kinetic and potential energy matrix elements respectively and λ_k = the corresponding energy.
The matrix itself is in square brackets (it also can be changed into diagonal form by a unitary transformation). The potential V_{ijkl} is non-local, i. e. its value at a point $\vec{r}$ depends on the situation at some other point $\vec{r}$. For a chosen state ψ_k the sum over all potentials of the other states should give the average one-body potential $V_o(k)$.

$$V_0(k)=\sum_{i}^{A}\left(V_{ki}-V_{ik}\right) \qquad (7)$$

The Hartree-Fock method gives the best results - i. e. when just one ground-state determinant describes the nucleus - if there are no unoccupied states having energies close to some of the occupied states. Since this situation is not the case with most nuclei however, the unified model must be used.

(iv) Unified Model

The concept of the unified model is based on the existence of collective modes of motion where all single particles cooperate in a certain manner. For instance nuclear matter travelling through the saddle point to scission gives a perfect example of collective cooperation. The unified model treats simultaneously collective and single particle motions so that the total Hamiltonian can be written as

$$H = H_{collective} + H_{particle} + H_{interaction}. \qquad (8)$$

The problem of too many degrees of freedom (more than the nucleus has) is not encountered because as far as the particle excitation is negligible these degrees of freedom of the particle are not used. The condition for this is that the collective period of motion be larger than the period of motion of the single particle, ($\tau_{collective} > \tau_{single\ particle}$).

Collective motion is treated by means of collective coordinates R, that determine the position of a point in a uniformly charged medium that is incompressible and whose flow is irrotational according to

$$R = R_0\left[1 + \sum_{\lambda\mu} a_{\lambda\mu} Y_\lambda^\mu(\theta,\varphi)\right] \qquad (9)$$

where $Y_\lambda^\mu(\theta,\varphi)$ = spherical harmonics of degree λ and order μ and $a_{\lambda\mu}$ are coefficients. R_0 is the equilibrium radius.

Spherical harmonics are chosen basically because of convenience. For instance, if the deformations are small, $\lambda = 2$ is sufficient for a complete description and the collective energy can be separated into vibrational and rotational terms. As will

be shown later, Brandt & Kelson (8) do not use this kind of collective coordinates for a description of the fissioning nucleus. The coordinates of equation (9) can describe uniquely a saddle-point shape; the calculations are, however, very complicated and will not be reviewed here. Even for deformations very far away from the spherical shape the degree λ is limited by the condition $\tau_{coll} > \tau_{sp}$, i. e. values more than six are excluded. Also the order μ is put equal to zero thus limiting the shapes to axially symmetric.

The unified model is concerned with small deformations so that the collective Hamiltonian can be written as

$$H_{coll} = \frac{1}{2}\sum_{\lambda\mu} B_\lambda \dot{a}^2_{\lambda\mu} + \frac{1}{2}\sum_{\lambda\mu} C_\lambda a^2_{\lambda\mu} = \text{Kin. E.} + \text{Pot. E.} \qquad (10)$$

where B_λ represents mass transport associated with the motion and C_λ the "stiffness" coefficient or effective surface tension (as in the semiempirical mass formula). ($\lambda = 1$ is excluded because it represents only translational motion).

The coefficients $a_{\lambda\mu}$ vary with time so that kinetic energy can be expressed too. The calculations of the saddle-point energy represent basically the potential energy in equation (10).

Deformation in ground-state nuclei is caused by several extra core nucleons. Whenever there are intrinsic and collective modes of motion there is also coupling between them ($H_{interaction}$ in equation (8)). If this coupling is weak the intrinsic states can be calculated as perturbed-shell spherical states. If the coupling is strong the intrinsic wave functions are calculated using a non-spherical average potential by means of the Nilsson

equation. The Nilsson equation, as given by Wilets (4) is

$$\mathcal{H} = \sum_i H(i) \tag{11}$$

where

$$H = \frac{p^2}{2m} + \frac{1}{2} m \omega_0^2 r^2 \left[1 - 2\beta Y_{20}(\theta)\right] - C\,\vec{l}.\vec{s} - D\,l^2 \tag{12}$$

where $\frac{p^2}{2m}$ is kinetic energy; $C\,\vec{l}.\vec{s}$ represents spin-orbit coupling. The $D.l^2$ - term modifies the shape of the well (flattens the bottom), $Y_{20}(\theta)$ are spherical harmonics and β is a term describing deformation.

The second term can also be written as

$$\frac{m}{2}(\omega_x^2 x^2 + \omega_y^2 y^2 + \omega_z^2 z^2) = \frac{m}{2}\omega_0^2 r^2 \left[1 - 2\beta Y_{20}(\theta)\right] \tag{13}$$

where $\omega_0, \omega_x, \omega_y, \omega_z$ are corresponding oscillator frequencies.

This equation shows the relationship between the vibrations in the direction of the x, y, and z axes and the deformations expressed in equation (12) by the term $2\beta Y_{20}(\theta)$.

For future reference it is important to realize that the situation described by equation (12) concerns an equilibrium state only, or a potential energy term in equation (10) if $\dot{a}_{\lambda\mu}=0$ because even in the case of deformed ground-states of the heavy nuclei, the deformation coefficients describe changes around certain equilibrium average values, while nuclear matter travelling towards scission is not in the equilibrium state.

The approach outlined above shows that it is always possible to express any nuclear state as a linear combination of some wave functions which form an orthogonal and complete set. If these are, for instance, ground-state single-particle wave functions corresponding to a spherical nucleus, and if the state

in question is rather far away from any of these single-particle states (and calculation of energy spectrum, as stated on page 172 in reference (11), becomes prohibitively large), a solution in the form of a Nilsson treatment can be used so that the single-particle character is "restored" again, even though in an average potential which is not spherical.

The calculations themselves are rather complicated for shapes far away from spherical and in the case of the single-particle theory of fission, Brandt & Kelson (8) use difference equations.

(v) Nucleus in Excited State

Excited states are not stationary and they decay with half-lives related to their total width Γ, as follows from the Heisenberg uncertainty relation. The half-lives determine the time scale, which becomes of basic importance for collectively-described motions (on the condition that the characteristic period of collective motion is greater than that of the single particle) and it is useful to recall the case where the time-dependent perturbation is used for describing the time evolution of a system.

If a state is stationary (the Hamiltonian does not depend explicitly on time) the energy of the system can be expressed as $E = \hbar.\omega$ and the time-evolution operator describing the change from the state at time t_o to the state at time t is

$$U(t\,t_o) = \exp\left[-i E (t-t_o)/\hbar\right]. \qquad (14)$$

If a state is not stationary and the Hamiltonian depends on time, the time-evolution operator cannot be written as above. Its solution can be obtained using time-dependent perturbation theory, where the perturbing energy admixtures other

states into the state in question. There are two extreme cases in the so-called adiabaticity ratio describing the speed with which the perturbation is applied. If it is applied slowly - adiabatically - (adiabaticity ratio goes to zero) the situation can be visualised as a succession of many steady states, obtained from time-independent perturbation theory, leading to the final state at the end of perturbation. If, on the other hand the perturbation is applied suddenly, there is no change in the states at all, as might be expected from the time-energy uncertainty relations.

The case for a given adiabaticity ratio is usually described in terms of a Hamiltonian H(t) as in equation (15) and in Figure 1.

$$H(t) = \begin{pmatrix} E_a(t) & H' \\ H'^* & E_b(t) \end{pmatrix} \qquad (15)$$

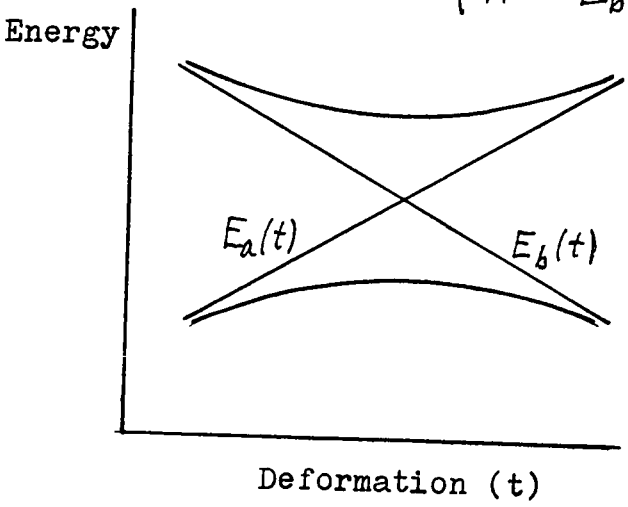

Figure 1.

where H' is interaction energy and $E_a(t)$, $E_b(t)$ are the energies corresponding to states a and b as shown in Fig. 1. In Fig. 1 the x-axis represents the applied perturbation connected with the deformation of the nucleus and the y-axis the energy of given states. If there is no interaction between states a and b the states cross as lines designated by E_a and E_b. This also happens when a deformation is applied suddenly, and the states do not change. However, if there is an interaction, and if applied

adiabatically, the states change into another as shown in Fig. 1 by curved lines. There are also in-between situations when there is finite probability of a jump from one curved line to the other, so-called "slippage", for medium adiabaticity ratios.

With respect to the problem of fission it is also important to trace out the fate of a single-particle state at higher excitation energy (up to 100 MeV), from another point of view than as discussed in the unified model section.

The first estimate is simple. The kinetic energy of all nucleons in a Fermi gas as shown in the previous section, is for heavy nuclei approximately 1200 MeV. To have substantial excitation energies of the order of 1000 MeV are needed, which are certainly never reached in any fission act. In other words, at low excitation energies the average potential will have roughly the same form when a single nucleon with excitation is inserted into the nucleus, "it will not greatly affect the self-consistent distribution of the large number of nucleons already present" (page 538 in reference (11)). To show this it is useful to recall the optical model. This is based on the notion of a "cloudy crystal ball" that reflects, refracts, and absorbs impinging nucleons using real and imaginary potentials. The magnitude of the imaginary potential is related to a total single-particle width of a compound state and is of the order of units of MeV, which is - in the resonance region - greater by a factor of 10^6 than the observed widths of the resonance states, which are directly connected with the level density as given by equation (3). The connection is again best explained in terms of unbunching and residual

interactions. If there were no residual interactions among nucleons the shell model and the optical model would be a complete description of the nucleus and all states would simply be single-particle states. The "smearing out" of single-particle levels, their unbunching and consequent half-lives increased by a factor of about one million are due to residual interactions. The quantity that reflects the admixture of single-particle states is called a strenth-function.

There are many theories treating the residual interaction and configuration mixing by means of perturbation theory and also nuclear reaction theories like R - matrix, etc. In the case of fission, theoreticians are not yet able to apply any rigorous treatment due to the enormous complexity of the problem, and the single-particle fission theory as used by Brandt & Kelson (8) based on the Nilsson treatment seems to be a justifiable approach. Before their theory will be reviewed a short synopsis of the most relevant experimental data is given in the next section.

2b. Experimental Facts about Fission

All nuclei having the parameter $Z^2/A \geq 18$ can fission spontaneously. However, most of the experimental data comes from a relatively narrow region of approximately $30 < Z^2/A < 40$ (a value of approximately 50 corresponds to a nucleus unstable towards fission in the ground-state). The quantity $(Z^2/A)/(Z^2/A_{critical})$ is called the fissionability parameter x. The region of experimentally investigated fission was divided by Jensen & Fairhall (11) into three regions according to Z:

1. $Z \geq 90$. Only in this region can some of the nuclei be caused

to fission with thermal neutrons, giving rise to two unequal parts (asymmetric fission). The ratio of the most probable fragments A_h/A_l decreases with Z of the target in this region, the value of A_l increasing faster than that of A_h. At higher excitation energies the valley between the peaks is continuously filled, typically by widening of the peaks, till one obtains a flat, wide, symmetrical mass distribution. The fission barriers B_f are typically of the order 5 to 7 MeV.

2. $Z < 84$. In this region fission is symmetric only and thresholds are much higher than for the previous case (more than 15 MeV), so that there is no low-energy fission in the same sense as for the heaviest elements. The width of the mass distribution is markedly narrower as shown by Blann (23) and Karamian et al. (24). With increasing excitation energy the width increases. The behavior follows basically the liquid-drop model calculations.

3. $84 < Z < 90$. In this intermediate region for low-energy fission (which has very low cross section) asymmetry is observed, at moderate energies symmetric and asymmetric coexist, and at high excitation energy (more than 100 MeV) symmetric fission prevails entirely. There is a considerable change in mass distribution within a relatively narrow energy region - an occurrence of great importance for explaining asymmetric fission. Recent work in this region was performed by Konecny & Schmitt (25). Some properties typical of this region "leak" into both neighboring regions.

The total kinetic energy release does not change appreciably with excitation energy nor does fissionability. As Remsberg et al. (39) point out the mechanism of fission remains

basically the same up to an excitation energy of 500 MeV (in the case of ^{238}U bombarded by protons at 2.2 GeV). The kinetic energy release is lower for symmetric fission as observed by Milton & Fraser (26).

In close relation to the kinetic energy release is the neutron yield in dependence on the mass of fragments. It shows the characteristic "saw-tooth" shape, as observed for instance by Terrell (27), for almost all asymmetrically fissioning nuclei. Since - according to Vandenbosch (28) - for the approximately symmetric fission (within 15 mass units around the mass equal to half of the fissioning nucleus) the fragments are not close to any closed-up shell structure, the maximum in the "saw-tooth" shape of the neutron yield is explained as determined by greater "softness" of these fragments with respect to those having a composition close to the closed shell. The maximum in the number of evaporated neutrons from low-energy fission corresponds to the maximum in the excitation energy of the fragments; and that must be reflected in lower kinetic energy release for the particular fragments. At the same time this behavior shows that the distance between the charge centers is greater for symmetric fission, otherwise the kinetic energy due to Coulomb repulsion could not be lower.

At higher excitation energies the saw-tooth shape disappears as Britt & Whetstone (29) and McHugh & Michel (21) observed and the number of evaporated neutrons becomes more and more proportional to mass of the fragment.

Charge dispersion, as defined by Friedlander et al. (30), is measured along an isobaric chain. It is dispersed around a

most probable charge, Z_p, in an approximately Gaussian distribution. The position of Z_p, measured mostly in terms of distance from the most stable charge Z_A, $Z_A - Z_p$, is described approximately by one of the following hypotheses:

1. UCD, unchanged-charge distribution, predicts that the two fragments will have the same charge density as the fissioning nucleus.

2. MPE, minimum potential energy, postulates that the nuclear charge distributes itself between fragments such that a minimum is achieved between the nuclear potential energy and the Coulomb energy.

3. ECD, equal-charge displacement, is essentially on one hand an empirical correlation of low-energy experimental data and on the other hand it is an MPE-based postulate. It states that the complementary products of the most probable charges Z_p lie an equal number of charge units away from Z_A and that the distribution function about the most probable charge Z_p is symmetric and the same for all mass splits.

The full-width at half-maximum, FWHM, for most low-energy fission charge dispersions is approximately 1.6 Z units. When odd-even effects are taken into account the width becomes narrower by approximately 10% as reported by Wahl (31).

At higher excitation energies both widths and Z_p change, reflecting the increased neutron evaporation and the occurrence of multichance fission. $Z_A - Z_p$, shifts towards the less neutron-rich isotopes as reported first by Pate et al. (32) and then by other workers of this laboratory whose findings have been summarized by Yaffe (33). The individual contributions will be

dealt with in great detail in the Results and Discussion sections. Here it will be stated only that the pattern of the shifts to less neutron-rich nuclides is mostly a fairly regular one and depends on the N/Z ratio of the target. However, slight deviations or "fine structures" do occur and it will be attempted later to explain some of them.

The full-width at half-maximum increases with higher excitation, even though the regularity is even more disturbed than in the case of $Z_A - Z_p$ functions. The overall trend is again summarized in Yaffe's paper (33). An attempt will be made in the Results section to explain some of these deviations. At energies between 100 MeV and 2.9 GeV Friedlander et al. (30) observed the charge dispersion in the mass region A = 125 - 140 and observed that the widths increasingly widened up to approximately 5 Z units and eventually resolved themselves into two curves corresponding to low and higher-deposition-energy fission. In the symmetric region Panontin & Porile (34) observed the charge dispersion curve at 450 MeV to be distinctly narrower for ^{208}Pb (1.9 Z units) than for ^{238}U (2.8 Z units). This is not unexpected because there should be no low-deposition-energy fission for ^{208}Pb. Both charge dispersion curves were measured in the region of mass A = 111. At the same energy Hogan & Sugarman (35) report 3.2 Z units FWHM for heavy-mass fragments (A = 139).

At higher excitation energies multichance fission is paralleled in the entire energy region by neutron evaporation. The neutron binding energy B_n and fission threshold B_f play an important role in determining the ratio of the fission width Γ_f to the neutron width Γ_n, as given by Huizenga et al. (36)

$$\Gamma_f/\Gamma_n \approx exp\left[2a_f^{\frac{1}{2}}(E^*-B_f)^{\frac{1}{2}} - 2a_n^{\frac{1}{2}}(E^*-B_n)\right] \approx exp\left[B_n - B_f\right] \quad (16)$$

where E* is excitation energy and a_f and a_n are level density parameters.

These estimates would seem to be in disagreement with the Harding & Farley (37) experiment, where it is argued that most neutrons evaporated are pre-fission. Blann (23) investigated a similar problem for fission of gold by ^{12}C ions. He used excitation functions of certain products and also concluded that most neutrons in this case were pre-fission. However, experiments by Cheifetz et al.(38) with 155 MeV protons on ^{209}Bi and ^{238}U show almost equal numbers of pre- and post-fission neutrons. It should be noted that the values B_n and B_f in relation (16) - which are in the exponent - are known only approximately from Myers & Swiatecki's (15) calculations and no final conclusion about the ratio can be made. (According to the relation (16) and Myers & Swiatecki's (15) values the situation where $B_n > B_f$ will be reached rather soon and consequently the fission width should prevail).

2c. Review of Most Recent Fission Theories, Hypotheses, and Conclusions

First consideration will be given to the time scale of the process. The time for an average bound nucleon to cross the nucleus is of the order $A^{1/3}/3 \times 10^{-22}$ sec. If this was the duration of the whole fission process no collective description would be applicable (for instance the surface harmonics necessary for such a description would be of the order of internucleon distances) and, among other things, the unchanged charge distribution (UCD) would apply. The compound nucleus has a lifetime of

the order of 10^{-15} sec., assuming configuration mixing, i. e. sharing the excitation energy among many degrees of freedom; then, if the formation of a compound nucleus is assumed for fission, the deformation leading to fission proceeds, at least up to the saddle point, collectively. Strong support for the assumption that the fission process is longer than 10^{-22} sec. up to very high excitation energies comes from Blann (23) who observed at excitation energies of 50 to 100 MeV that the fission products from the reaction Au (^{12}C, f) were produced according to the minimum potential energy (MPE) rule, which assumes a certain minimum duration to allow for rearrangements. Similar observations were made by Karamian et al. (24) at excitation energies between 40 and 120 MeV. Also Remsberg et al. (39), as mentioned before, found the process at 500 MeV excitation energy not very much different from low-energy fission, so that any sudden disruption seems unlikely. The seemingly contrary observations made by Saha & Yaffe (40) and Yaffe (33) - that UCD better agrees with the observed data - for the case of Cs fission products for various targets will be explained in the Discussion section.

In the previous section the time scale was shown to be of such an order that the collective treatment is justified. With this question settled the adiabaticity ratio comes into the picture, not only with respect to its value for fission as a whole but also to its changes during the process itself. Three main cases can be described depending on the adiabaticity ratio (according to Wilets (4)): if it is low, i. e. the collective characteristic passage time is much longer than the periods of of particle motion, the process is adiabatic and no crossings of

levels take place. If the ratio is moderate, the statistical model is valid, and thermodynamic equilibrium sets in and some level crossings do occur. This corresponds to a transfer of the collective kinetic energy into nucleonic excitation - a process somewhat analogous to "viscous heating". This phenomenon is also called "slippage". Finally, if the ratio is large the sudden approximation applies and the states keep their quantum numbers. Griffin (41) argues that the latter is the case for the last stage of fission, the plunge from the saddle point to scission when the nuclear matter "runs" into asymmetrical scission. He also argues that up to the saddle point the process is slow and that the residual interactions force the orbits to scatter in such a way as to follow the liquid-drop potential surface, which is symmetrical. He identifies this as a thermodynamical equilibrium and excludes the possibility of introducing asymmetry adiabatically in the potential energy surfaces. Naturally, according to Griffin (42), in the final stage of fission the main feature determining the final distribution cannot be the available phase space and fragment level densities as proposed by the statistical models (Fong (43)). Wilets (4) points out that the statistical model has been only partially successful. Griffin (42) admits the possibility of the statistical model being "locally" applicable. However, since well-defined quantum states have been observed many times in the angular distribution of the fission products, he excludes the possibility of the universal applicability of the statistical model.

Griffin (42) in his latest article reformulates his previous approach by using the concept of kinetic energy dominance.

This can be seen in equation (10) where simply the kinetic energy term becomes so predominant that potential energy can be neglected. The sudden approximation is then applied and the corresponding changes in the inertial mass parameter B are expressed using the complicated treatment of the cranking model.

Unfortunately there seems to be no evidence for assuming any of the time scales and accompanying hypotheses to be correct. The solution for the time being seems first to investigate the potential energy term alone, i. e. not putting any explicit requirements on the time scale at all (except that which justifies the collective treatment, i. e. it is longer than 10^{-22}sec.). This approach was adopted by Brandt & Kelson (8) in their Single Particle Theory of Fission. Most of what follows is based on their article. It is the most recent and thorough work embracing many facets of fission. However, the authors argue that it "does not constitute an independent and self-consistent model of fission. Rather it is an attempt to illuminate various aspects and concepts in relation to other existing models."

The first important statement is that an independent-particle model reproduces the liquid-drop model potential surfaces if the particles occupy the lowest available energy states. This gives a new justification for the liquid-drop model, which originally was based on an obviously inadequate assumption of a homogeneously-charged medium with a very short mean free path of the constituent hypothetical particles. The independent-particle model assumes a long mean free path of the nucleons (due to the Pauli principle).

To clarify the above statements one should note first

the resemblance to the unified model. Various parameters play the role of the collective coordinates. These parameters describe the shape of the fissioning nucleus as two spheres joined through a neck of parametrized length and width and the point where the neck joins the spheres, together with the asymmetry parameter α. (They did not use the spherical harmonics as in the unified model). The single-particle states are a direct extension of the Nilsson model states with deformation more appropriate to fission, axially symmetric and extending, according to estimates by Griffin (42) and Krappe and Wille (44), (based on different calculation techniques) deformation up to 0.8 of the deformation parameter δ. The independent particles moving in some average single-particle potential can be treated by the Hartree-Fock variational method. This approach is extended to other than ground-state shapes, to states with subsidiary restrictive conditions, using the method of Lagrange multipliers. It can be visualized as external forces restricting the single-particle states within a certain shape. If these restrictions are maintained long enough and the system is allowed to attain as low energy as possible the potential energy of the system is obtained. It is equivalent to putting $\dot{a}_{\lambda\mu}$ equal to zero in equation (10). It also represents the link to the liquid-drop model because the potential reproduces the liquid-drop model potential. (The liquid-drop model becomes a special case of a more general treatment). Clearly, it is the case mentioned earlier where there is no equilibrium because the external forces are used to keep the nuclear matter in a shape appropriate for fission while in the case of Nilsson treatment the nucleus is in the ground state. It can happen, as mentioned at the end of the section on the shell model, that the result of the Hartree-

Fock treatment renders the equilibrium shape non-spherical even without any external forces, if there are several extra core nucleons present.

Another justification for investigating the potential energy term only (of course, it includes a great deal of kinetic energy of the individual nucleons) is that even at the last stages of fission when presumably the kinetic energy should be predominant, Nix (45) argues that the nucleus does follow the potential energy valley even though the importance of kinetic energy term increases.

The performance of the self-consistency program was avoided by postulating ("guessing") the solution to this problem. Brandt & Kelson (8) state that "one must hope that the results are not affected considerably and that no appreciable physical insight is lost."

The extension of the Hartree-Fock method to non-equilibrium highly-deformed shapes is possible because the residual interactions are short-range. This has a very important consequence: residual interactions are independent of shape and they need only be known in relation to a proportionality constant. The same that holds for the residual interactions (which are responsible for "unbunching" mentioned earlier and for level density as approximated in equation (2)) holds for the pairing force, so that the result of the variational problem is independent of the shape.

This is an important assertion, contrary to that of Griffin (41), who considers these residual interactions as mainly responsible for the rearranging of the states during the first

slow motion towards the saddle point (so that its liquid-drop model potential is maintained). As mentioned earlier, Griffin's (41) view excludes the possibility of an adiabatically-introduced deviation from the liquid-drop potential and is also in disagreement with Wilets (46) who argues that adiabaticity also leads to asymmetry. Brandt & Kelson (8) also argue that the requirement that nuclear matter follow the liquid-drop model potential surface amounts to an unjustified assumption that any additional kinetic energy imparted to the system (to nucleons) will become purely collective kinetic energy, i. e. no particle will be allowed to become excited, that nothing will ever happen to disrupt the liquid-drop advancement to the saddle point and to scission.

To conclude these considerations one should note that if there are no residual interactions (i. e. if they are short-ranged, H', from equation (15), = 0) there is no level crossing in the sense of Fig. 1. and automatically the individual quantum numbers are conserved, disregarding the adiabaticity ratio. More about this appears in the Discussion section together with some experimental evidence.

The important thing to decide is which quantum numbers are going to be conserved. Charge conservation and spatial reflection symmetry along the z-axis (along which the fission proceeds) seem to be suggested by typical paths leading to fission. As the last good quantum number, the z-component of the angular momentum is chosen. The quantum numbers are labelled by π, γ_z, m. Perhaps it should be stressed that these concern a one-body Hamiltonian; the total Hamiltonian has the angular momentum $\vec{J}$ con-

served also. It has been observed many times that K, the projection of total angular momentum along the z-axis ($or \langle\Omega\rangle$), is conserved as shown in experiments which give a typical angular distribution pattern (Griffin (42)). Ω is the single-particle state z-component of the angular momentum.

All solutions of the variational problem satisfy

$$\langle\psi_\mu | H | \psi\rangle = 0 \qquad (17)$$

where ψ_μ differs from ψ by a one-particle state. It reflects the relative stability against excitation of particles by the total Hamiltonian. A similar point about the persistence of the single-particle state has been mentioned in previous sections. The single-particle character is believed to be preserved.

Perhaps the most important contribution of Brandt & Kelson's(8) theory is the view of single-particle localisation during the fission process. The individual-particle model obviously localizes the particle within the entire nucleus. This is a consequence of the Pauli principle. On the other hand the liquid-drop model, with its short mean free path, highly localizes an individual-particle. When the shape of the fissioning nucleus reaches the scission stage (one part being labelled as left, the other as right) there are states which previously were either node or crest on the symmetrical plane. The reflection symmetry quantum number π_z which is conserved determines if the state has a crest or a node on the symmetrical plane simply because it determines which state is symmetrical (geräde) or antisymmetrical (ungeräde) with respect to the z-axis (see Fig. 4.) It is not identical with parity, which depends only on the l orbital angular momentum. To visualize this, Fig. 2. according to Griffin (41)

is presented. The extension to states with more nodes is presented in Fig. 3. according to Kauzman (47). It can be seen how symmetrical states of odd number of crests become degenerate with respect to antisymmetrical states which had an even number (one less) of crests. Perhaps it should be pointed out that the pictures on Fig. 2. and Fig. 3. show the situation schematically only, since in spherical harmonics subjected to spatial reflection symmetry along the z-axis (which is performed by changing in wave function $\psi(r,\theta,\varphi)$ $\varphi \to \varphi$ and $\theta \to -\theta$) the poles are not nodes as they appear in Fig. 2. but places with "plus" or "minus" densities. However, the essential point of the behavior with respect to a potential wall being built up in the middle of the nucleus and consequent changes of nuclear states is shown sufficiently by Fig. 2.

When degeneracy is introduced by fission (as in Fig. 3.) the orbits may be filled by a pair of symmetric and antisymmetric states. These two states are indistinguishable and when antisymmetrization is performed it is found that such a properly antisymmetrized state (the particles are, of course, assumed to be of one kind) is zero (the 2 x 2 determinant has two identical columns), everywhere except in the case when one particle is completely localized in the left region and the other completely in the right. In other words there can be no particles simultaneously in both halves. The only states which can be in both halves are those that are not paired (i. e. symmetrical with antisymmetrical - they have the amplitude $1/\sqrt{2}$). From this arises the main Brandt & Kelson (8) phenomenological rule that the ratio of symmetrical to antisymmetrical states of the ground-state (spherical) configuration, A_+/A_-, determines the double-humped mass distribution.

When the actual calculations of the Nilsson states in a deformed nucleus are performed, many level crossings happen (as in Figure 1). In the IAEA 1969 Fission conference (48) many papers on this subject were presented, however it was not possible to include them into this introduction in any more systematic degree because of time and space limitations. Undoubtedly those calculations are very important for any further development of the Brandt & Kelson (8) theory. Brandt & Kelson (8) performed calculations for ^{252}Cf but they did not present any details, only the observed trends. For instance, if the symmetry of the fissioning fragments is released, many of the above mentioned crossings are eliminated. It has also been observed that symmetric levels go down in energy with the asymmetry in fissioning shapes introduced, while the antisymmetric levels go up. This can be interpreted in a simple way; the symmetric states tend to localize in the larger region, the antisymmetric states in the smaller. Obviously, the symmetric states "resist" the perturbing potential less as shown in Fig. 2. if there is some asymmetry in the fissioning nuclear shape, because the "crests" occurring just in the fissioning x-y plane are not "so much in the way". The nodes of the antisymmetric states do not resist the perturbing potential at all. Another observation made on the basis of the calculations was: the lower the magnetic quantum number m the less the wave function is affected by the introduction of the asymmetry in fission. This can be explained in a simple way using Fig. 4. taken from Pauling & Wilson (49). One can see the lower the quantum number m the more the wave function is centered around the symmetry axis and therefore the less it is affected by introducing the asymmetry in the fissioning shape which occurs in

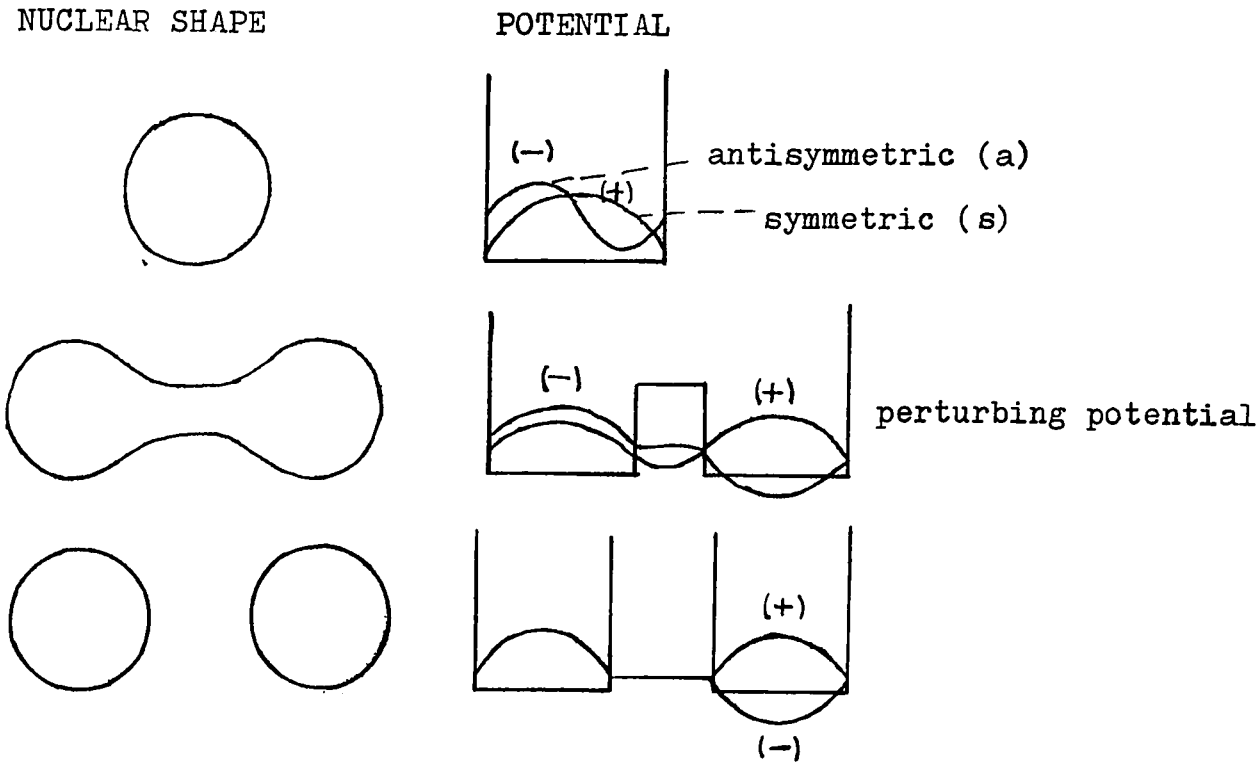

Figure 2

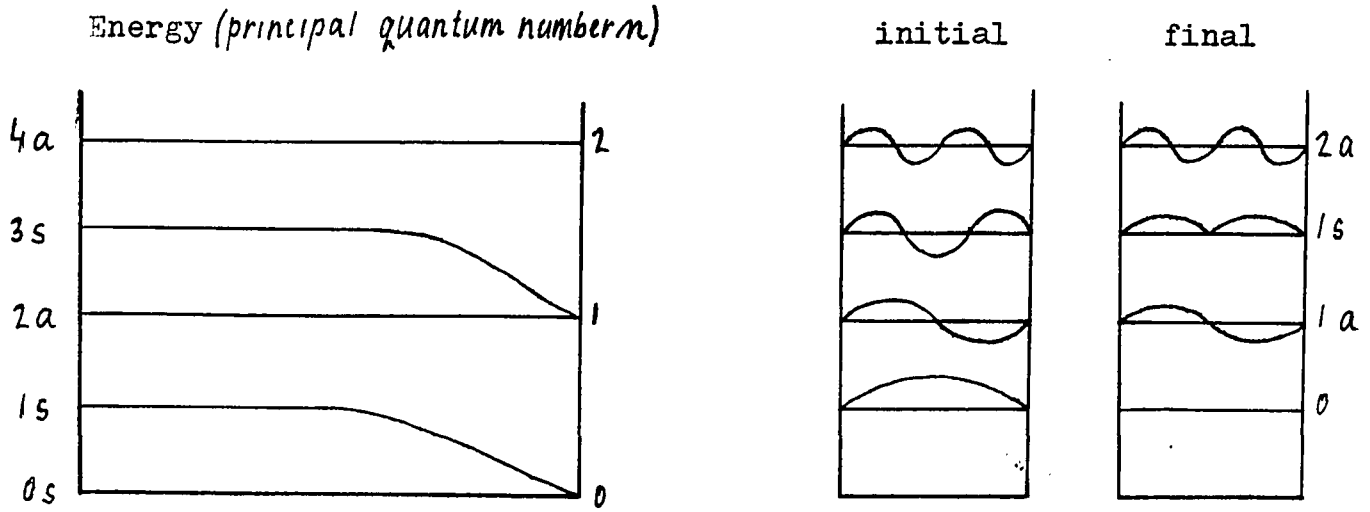

perturbation corresponding to that in Figure 2.

changes in wave functions corresponding to the initial and final states

Figure 3

in x-y plane). One more general feature is that the same trend holds for principal quantum number n, the explanation being the fact that the more nodes the state has the more evenly it is distributed in the nucleus and the less affected by asymmetry changes. Brandt & Kelson (8) report that one can see the effect of single-particle states - subject to asymmetry in the last stage of fission ("pinching" mode) - by taking the energy differences between the degenerate states as a measure of localization of these symmetrical or antisymmetrical states in either region. It shows that extreme localization occurs even at relatively early stages of pinching, the probability of finding the lowest symmetric state in the bigger region is almost unity.

These considerations showed only the trends and do not give any real probabilities of finding the particles in the fission process.

The problem now is how to incorporate these findings into the collective picture of fission. It is obvious that the single-particle effects must be a few units of MeV within the liquid-drop model calculations (the circumstances of fission in terms of individual surface and Coulomb energy contributions are given later in the Discussion and in Fig. 28) so that is is natural to include the facts mentioned above into the picture just as perturbations of the liquid-drop model. Here again Brandt & Kelson (8) chose not to present any detailed calculations, only the main features.

The starting point is the fact that liquid-drop model surfaces are reproduced if the lowest energies of the single-particles are occupied. There are, however, certain deviations

a) $l = 3$, $m = 0$

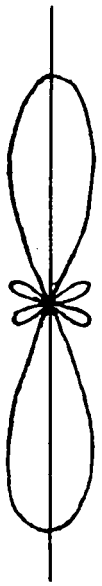

z axis

b) $l = 4$, $m = \pm 4$

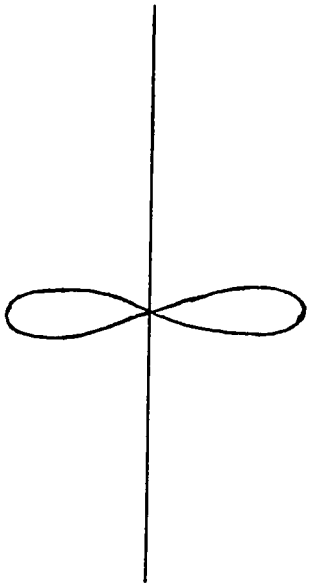

z axis

Fission proceeds along z axis. It can have $\gamma_\pi = 1$ or $\gamma_\pi = -1$ according to

$$\gamma_\pi = (-1)^{l-m}$$

in a) the state is antisymmetrical (it has node at x-y fission plane).

in b) the state is symmetrical (it has crest at x-y fission plane).

Figure 4.

from the smooth liquid-drop energies because of shell effects. The shell effects will be dealt with later. The first choice of a state where not all the single-particle states are the lowest is a configuration in which all single particles keep their original ground-state configuration. These have always higher energy, i. e. even the fission barrier should be higher, and the differences are used by the authors to extract surface-energy coefficients for a given single-particle configuration labelled by π defined by

$$C^{\pi}_{surface}(shape)\Big|_{\xi_i} = \left(\frac{\partial V(\pi, \xi_i)}{\partial \xi_i}\right)\left(\frac{\partial[\text{surface area(shape)}]}{\partial \xi_i}\right)^{-1} \quad (18)$$

where ξ_i is the given shape mode (like "pinching", "asymmetrizing", etc.).

The idea that these "constants" may not be constant during fission has been mentioned by some other authors (for instance Wilets (4)). In the expression above, the first bracket shows how the potential of a certain fixed single-particle configuration varies with changes of individual "modes" of collective motion. It is understandable that these changes should not be the same with respect to all possible shape changes, and, indeed, it is found that for the asymmetrizing parameter α, the surface-energy coefficient is much higher. Moreover, on reaching a certain magnitude of the asymmetry parameter α, the coefficient becomes much smaller and practically equal to the other coefficients associated with other collective modes. This has the basic effect of shifting the saddle-point shape from symmetry to asymmetry.

The question of the actual shape of the potential surfaces (and of all others which have the single-particle occupancy

different) is, according to Brandt & Kelson (8) not too important and these shapes are not mapped in their article because the charting is unwieldy and because they differ from the liquid-drop potential basically only by addition of the energy difference between the pertinent occupied single-particle states and those of the lowest occupied ones and because the authors do not want to "overprejudice the reader as to its significance". The authors mention only the features of the perturbation treatment using the potential for the saddle point expanded around the saddle point and they then expand this expansion again for small perturbations.

Shell effects obviously play an important role not only in affecting the fission barrier height but, as many researchers argue, in causing asymmetry in fission. Here there should be discerned several cases of the shell effects:

1. Those associated with any shapes having more degeneracies than some neighboring shapes. This characterisation is the extension of the "bunching" concept of Myers & Swiatecki (15), i. e. any bunching, not only that associated with spherical shape, is more stable. This theory can explain the existence of fissioning isomers for many nuclei as shown by Vandenbosch (16). However, asymmetric fission does not follow from the existence of isomeric states. A complete understanding of the isomeric states, and, as Strutinski (9) points out, a third isomer state, or better a third hump in the fission barrier, would have to be discovered or inferred to explain fission asymmetry.

2. Those associated with spherical shapes.

It seems that Brandt & Kelson (8) concern themselves with both kinds of shell effects. In any case, they divide them

into two cases, those concerning the total energy and those associated with "the response of the system to variations and stimuli". Their conclusion is that shell effects in the important stages of fission are second-order effects and that they tend to average out during the process. Hill & Wheeler (50) point out that fine structures in mass distribution, (the small hump around A = 130, for instance) are obviously associated with closed shells and they are second-order effects. It is very difficult to make a strong case that the same causes could make the fission asymmetric (the first-order phenomenon). Griffin (41) argues, disregarding the possibility mentioned in the previous paragraph 1., that the shell effects are so much associated with the spherical shapes that they would be unable to cause such enormous changes in saddle-point shapes that are far from sphericity.

Brandt & Kelson (8) leave the question of some preferential formation of "clusters" open besides concluding that the shell effects are of the second order. In the Discussion, a method will be suggested which might indicate the strengths of shell and other effects. Recent experiments by Glendenin et al. (51), as shown in Section 6c, seem to bear out Brandt & Kelson's (8) assumption.

The last point which Brandt & Kelson (8) explain successfully is the width of the mass distribution. It is well known that at the heavy mass region the $\vec{l}.\vec{s}$ coupling is very strong because the shape is highly deformed (or as Hyde (52) stated, because of the strong $\vec{l}.\vec{s}$ coupling there is a prolate deformation). This coupling makes j (which is a sum of orbital and spin quantum number) a good quantum number and this complicates the determination of which state is symmetric and antisymmetric

in the procedure as shown in Fig. 4. The answer lies in linear combinations of l and s wave functions as given by the rules for addition of two angular momenta (as given in M. A. Preston (11).

$$|l;\tfrac{1}{2};j;m_j\rangle = \langle l;\tfrac{1}{2};m_j-\tfrac{1}{2};\tfrac{1}{2}|j;m_j\rangle\,|l;m_j-\tfrac{1}{2}\rangle|\tfrac{1}{2};\tfrac{1}{2}\rangle + \langle l;\tfrac{1}{2};m_j+\tfrac{1}{2};-\tfrac{1}{2}|j;m_j\rangle\,|l;m_j+\tfrac{1}{2}\rangle|\tfrac{1}{2};-\tfrac{1}{2}\rangle \tag{19}$$

The states $|l;\frac{1}{2};j;m_j\rangle$ are not pure eigenstates with respect to spatial reflection along the z-axis, R_z, but mixtures of those with $\gamma_R = 1$ (symmetric) and $\gamma_R = -1$ (antisymmetric) and the probabilities of these states are given by the squares of the Clebsch-Gordan coefficients.

$$C^{\gamma_R} = |\langle l;\tfrac{1}{2};m_j\mp\tfrac{1}{2};\pm\tfrac{1}{2}|j\,m_j\rangle|^2 \tag{20}$$

To determine γ_R the expression of Fig. 4. is used

$$\gamma_R = (-1)^{l-m_j\pm\frac{1}{2}} \tag{21}$$

If all possible combinations obtained using the above prescriptions are summed one gets the probability of obtaining a certain mass division as given by the amount of symmetric states A_+ and antisymmetric A_-

$$P(A_+,A_-) = \sum_{\alpha,\beta}\left\{\prod_{\lambda=1}^{A_+} C^{+}_{\alpha\lambda}\right\}\left\{\prod_{\lambda=1}^{A_-} C^{-}_{\beta\lambda}\right\} \tag{22}$$

where the summation extends over all possible combinations α and β . The number of these combinations has a Gaussian distribution around a certain most probable division so that it can be written as

$$P(A_+A_-) = \frac{1}{(2\pi\Gamma)^{\frac{1}{2}}}\, e^{-\frac{(A_+-\langle A_+\rangle)^2}{2\Gamma}} \tag{23}$$

where

$$\langle A_+\rangle = \sum_{\alpha=1}^{A} C^{+}_{\alpha} \qquad \Gamma = \sum_{\alpha=1}^{A} C^{+}_{\alpha}\cdot C^{-}_{\alpha} \tag{24}$$

For A can be substituted number of neutrons or protons. It is obvious that there are great possibilities in comparing these suggestions with experimental data with respect to the observed mass and charge distribution and dispersion and state assignments for the single-particle states for the ground-state fissioning nucleus. An attempt will be made in the Discussion section to draw some conclusions from the observed data using Brandt & Kelson (8) theory.

It should be mentioned that the "shell structure" theory of Strutinski (9) and Vandenbosch (16) may well be successful in all respects concerning the unsolved problems of fission, however, it is not worked out in as great detail as the Brandt & Kelson (8) theory. Because of that the latter can be used more readily in comparing with experimental data than the former.

It is quite likely that both theories will contribute since they are not mutually exclusive.

2d. General Methods of Determination of Independent Yields

The independent primary product yields give the basic information for the charge dispersion studies. The methods most widely used are either radiochemical or physical, like, for instance, measurement of the number of β particles emitted in the decay of a specific mass chain (Armbruster et al. (53), or of the characteristic K X-rays associated with the primary charge (Glendenin et al. (54) or by mass spectroscopy (McHugh & Michel (21)).

The main problem is to distinguish between the independently-formed products and those that are formed cumulatively by consecutive β decays of their precursors. At moderate and higher energy fission the situation is further complicated by a multichance fission which results in fragments of varying excita-

tion energies.

The physical methods suffer from various factors. For instance, most mass spectrometers have relatively poor mass resolution. The K X-ray method is difficult to use because the sources of the K X-rays are not uniquely determined. They can arise from the disruption of the electron cloud during the fission process (half-life of the order of 10^{-16} sec.) and/or from the internal conversion of the prompt γ-rays from the de-excitation of the primary fission fragments after neutron emission (half-life of the order of 10^{-10} to 10^{-7} sec.). On the other hand, these methods are very useful for measurements of short-lived precursors where radiochemical methods fail completely and for obtaining fragment mass and charge distributions which are never directly accessible by radiochemical investigations.

When the two methods are compared it must be pointed out that there are discrepancies, especially between mass spectrographic results and the radiochemical ones. The K X-ray method seems to give results which are in good agreement with the radiochemical ones, especially in the case of the spontaneous fission of ^{252}Cf (Glendenin et al. (54)).

The most convenient case for radiochemical measurements is to study a nuclide that is shielded by a stable precursor; then the obtained cross sections are always the independently formed products. Unfortunately, in most cases the nuclides are not shielded and "milking" or time-extraction methods must be used where as many different separations (or "milkings") must be made as there are unknown cross sections which are to be investigated. The main point of these separations ("milkings") is to

allow for the contributions from the precursor to the nuclide in question. The limitation is the half-life of the precursor; no meaningful separation can be performed if the precursor's half-life is less than one minute.

If the half-lives of the investigated nuclides are known as well as the separation times it is possible to obtain the cross sections of the independently-formed nuclides. In theory the number of the cross sections determined can equal the number of separations. Since the errors of the radiochemical measurements of half-lives determinations and of many others are relatively large it is difficult to extend the number of separations beyond two. The method is then called "double-time extraction". If the case for three separations ("triple-time extraction") is to be successfully applied, the half-lives of the isotopes should be approximately within one order of magnitude.

2e. Decay Chains Studied

The properties of the nuclides studied are given in Table 3 and the genetic connections in Table 4. The nuclides in this region lie just outside the closed shells N = 82 and Z = 50, so that even ^{140}Ba, a nuclide stabilized by the even-even effect, and close to Z_A, is unstable. Since the half-life of ^{140}Ba is, however, about ten times longer than that of its daughter ^{140}La it can be considered a case of semi-shielding. The appropriate method used for this case to obtain the independent yield of ^{140}La is described in the Treatment of Data section.

In the isobaric chain most thoroughly studied in this work, mass A = 141, the half-lives are such that the "triple-time extraction" method could be used. However, as previously mentioned, the data from independently-measured ^{141}Ba, from barium

separation samples were essential for obtaining the independent yields for ^{141}La as well as for ^{141}Ce. The details of the calculations are given also in the Treatment of Data section.

The properties of ^{141}La and especially ^{141}Ce are well known. In the case of ^{141}Ba, although the half-life and the energy of the 190-keV peak followed in this work were determined recently by Carlson and Schick (55) using the most advanced techniques, the branching ratios were not reported and had to be inferred from the ^{141}Ce measurements, the last radioactive member of the isobaric chain.

The chains of mass A = 143 and A = 139 are subject to larger error because of the shorter half-lives of ^{139}Cs and ^{143}La. In the case of cerium the more time-consuming chemical separation also affected to a certain degree the accuracy of the independent yield determination of ^{143}Ce.

B. EXPERIMENTAL

1. Targets and Irradiations

Thorium metal foil of thickness 0.002" was used as a target material. The ^{65}Cu (p,pn) ^{64}Cu reaction was used as a proton beam monitor. The copper foils were 0.001" thick. Since there were significant variations in the superficial densities of both foils it was considered necessary to weigh the same area of both foils before each irradiation in order to get the ratio of superficial densities more accurately. The ratios (including the percentage of ^{65}Cu) varied from 0.29 to 0.42. The areas were about 0.7 cm^2.

To eliminate recoil losses three copper and three thorium foils were used. The former were placed upstream with respect to the thorium foils. For chemical processing only the middle foils were used. All six foils were carefully sheared with scissors to ensure their alignment, wrapped with 0.0008" thick aluminum foil and placed inside the cyclotron at a chosen radial distance corresponding to the desired bombarding energy. These were determined from the data given by the Foster Radiation Group with an uncertainty $\pm$ 2 MeV. The energy degradation was estimated and found to lie within the above uncertainty limit. The total superficial density of all foils in front of the target was approximately 100 mg/cm^2. The target holder is shown in Figure 5.

2. Chemical Separations

After irradiation the target and foils were dismantled and the middle thorium foil was dissolved in 3 - 4 ml of concen-

trated HCl along with traces of HF. In this process HF served as a catalyst and although the amount needed is very small, about 10^{-5} M, however, its presence for fast dissolution was essential. If this amount exceeds a certain optimal value, determined by trial and error, there is a tendency for a colloidal precipitate to form at a later time in this mother solution.

After dissolution was complete, the volume was made up to 10 ml with H_2O and all the following separations were performed on aliquots from this mother solution.

The chemical separation procedures for barium were taken from "Collected Radiochemical Procedures" (56) and for cerium from "Rapid Chemical Separations" (57). In the case of cerium an additional step was added, separating cerium from thorium. A brief description of each of these procedures is given below.

All carrier solutions contained 10 mg of carrier per ml and were standardized as follows:-

Barium Carrier Standardization

5 ml of the carrier solution was pipetted into a 250-ml beaker and diluted to approximately 100 ml. Then 10 ml of 6M $H_4C_2O_2$ and 3M $NH_4C_2H_3O_2$ were added, placed on a hot plate, and brought to boiling. 5 ml of 1.5M Na_2CrO_4 were added dropwise and stirred, boiled for 1 minute with stirring, cooled to room temperature and filtered into a weighed fine sintered glass crucible which had been washed and dried previously and dried at 110°C for 15 minutes. The precipitate was washed several times with 5-ml portions of H_2O and EtOH and dried, cooled and weighed in the same way. This standardization procedure was repeated three times and the spread in results was about 3%.

Cerium Carrier Standardization

5 ml of the carrier solution was pipetted into a 100-ml beaker and diluted to about 20 ml with H_2O. Then it was warmed slightly and approximately 50 ml of saturated $(NH_4)_2C_2O_4$ solution were added. The solution was cooled in an ice bath for 15 minutes and filtered through an ashless filter paper (No. 42 Whatman). The precipitate was then ignited in a furnace at 800°C. for 30 minutes, cooled and weighed as CeO_2. Three standardizations were made during the course of the experimental work and they agreed within 3%.

The two above standardizations were taken from reference (58).

Barium

A 2-ml aliquot of the mother solution was pipetted into a 40-ml centrifuge tube, 2 ml of standardized barium carrier solution added and the tube placed in an ice bath. About 30 ml of a mixture of hydrochloric acid and diethylether (5 parts of HCl to 1 part of $(C_2H_5)_2O$) were added and after stirring for one minute a white precipitate of $BaCl_2.H_2O$ was formed. This time of the beginning of the precipitate formation was recorded carefully because one of the followed isotopes, ^{139}Ba, has a precursor with a 9.5 minute half-life and any larger error in timing would affect the cross section determination substantially. This separation time was always about 10 to 15 minutes after the end of bombardment time. For the double-time extraction procedure described in the Introduction one more separation was performed 40 to 70 minutes later.

When the precipitation was complete (approximately in one minute) the solution was centrifuged and the supernate discarded. The precipitate was dissolved in 2 ml of distilled water,

1 drop of phenolphthalein and 3 drops of Fe^{3+} carrier were added and the mixture neutralized with 6M NH_4OH (with 12 drops in excess over the equivalence point). $Fe(OH)_3$ acted as a scavenger removing most of the insoluble hydroxides. The precipitation was repeated, La carrier added and the solution then scavenged with $La(OH)_3$. Neutralization was performed again with 6M NH_4OH and when the equivalence point was reached 10 drops of 6M NH_4OH were added in excess. This mixture was heated. The mixture was heated to boiling to complete the precipitation and centrifuged. 10 ml of a buffer solution (mixture of 6M CH_3COOH and 3M NH_4OH) were added to the supernate. The solution was heated to boiling and 2 ml of 1.5M Na_2CrO_4 were added dropwise. The mixture was boiled for one minute and stirred constantly. The characteristic dark orange and later light yellow precipitate of $BaCrO_4$ formed, which was subsequently centrifuged and the supernate discarded. In the case of the first separation the precipitate was slurried with water and filtered on a fibre glass filter paper using a filter chimney and ground-off Hirsch funnel, mounted immediately (after washing twice with 5 ml portions of EtOH) and measured as soon as possible on the Ge-Li detector. This procedure of leaving out the step involving the chemical yield determination was followed when the time elapsed from the end of bombardment exceeded 70 minutes. As will also be mentioned later, there was always the possibility of determining the chemical yield by comparison with Ba measured directly from the mother solution. However, if there was enough time, and in the case of the second separation, the following longer procedure was used. The glass filter was weighed beforehand, dried, and the filtered $BaCrO_4$ precipitate dried again at 110° Centigrade and weighed

again and mounted.

This separation is very reliable and removes all contaminating elements so that barium isotopes are in a radiochemically pure form. Several very thorough checks were made in the course of the experimental work and no gamma-emitting impurities were ever observed. However, considerable difficulty was found in determining the exact separation time, not only in the case of the $BaCl_2.H_2O$ formation after which the ^{139}Cs precursor no longer contributes to the ^{139}Ba, but also in the case of the $La(OH)_3$ scavenging. At the moment of $La(OH)_3$ scavenging all lanthanum isotopes are removed and from that time the ^{141}Ba isotope decays to ^{141}La and then into ^{141}Ce. The known properties of ^{141}Ce were used to infer the branching ratio, I_γ, for ^{141}Ba. Because of the difficulties these measurements were performed separately for I_γ in three separate experiments. The result is given in Table 3. The above-mentioned separation-time difficulties caused the error to be estimated as between 10 and 15%.

Cerium

A 2-ml (or sometimes 1-ml) aliquot was removed from the mother solution into a 40-ml centrifuge tube and the solution was carefully evaporated to dryness. The residue was dissolved in 1 ml of Ce carrier, then 2 ml of 2M $NaBrO_3$ added and the solution allowed to cool to room temperature before the addition of 5 ml of concentrated HNO_3. The cooling was necessary in order to prevent HNO_3 decomposition (release of nitrogen oxides). This oxidizing medium changed all the cerium into the 4+ state, coloring the solution a characteristic transparent yellow. It was found that if the HCl mother solution is not evaporated to dryness the separation does not proceed well. The next step was solvent

extraction of the cerium by hexone (methyl iso-butyl ketone). The extraction was done in 100ml separatory funnel containing 50 ml of methyl iso-butyl ketone (previously equilibrated with 50 ml of 9M HNO_3 and 2 ml of 2M $NaBrO_3$). The mixture was shaken for exactly one minute and the middle of the shaking time was recorded as the time of separation. The organic phase was then washed twice with 1 ml of 9M HNO_3, with two drops of $NaBrO_3$ and back-extracted with 5 ml of H_2O with two drops of H_2O_2 serving as a reducing agent.

The aqueous phase was neutralized by concentrated NH_4OH(1 - 3 ml) until the insoluble hydroxide precipitates just appeared and acidified with a small amount of 6M HNO_3 until the solution was clear. The solution was then diluted with water to 15 ml and heated to boiling. Then 15 ml of saturated $H_2C_2O_4$ were added and the thorium rapidly formed a colloidal precipitate of insoluble oxalate which was followed by the formation of insoluble cerium oxalate after the solution was cooled for two minutes in an ice bath. It was centrifuged and the supernate discarded, 1 ml of 6M HNO_3 was added and the mixture heated to boiling if necessary depending on the ease with which the cerium oxalate dissolved, the thorium oxalate remaining undissolved. After centrifugation the supernate of pure cerium oxalate was poured into a clean test tube and the oxalate precipitation was repeated. If the yellowish color and the oxalate precipitates appeared immediately after addition of saturated $H_2C_2O_4$ the whole step of thorium-cerium separation was again repeated. Unfortunately this decreased the chemical yield to 40 - 50%. However, it was never necessary to repeat this purification for the third time. The final mixture was cooled in an ice bath, centrifuged, washed with water, and

filtered with suction on an ashless filter paper, washed three times with EtOH to dissolve any $H_2C_2O_4$ and heated in a furnace at 800^o for 30 minutes to convert the oxalate into CeO_2. After this the yellowish CeO_2 was slurried with EtOH and filtered on a previously dried and weighed fibre glass filter paper, dried and weighed again and finally mounted on cardboard in the usual way.

This chemical procedure was checked for possible thorium contamination by performing a blank chemical separation on an unirradiated thorium foil. The activity of the sample was then measured and compared to a thorium spectrum (namely thorium plus its daughters up to ^{228}Th which reaches an equilibrium in several days) and no thorium activity found at all. Another way of checking this was by performing the same experiment but without addition of Ce carrier, in which case no appreciable weight was obtained and thus no measurable thorium contamination by weight.

Copper

The copper foil was weighed and dissolved in 2 ml of concentrated HCl and a few drops of H_2O_2. No carrier for copper was necessary because the irradiated copper foil acted as the carrier. The solution was evaporated to dryness and then dissolved in two ml of 4.5M HCL. The solution was passed through a Dowex-IX8 anion-exchange resin column (58). The column was washed with 4.5M HCl to free it from zinc, cobalt, and iron. When the yellow copper band appeared at the bottom of the column, the column was eluded with 1.5M HCl and the middle fraction of this eluate was taken for the copper fraction. The solution was diluted to about 5 ml and copper was reduced with $NaHSO_3$ and precipitated as CuCNS

with NH_4CNS from dilute HCl solution. The precipitate was digested, filtered, washed with water and with EtOH, dried at 110^0 C. for about 15 minutes, weighed and mounted on cardboard.

3. Radioactivity Measurements

The activities were measured by gamma spectroscopy using a 3" x 3" thallium-activated sodium iodide crystal detector and a $2cm^3$ lithium-drifted germanium semiconductor detector. A brief description of each of these detectors is given below.

3a. Scintillation detector:

The crystal, hermetically sealed in an aluminum capsule, and optically coupled to an RCA A6342-A photomultiplier was shielded in a lead box to reduce the background. The inside of the lead shielding consisted of iron and copper layers to reduce the γ-ray backscattering.

The output pulses from the amplifier were analyzed by a 400-channel Pulse Height Analyzer (Nuclear Chicago Corporation, Model 34-12B, RIDL). The spectrum of the measured data could be displayed on the screen of the cathode ray tube, printed out by printer, and plotted with an X-Y plotter.

The dead-time loss was eliminated by using the timer in the "live" mode on the analyzer. The detector efficiency was calibrated both with standard gamma sources, ^{57}Co, ^{203}Hg, ^{22}Na, ^{88}Y, ^{137}Cs and ^{60}Co in the form of precipitates on the standard cardboards of approximately 4 cm^2 area and with more recent solid sources (IAEA) in the form of weightless "point" sources sealed in plastic holders. The differences between these two calibrations were within the limits of expected error. For liquid samples the calibration was performed only with the former standards.

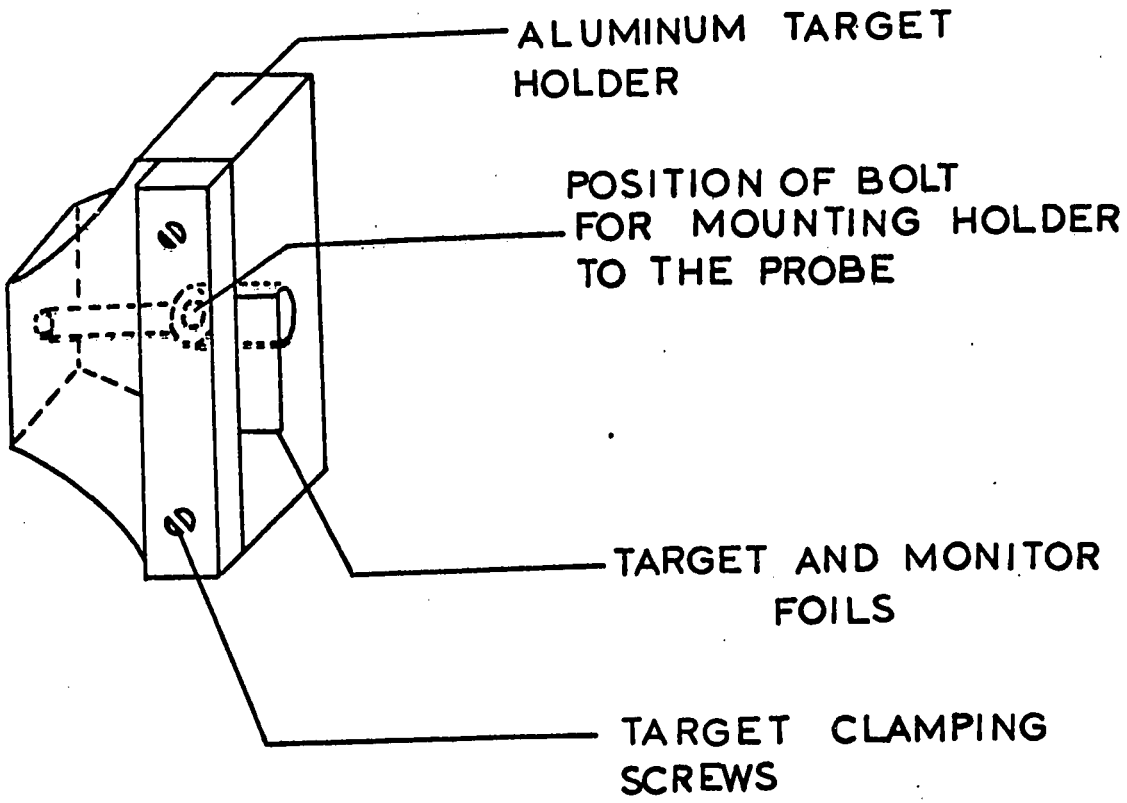
ALUMINUM TARGET HOLDER
POSITION OF BOLT FOR MOUNTING HOLDER TO THE PROBE
TARGET AND MONITOR FOILS
TARGET CLAMPING SCREWS

Figure 5

3b. Germanium-Lithium Detector:

The detector with 4.0 cm^2 active area was encapsulated in a Model 80 Vertical Cryostat, which provides the required vacuum and temperature conditions for the detector. The cryostat was placed in a 25-l Dewar filled with liquid nitrogen. A Model 118 preamplifier was mounted directly on the cryostat. The pulses were amplified by an Ortec 440 multimode amplifier, stretched in a pulse stretcher (Ortec 411) and fed into a 1600-channel Victoreen SCIPP analyzer. The block diagram is shown in Fig. 6.

Since the active volume of this detector was only $2cm^3$ and consequently the efficiency approximately one tenth that of a sodium-iodide detector, the former was used only in cases when its superior resolution was essential for separating the γ-rays of barium and cerium isotopes. The resolution of this detector was 4.5 keV full-width at half-maximum for the ^{137}Cs 662-keV peak, while for the sodium-iodide detector the corresponding value was 50.3 keV.

All the calibration work was in agreement with the calibration curves of other workers from the laboratory and also intercalibration between both counters was performed and found to be satisfactory.

The gamma intensity of the ^{141}Ba 190-keV peak was determined in later experiments on the new Ge(Li) detector of active volume $30cm^3$ with appropriate calibration. This measurement was found more reliable than any similar measurement on the $2cm^3$ detector because of better peak-to-Compton ratio.

The 1600-channel analyzer could be operated in "live" mode and "recycle" plus "destruct" mode. The latter combination enabled one to measure short-lived isotopes, for example ^{141}Ba

continuously in short-counting times. If the dead-time losses exceeded 20% all resolution was lost.

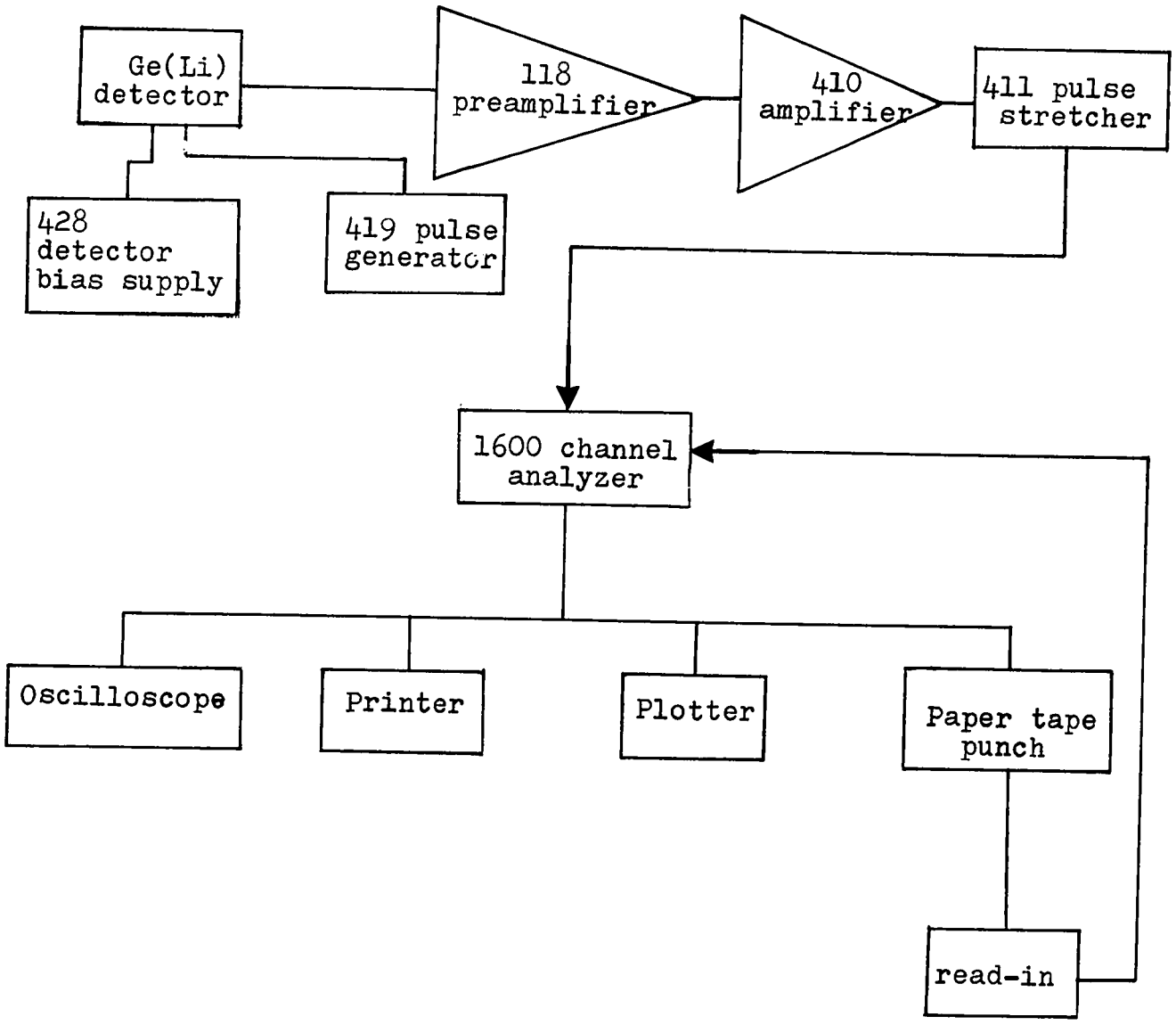

Figure 6

4. Treatment of Data

A list of all nuclides studied, their gamma rays and other pertinent properties are given in Table 3. In this Table are also listed the efficiency coefficients for the Ge(Li) and/or NaI(Tl) detector assemblies. One or the other was used for each nuclide depending on the availability of the Ge(Li) counter, activity of the isotope, and complexity of the spectra.

As shown in Table 3, the activities of ^{139}Ba, ^{141}Ba, and ^{139}Ce were measured only with the Ge(Li) detector. In the case of the first two the energies of the gamma rays were very similar, and their activities high enough so that short-counting times gave sufficient total accumulated counts. The peak from ^{139}Ce was completely obscured by other cerium peaks if the NaI(Tl) were used. All the rest of the isotopes were measured on the NaI(Tl) counter. In the case of ^{141}Ce and ^{144}Ce isotopes one composite peak was followed, while in all other cases single peaks were measured three times per half-life for three half-lives. If the duration of the measurements on the NaI(Tl) detector exceeded 100 minutes the background was automatically subtracted using the subtraction and addition modes. At bombarding energies higher than 70 MeV the 1692-keV peak from ^{124}Sb interfered with the measurement of the 1596-keV peak from ^{140}La. However it was easy to resolve this composite peak since the ^{124}Sb peak was longer-lived (60-day half-life) and of lower cross section.

Since escape and backscatter peaks did not constitute a problem the spectra were simple. Typical examples are shown in Figure 7. The escape peak for iodine formed a small hump on the low energy side of the main peak and it was not difficult to

include it into the peak area. Also the Compton edge and continuum did not interfere with the peak area determination. Background subtraction was done in a simple way by subtracting the background trapezoid from the total peak area.

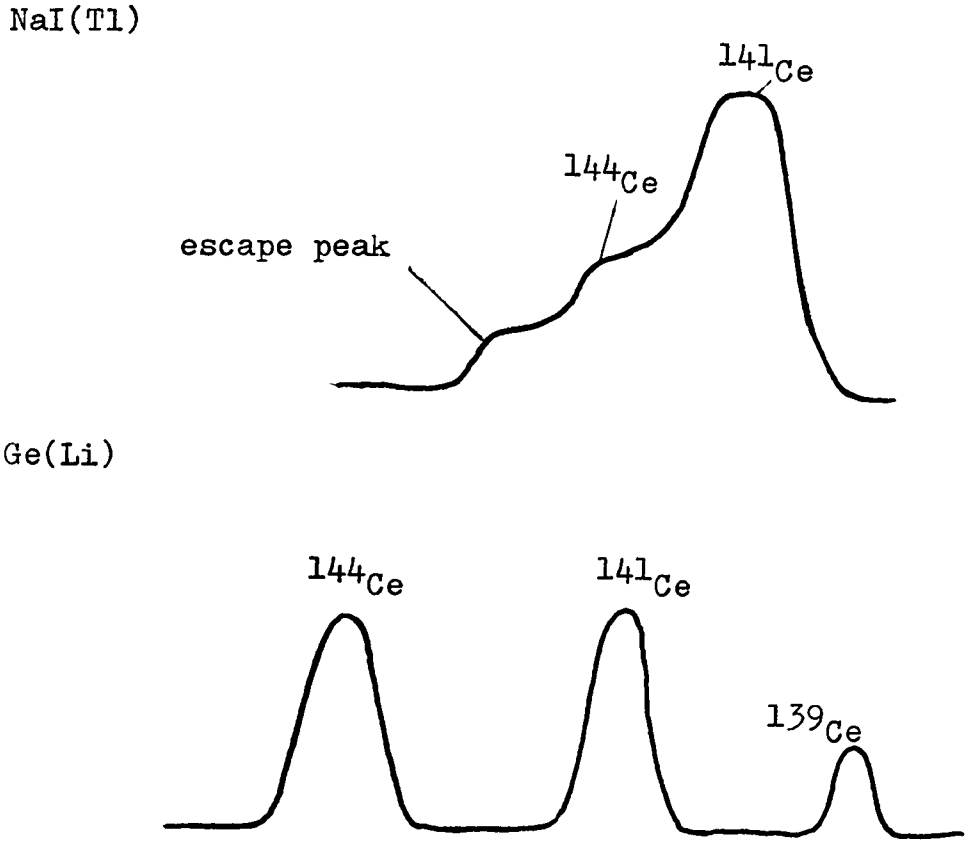

Figure 7

The photopeak areas, after background subtraction, representing the total number of registered counts were subjected to CLSQ analysis (59), and in this way the number of counts per minute at the end of bombardment, CPM^{EOB}, was obtained. These were then converted into disintegrations per minute at the end of bombardment, D^{EOB}, using the equation

$$D^{EOB} = CPM^{EOB} \times \frac{1}{C.Y.} \times \frac{100}{B.R.} \times \frac{100}{Eff.} \times A \qquad (25)$$

TABLE 3

List of Nuclides and their Pertinent Properties

	E (keV)	Branching Ratio in (%)	Counter Efficiency in (%) Ge(Li)	Counter Efficiency in (%) NaI(Tl)	$\frac{\lambda_{La}-\lambda_{Ba}}{\lambda_{La}}$	C_c* Ge(Li)	C_c* NaI(Tl)
^{139}Ba	166.	23.	1.4	---		1552.8	---
^{141}Ba	190.	54.	1.1	---		771.6	---
^{139}Ce	165.	80.	1.4	---		446.4	---
^{140}Ba - ^{140}La	1596.	96.	---	1.65 .54**	.86908	---	274.2 839.5**
^{141}Ce	145.	48.	1.35 2.**	13.1		520.8 771.**	79.5
^{143}Ce	293.(493.)	50.14***	---	8.2		---	121.6
^{144}Ce	134.	11.	1.58 2.2**	13.5		2066. 2876.**	336.7
^{64}Cu	511.	38.	---	3.1		---	84.89

** for liquid samples
*** weighted Branching Ratio

$$*C_c = \frac{\text{aliquot} \times 10^4}{\text{efficiency (\%)} \times \text{Branching Ratio (\%)}}$$

where C.Y. = chemical yield, Eff. = counter efficiency, A = aliquot and B.R. = branching ratio in %.

For most of the decay curves the "fit" parameter of the CLSQ program, which is a measure of the scatter of the points, did not appreciably exceed 1.5; in the case of ^{141}Ba it was 2.5. For ^{144}Ce in the composite peak (^{141}Ce - ^{144}Ce) where its activity was mostly very much lower than that of ^{141}Ce it was occasionally necessary to discard the measured value as unreliable. The scatter of the points was evenly distributed. The decay factor varied between 1.5 and 3. in most cases; for ^{141}Ba it was rather large; up to 20. However, the fit parameter was satisfactory and duplicate experiments were well within the estimated error.

The fission products studied in this work are given in Tables 3 and 4. All data are taken from Lederer et al. (60) and the half-life and energy of ^{141}Ba from (55).

As mentioned earlier, none of the nuclides studied is shielded so that only cumulative cross sections could be obtained in straightforward fashion. These were obtained using the well-known equation

$$\sigma = D^{\infty} \times \frac{W_M}{W_{Th}} \times N.A. \times \frac{A_{Th}}{A_M} \times \frac{\sigma_M}{D_M^{\infty}} \qquad (26)$$

where W_M and W_{Th} are the superficial densities of the monitor and thorium foils respectively, N.S. = natural abundance of the ^{65}Cu isotope, A_{Th} and A_M are atomic weights of thorium and the monitor respectively, $D^{\infty} = \frac{D^{EOB}}{1 - e^{-\lambda t_0}}$ and $D_M^{\infty} = \frac{D_M^{EOB}}{1 - e^{-\lambda_M t_0}}$

where λ and λ_M are the decay constants of the nuclide and of the monitor respectively and t_0 = duration of the bombardment. D^{EOB} and D_M^{EOB} are as given in equation (25).

TABLE 4

Pertinent Decay Chains

^{139}Cs ——9.5 m——→ ^{139}Ba ——83.0 m——→

^{140}Ba ——12.8 d——→ ^{140}La ——40.2 h——→

^{141}Ba ——18.2 m——→ ^{141}La ——3.9 h——→ ^{141}Ce ——32.5 d→

^{143}La ——14.0 m——→ ^{143}Ce ——33.0 h——→

^{144}Ce ——285.0 d——→

^{139}Ce ——140.0 d——→

From this equation the cumulative cross sections for ^{139}Ba, ^{141}Ce, ^{143}Ce, ^{140}Ba, ^{144}Ce and ^{139}Ce were obtained. In order to determine the best approach for the time-extraction methods a reasonably simplified situation, based on real data, is given in Figure 8, showing the time dependence of the number of atoms for the individual members of mass chain A = 141. Curve 1 shows the growth of the total number of ^{141}La atoms and curve 2 gives the decay of independently-formed ^{141}La. Curve 3 gives the growth and decay of ^{141}Ba. One can see that in 100 minutes all ^{141}Ba is changed into ^{141}La, so that, in order to determine the independent yield of ^{141}La, the first separation must be performed as soon as possible after the end of bombardment, and the second separation after about two or three half-lives of the parent isotope (^{141}Ba), since at that time most of the relations between the genetically connected components are still affected by the parent-daughter relationship. In this work only barium and cerium chemical separations were performed so that there was a choice between two possibilities in the case of the 141 mass chain:

1. To let all ^{141}Ba atoms decay into ^{141}La, perform the first separation of cerium and then do the second separation about 12 hours later. This approach is typical for radiochemical studies and is basically a double-time extraction method.

2. To separate four times (the fourth separation is performed only to obtain the total cumulative yield). The first separation is to be done as soon as possible, the second a few hours later, and the third a day later. In addition the cumulative yields of ^{141}Ba and ^{141}Ce (obtained using equation (26) from separate measurements) can be used to obtain two independent yields for ^{141}La and ^{141}Ce, a method which we may call "triple-time extraction".

The second possibility was chosen mainly because the cross section for independently-formed ^{141}Ce was very low. This method gives better results since the error resulting from subtraction of two approximately equal numbers is smaller in the second case. From the four separations it was possible to employ the double-time extraction method in addition to that of triple-time extraction. It was found that for the systems studied each time extraction method has its own optimum number of separations and separation times. Theoretically, all data could have been subjected to a weighted least-squares analysis - simply because there were more data than unknown cross sections and because the data were coupled by measuring the same isotope in the barium and cerium samples (more detail will be given about this at the end of this section). However, a rigorous mathematical treatment of this problem would have been extremely laborious and time-consuming. To a certain degree it was possible to weight the results

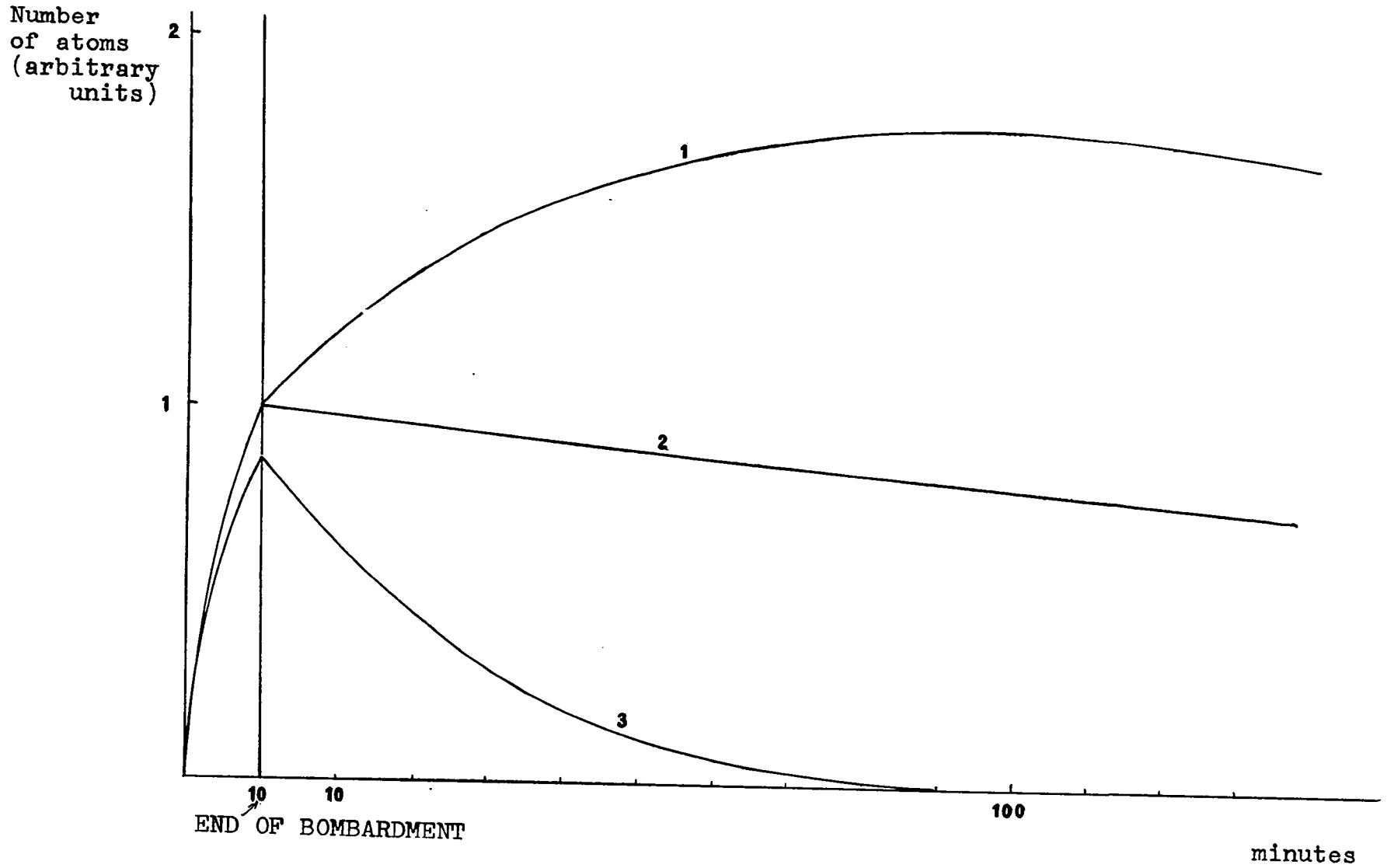
Number
of atoms
(arbitrary
units)
2
1
1
2
3
10
10
100
END OF BOMBARDMENT
minutes

Figure 8

of various calculations, namely discard the results when the method showed itself to be unstable with respect to small changes in the input data which were within the experimental error. (By unstable we mean a situation where, for instance, a change of the order of 1% in the input data creates a change in the output of several orders of magnitude.)

For the cases of two chemical separations and two cross sections (independent and cumulative) another well-known equation was used

$$D_d = \frac{\lambda_d}{F}\left(K_1 \sigma_p + K_2 \sigma_d\right) \qquad (27)$$

where $F = W_M/W_F \times N.A. \times A_{Th}/A_M \times \sigma_M/D_M^{\infty}$

$$K_1 = \left[e^{-\lambda_p t}\left(1-e^{-\lambda_p t_0}\right)-(\lambda_p/\lambda_d)e^{-\lambda_d t}\left(1-e^{-\lambda_d t_0}\right)\right]/(\lambda_d-\lambda_p)$$

$$K_2 = \left[e^{-\lambda_d t}\left(1-e^{-\lambda_d t_0}\right)\right]/\lambda_d$$

D_d = activity of the daughter at time t, t_0 = duration of bombardment and λ_p and λ_d are the decay constants of the parent and daughter respectively. The rest of the quantities are as given in equation (26).

From two measurements of D_d two equations of this kind were obtained and both cross sections calculated. This method was applied in the case of ^{139}Cs and ^{139}Ba with satisfactory results, and in the case of ^{143}La and ^{143}Ce with semi-satisfactory results (the error reaching in some cases up to 50%). For the ^{141}La - ^{141}Ce chain the activities in the second and third separation gave satisfactory results, but in the third and fourth separation the method showed itself to be unstable. The derivation of equation (27) is included in Appendix B where it is the second step in the derivation of a similar expression for the case of the triple time-extraction. A FORTRAN program was used in this

case as well as for the actual calculation.

In the case of the ^{140}Ba - ^{140}La parent-daughter chain the independent yield of ^{140}La was obtained by the simple method of following ^{140}La activity in an aliquot of the mother solution. The measurements were performed in two sequences. The first eight to ten measurements were taken during the second and third day after the irradiation (on the first day the peak-to-Compton ratio was very unfavorable) to follow the decay of the independently-formed ^{140}La and in the second sequence after 10 days when the equilibrium between ^{140}Ba and ^{140}La was established, an ordinary set of measurements for three half-lives was performed. By that time all the activity from the independently-formed ^{140}La had decayed. Calculations were based on equation (28) for the first sequence

$$D_d^{EOB} = D_p^{EOB} \frac{\lambda_d}{\lambda_p - \lambda_d} \left[1 - e^{(\lambda_d - \lambda_p)t} \right] + D_d^{EOB} e^{\lambda_d t} \qquad (28)$$

where t is the time when the measurements were taken and the other symbols are as defined in equations (27) and (25) and on equation (29) for the second sequence,

$$D_p^{EOB} = CPM_d^{EOB} \frac{C_c}{C.Y.} \qquad (29)$$

where the symbols are as defined in equation (25) and the constant C_c is given in Table 3. Equation (28) gives the cross section for the independently-formed ^{140}La while equation (29) gives the cumulative cross section for ^{140}Ba. (It was not necessary to convert to counts per minute, CPM, because only one peak was measured in both cases). Derivations of equations (28) and (29) are given in Appendix A. Count rates giving counts/minute at the end of bombardment in equation (29) were obtained by CLSQ analysis. The

values for the ^{140}La independently-formed activity were processed by a very simple method included in the FORTRAN program used for calculations from equation (28), namely by calculating the arithmetical average. The accuracy of this method was checked by analyzing the count rates by CLSQ for two cases and it was found that the difference was negligible. This was not surprising since the measurements were taken during the linear part of the decay curve, so that the least-squares analysis and the arithmetical average should give the same number if done correctly

Finally the case of the chain $^{141}Ba - ^{141}La - ^{141}Ce$ was treated by the triple time extraction method previously discussed. It was virtually impossible to arrive at a simple expression of the type of equations(27) and (28). The derivation is given in Appendix B. In the final calculation the following equation

$$^{141}Ce\,\sigma_{cum} = {}^{141}Ba\,\sigma_{cum} + {}^{141}La\,\sigma_{ind} + {}^{141}Ce\,\sigma_{ind} \qquad (30)$$

was used, where $^{141}Ba\,\sigma_{cum}$ and $^{141}Ce\,\sigma_{cum}$ were known.

Besides the expressions shown in Appendix B an expression for the same case, derived, however, in a different way by Saha (61) was used for comparison. The results for the case of the cerium separation were practically identical using both sets of expressions. In the case of the second separation the difference was slightly greater. In the case of the third separation the values differed significantly. This is not surprising if it is noted that basically at least three inaccurate numbers are fed into these equations ($\lambda_{^{141}Ba}$, $\lambda_{^{141}La}$, $\lambda_{^{141}Ce}$, $D^{EOB}_{^{141}Ce}$, $^{141}Ce\,\sigma_{cum}$, $^{141}Ba\,\sigma_{cum}$) and they are treated in differently arranged expressions (the errors are therefore propagated in different ways).

In conclusion the nuclides measured in each run several times independently are given below:

^{140}Ba - measured as ^{140}La in both barium samples (labelled by "I" and "II") and in the fission products mother solution. In all it was measured three times.

^{143}Ce - measured directly, also could be calculated from the two triple-time extraction equations using the first and second separation samples. These results, however, were not satisfactory.

^{141}Ce and ^{141}La - from triple-time extraction and from double-time extraction using two pairs of separation samples: the pair including the second and the third separation and the pair using the third and fourth separations. The triple-time extraction method gave very good results, the rest were satisfactory.

5. Monitor Cross Section

For the whole energy range the ^{65}Cu (p, pn) ^{64}Cu reaction was used to monitor the proton beam. The cross sections used in this work are given in Table 5 as measured by Meghir (62).

TABLE 5

proton bombarding energy (in MeV)	monitor cross section (mb)
28	420
37	280
44	220
59	180
68	160
75	150
83	140

6. Errors

In experimental work two kinds of errors occur, systematic or constant and random errors.

The constant errors are associated with absolute branching ratios, half-lives, efficiency curves and monitor cross sections. The random errors are associated with the determination of disintegration rates, including determination of peak areas, decay curves resolution, chemical yield determinations, weights of the targets, and non-uniformity of the target foils.

The statistical errors in counting rates were minimized by making sources as active as possible, consistent with safety considerations.

Approximate estimates of the errors are given below:

Determination of photopeak area gives rise to one of the main sources of error and was estimated to be within ± 4 to $\pm 10\%$ depending on the complexity and peak-to-Compton ratio for the measured peak.

The error in chemical yield determination was estimated from the duplicate measurements discussed at the end of Treatment of Data section, which agreed within $\pm 5\%$. Even though this was only a rough estimate where one could not distinguish the chemical yield error from the statistical photopeak area determination errors, it was considered as acceptable that the chemical yield error does not exceed $\pm 4\%$.

Weighing of the targets was estimated to be accurate to $\pm 1\%$.

The uncertainty in the determination of counter efficiencies was estimated to be $\pm 10\%$.

The error in pipetting aliquots was estimated to be $\pm 1\%$.

The error in the determination of the separation time was ±1% in the case of solvent extraction and ±5% error in the case of precipitate separation as to the determination of the exact moment when the precipitate separates from the solution.

No attempt was made to evaluate systematic errors arising from absolute branching ratios and half-lives reported in literature and they were not re-checked in this work.

To make sure the methods used were reliable the runs for 28, 37, 59 and 68 MeV were duplicated. In most cases the agreement was within ±5%, never exceeding ±15% except in the case of ^{144}Ce. However, the cross sections obtained using the double-time extraction method in the case of mass chain A = 143 had poorer reproducibility (the values differed in some cases as much as 50%) showing how the errors listed above can be propagated by the exponential relations used in the double-time extraction method calculations. The duplicate experiments are considered as the main indication of the reliability of the methods used.

The rigorous total error calculation including the exponential relations would be very time-consuming. It was considered sufficient for the purpose of this section to give an indicative total error by taking the sum of the squares of the individual errors. It was found to be between ±10 and ±20%.

C. RESULTS

1. Excitation Functions

The measured cross sections of all nuclides studied are given in Tables 6 to 9. Excitation functions of various products are given in Figures 9 to 13. For completeness the results of duplicated experiments are also shown.

From Figures 9 to 13 one can observe the following. The cross section for the independent formation of ^{139}Ba reaches a maximum, rather poorly defined, at approximately 40 MeV. The scatter of the experimental points is probably due to the time-extraction method difficulties. The cross section for the cumulatively-formed ^{139}Ba formation in Figure 9 was obtained by summing up the ^{139}Cs cumulative and ^{139}Ba independent cross sections. This gives an indication of which errors are due to time-extraction problems and which are of different origin. For instance the deviation at 75 MeV for the independent formation of ^{139}Ba also shows up in the cumulative cross section for ^{139}Ba so that it is not considered as an indication of a peak.

The cross sections for the independent formation of ^{140}La and ^{141}La, shown in Figures 10 and 11 respectively, exhibit maxima at 60 MeV and 45 MeV respectively. The cross section for ^{141}Ce (Figure 11) increases very little with increasing bombarding energy and that for ^{143}Ce (Figure 12) shows only a poorly-defined peak at bombarding energies around 50 MeV.

Friedlander et al. (30) were the first to observe a correlation between the neutron-to-proton ratios of the fission products, N/Z, and their excitation function maxima, $E_p(max)$. According to the prescriptions given by these authors, the maxima

of different products, $E_p(max)$, have been plotted against their neutron-to-proton ratio, N/Z, in Figure 14. It can be seen from Figure 14 that the curves for ^{233}U and also for ^{232}Th display certain deviations from straight lines, unlike the curves for ^{238}U and ^{239}Pu. The basic trend pointed out by Tomita & Yaffe (63), that the peak of the excitation function, $E_p(max)$, of a given product occurs at a lower energy for a target of lower N/Z was again verified. This is discussed in greater length in a later section.

TABLE 6

Cross Sections of Mass Chain A = 139

Ep (MeV)	^{139}Cs σ_{cum} (mb)	^{139}Cs fraction of cum	^{139}Ba σ_{ind} (mb)	^{139}Ba fraction of ind	^{139}Ba σ_{cum} (mb)	% added	A = 139 estimated
28	24.	.67	11.	.25	35.	8%	38.
37	23.	.62	11.	.29	34.		38.
	19.	.50	15.	.41	34.	10%	38.
44	19.	.56	12.	.35	31.		33.
59	14.	.51	10.	.37	24.	12%	27.
68	11.	.44	10.	.42	21.		25.
	14.	.50	11.	.37	25.		29.
75	11.	.42	12.	.45	23.	14%	27.
					25.		29.
83	10.	.44	9.	.42	19.	16%	22.

TABLE 7

Cross Sections of Mass Chain A = 140

Ep (MeV)	^{140}Ba σ_{cum} (mb)	^{140}Ba fraction of cum	^{140}La σ_{ind} (mb)	^{140}La fraction of ind	^{140}La σ_{cum} (in mb)	% added	140 total estimated
28	32.	.96	1.1	.05	33.	0	
37	25.	.87	3.8	.13	29.	0	
44	23.	.85	4.0	.15	27.	0	
59	18.	.77	5.5	.23	23.	0	
68	17.	.75	5.2	.23	22.	2%	23.
75	16.	.73	4.8	.23	20.	4%	21.
83	14.	.72	4.0	.22	17.	6%	18.

TABLE 8

Cross Sections of Mass Chain A = 141

Ep (MeV)	^{141}Ba σ_{cum} (in mb)	^{141}Ba fractional	^{141}La σ_{ind} (in mb)	^{141}La fractional	^{141}Ce σ_{ind} (in mb)	^{141}Ce fractional	^{141}Ce σ_{cum} 141 total
28	19.	.78	5.3	.21	.20	.008	25.
37	13.	.60	8.5	.37	.46	.02	22.
	12.	.53	10.	.44	.5	.02	24.
44	12.	.52	9.8	.44	.65	.03	22.
59	10.	.53	7.4	.39	1.2	.06	19.
68	9.2	.48	8.2	.43	1.5	.08	19.
	10.	.52	7.9	.39	1.7	.08	20.
75	10.	.52	7.5	.38	1.6	.08	19.
83	8.6	.50	6.4	.37	1.9	.12	17.

TABLE 9

Cross Sections of Mass Chain A = 143, 139, 144

Ep (MeV)	^{143}La σ (in mb) cum	^{143}Ce σ (in mb) ind	^{143}Ce σ (in mb) cum	^{139}Ce σ (in mb) ind	^{144}Ce σ (in mb) cum
28	14.	7.	20.	0	14.
37	12.	8.	20.	0	16.
44	--	--	16.	0	12.
59	8.	6.	14.	0	9.
68	7.	7.	14.	.002	9.
75	7.	6.	13.	.008	10.
83	6.	5.	11.	.016	8.

Figure 9

Excitation functions for the mass chain A = 139

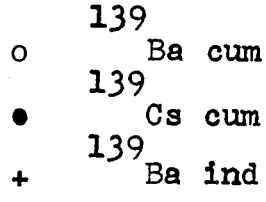

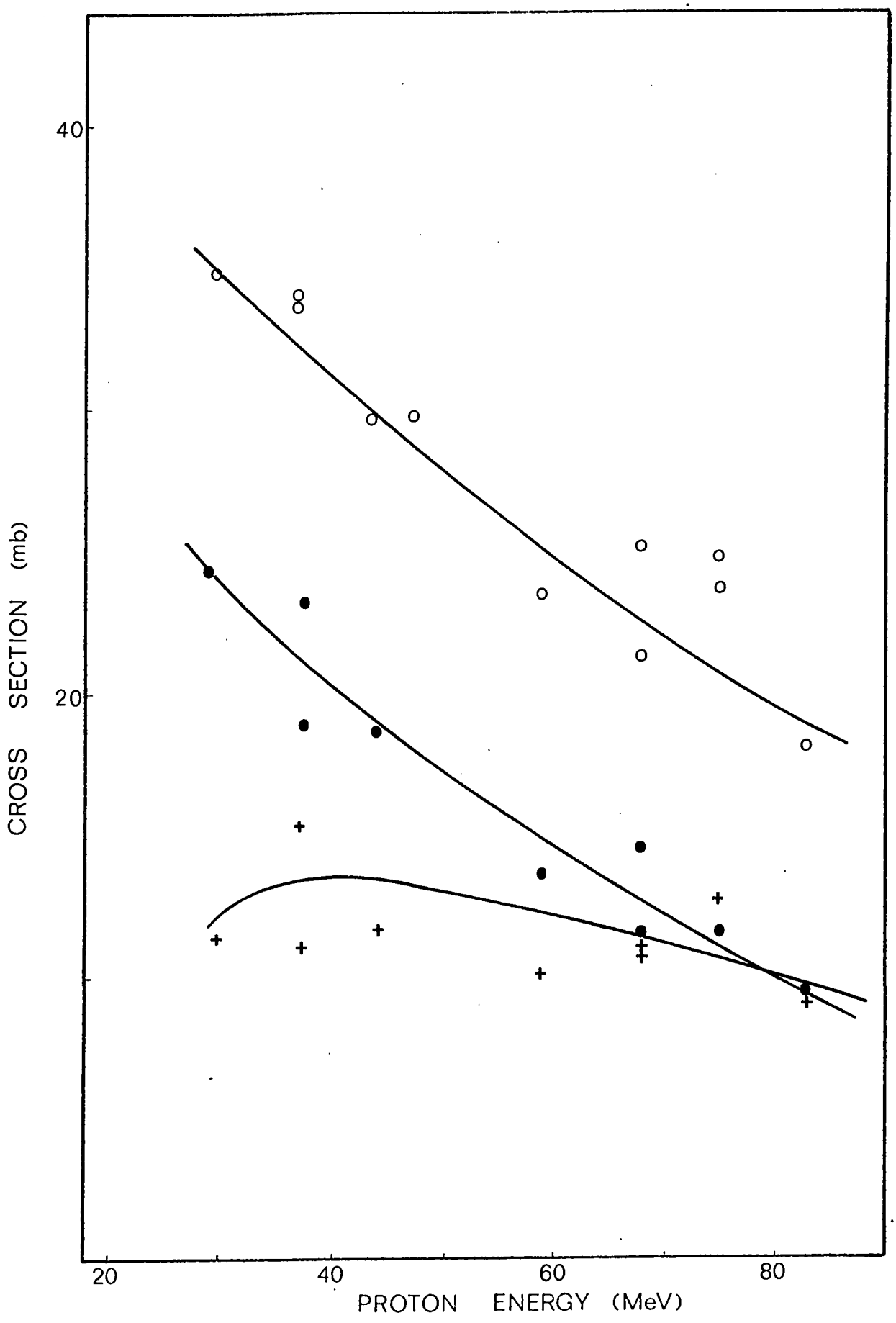
40
20
CROSS SECTION (mb)
20
40
60
80
PROTON ENERGY (MeV)

Figure 10

Excitation functions for the mass chain A = 140

o ^{140}Ba cum

• ^{140}La ind

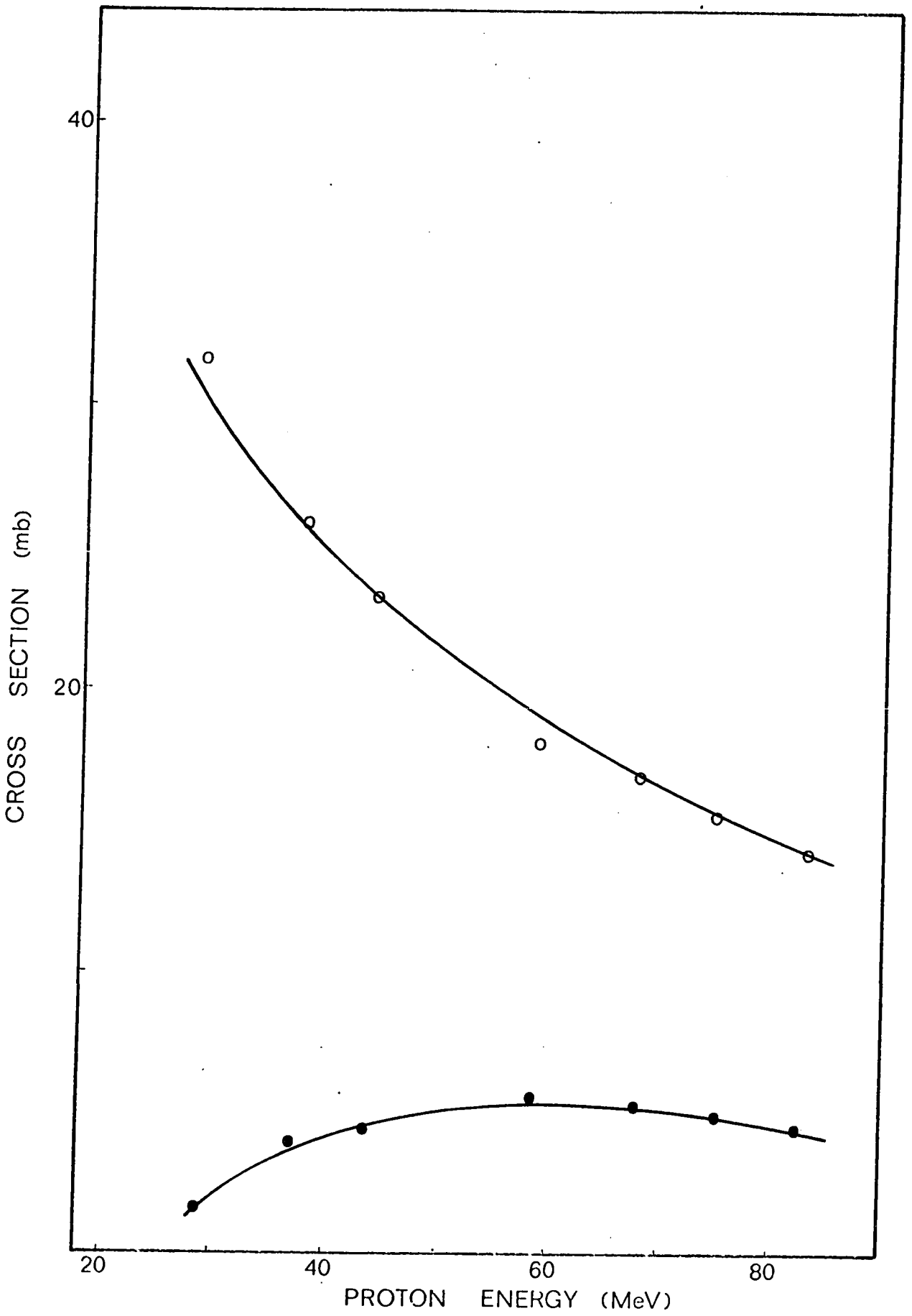
40
20
CROSS SECTION (mb)
20
40
60
80
PROTON ENERGY (MeV)

Figure 11

Excitation functions for the mass chain A = 141

o ^{141}Ba cum

● ^{141}La ind

\+ ^{141}Ce ind

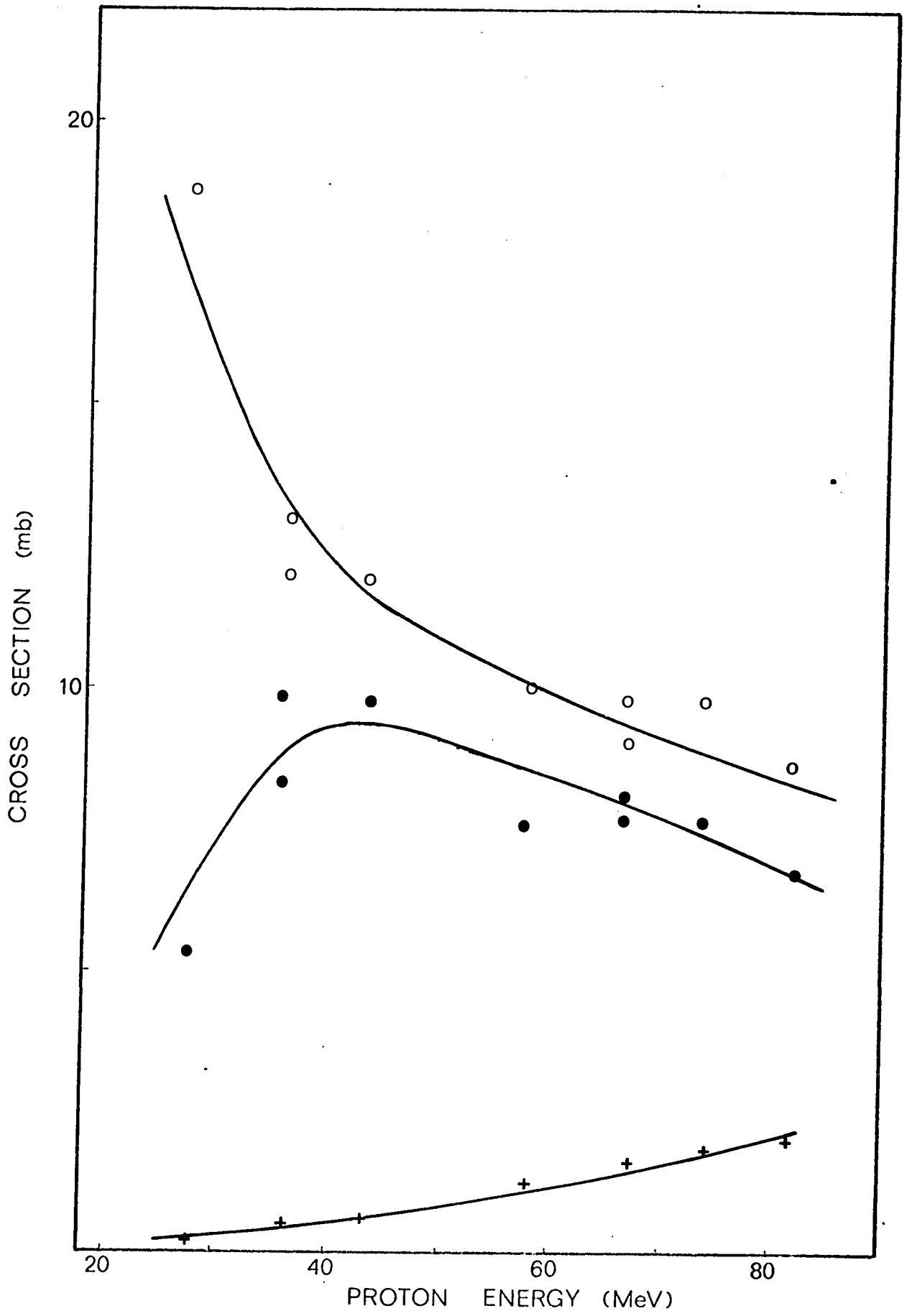
20
10
CROSS SECTION (mb)
20
40
60
80
PROTON ENERGY (MeV)

Figure 12

Excitation functions for the mass chain A = 143

o ^{143}La cum

• ^{143}Ce ind

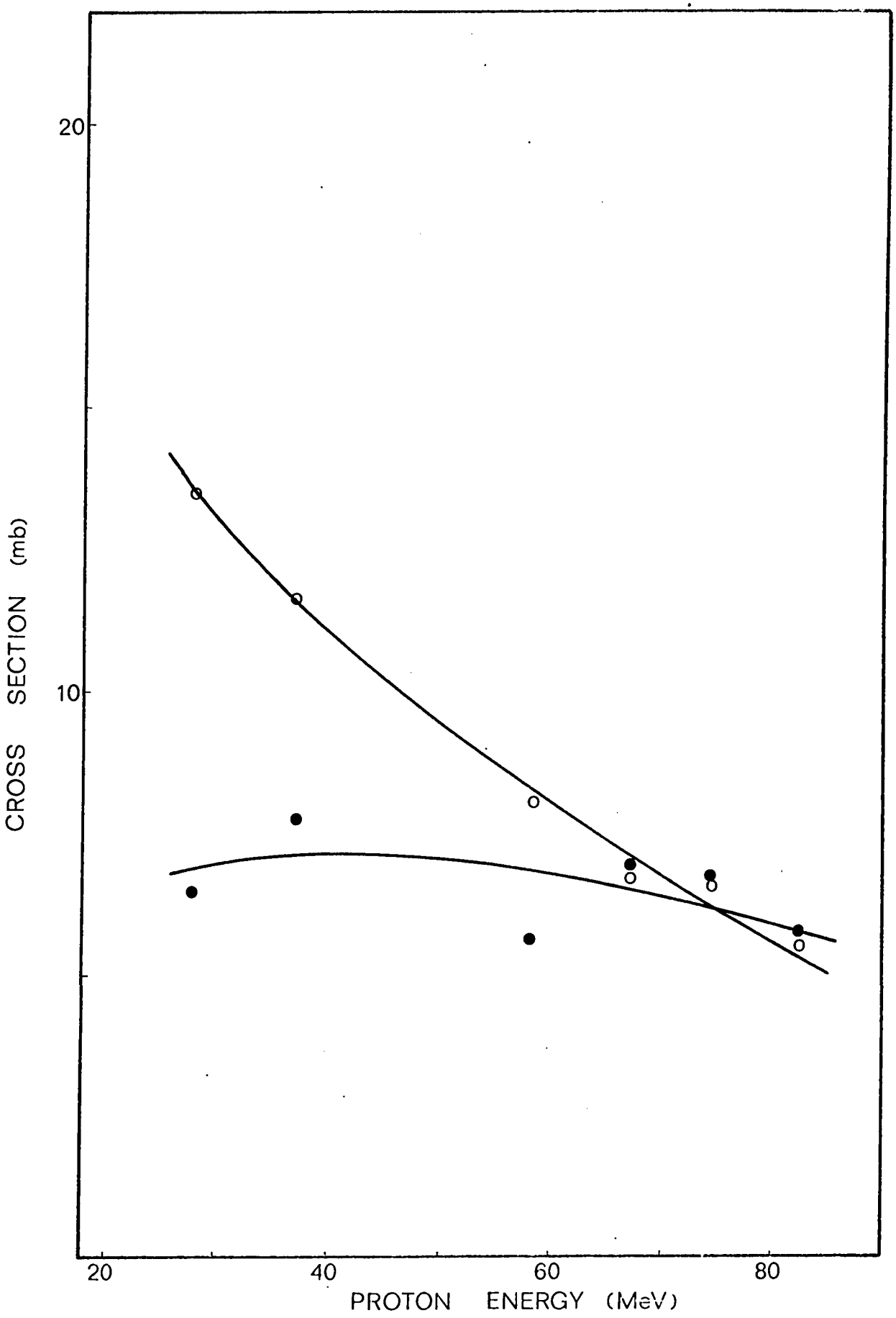
20
10
CROSS SECTION (mb)
20
40
60
80
PROTON ENERGY (MeV)

Figure 13

Excitation functions for the cumulative yields of the last members of the mass chains A = 139, 140, 141, and 143

△ ^{139}Ba cum

o ^{140}La cum

● ^{141}Ce cum

\+ ^{143}Ce cum

□ ^{137}Cs cum (taken from Benjamin et al. (64))

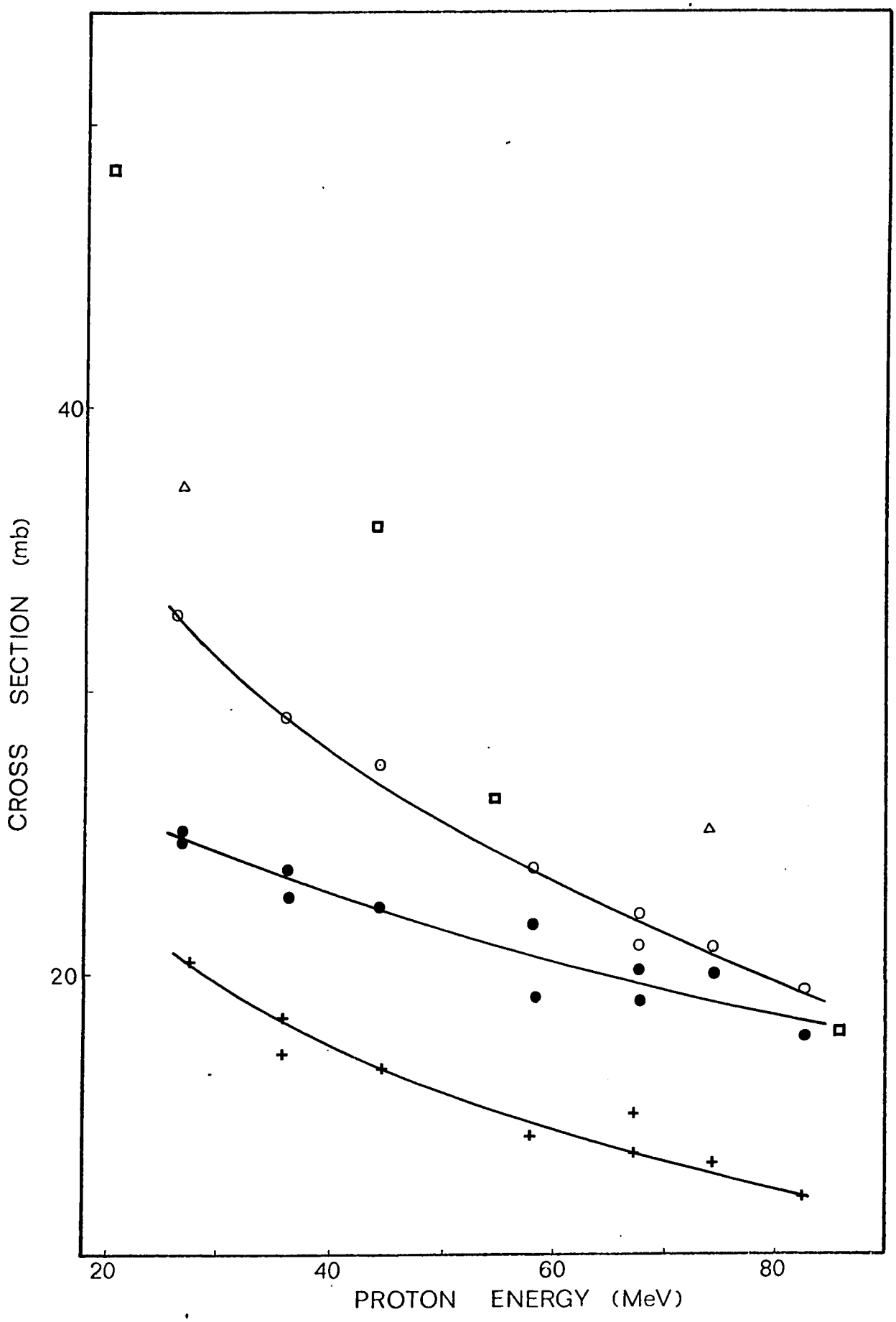
CROSS SECTION (mb)
40
20
20
40
60
80
PROTON ENERGY (MeV)

Figure 14

Energies at which the excitation functions of various isotopes reach their maxima

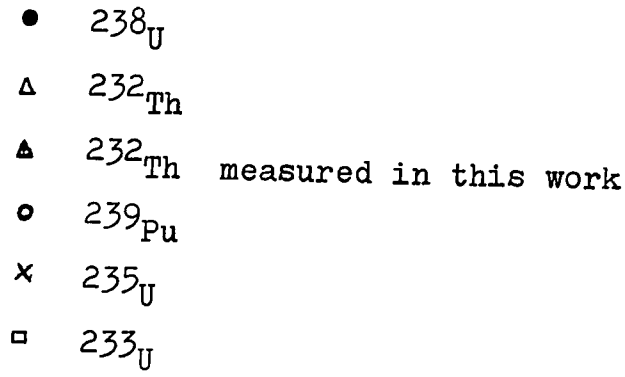

taken from Yaffe (33)

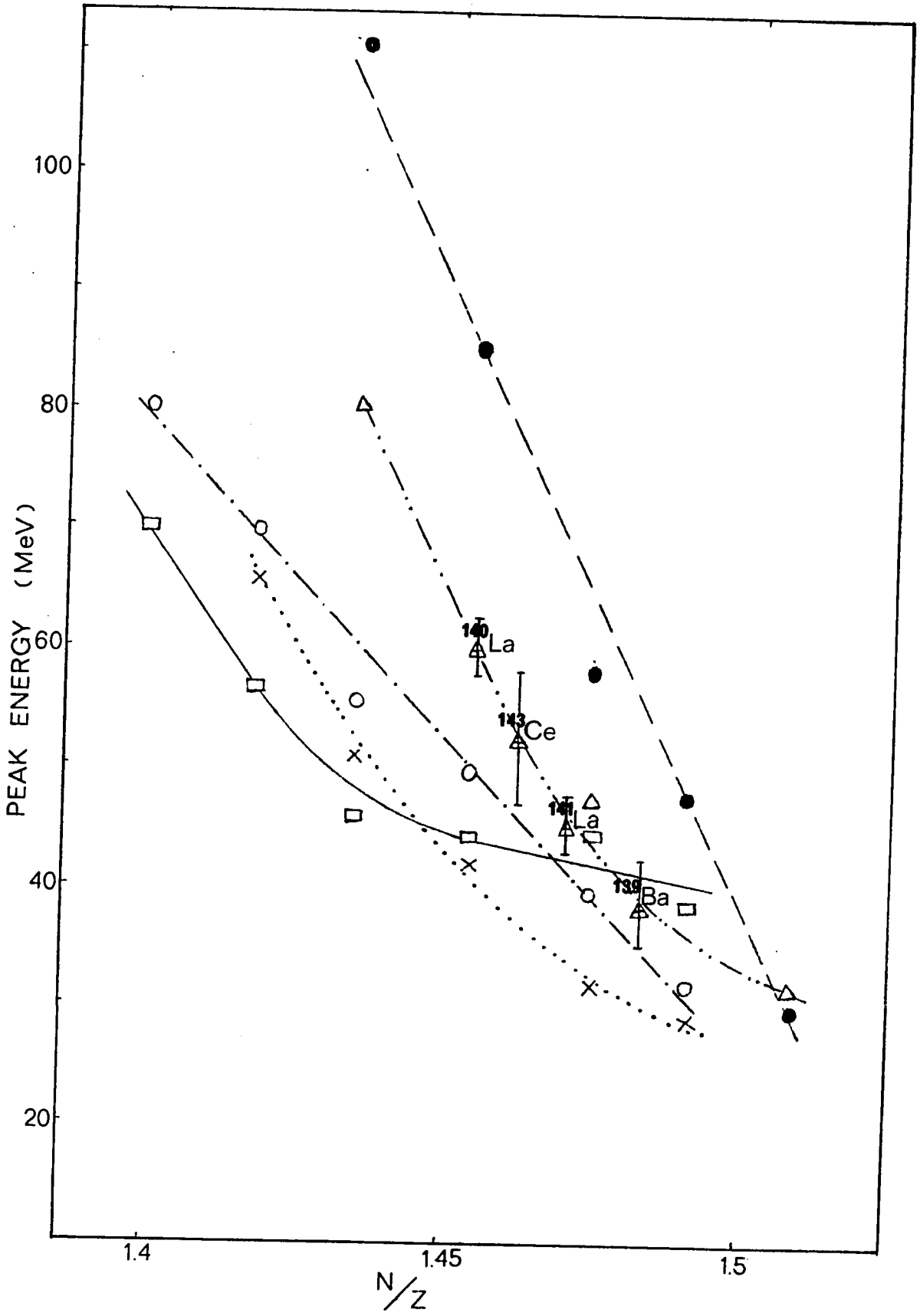
PEAK ENERGY (MeV)
100
80
60
40
20
1.4
1.45
1.5
N/Z
140La
143Ce
141La
139Ba

2. Charge Dispersion

The charge dispersion curves drawn at various energies are shown in Figure 15 to 21. The results of repeated experiments are also given.

The construction of the charge-dispersion curves in this mass region could not be performed assuming the mass-yield curve to be essentially flat, as other workers have done in other mass regions. Unfortunately, no reliable data giving the mass yields were available so that the measured cross sections had to be changed into usable data using corrections summarized in the Discussion section.

The fractional cross sections are given in Tables 6 to 9. In Figures 15 to 20 both independent and cumulative cross section curves are displayed (note that in this method of presentation all cumulative fractional cross section curves must pass through the point corresponding to 50% of the yield at a point exactly half a charge unit from the most probable charge, Z_p.). The independent cross sections of those nuclides not accessible to direct measurements were presented in such a manner that the sum of the independent yields read from the curves must add up to the measured cumulative yields which are also shown.

For each charge dispersion curve the mass A = 141 was used to obtain the most probable charge, Z_p. The full-widths of half-maxima, FWHM, of the curves in Z units were similarly obtained. The Z_A-Z_p values were calculated using Z_A values given by Coryell (19). The values of FWHM and Z_A-Z_p are given in Table 10 and the values of Z_A-Z_p are plotted, together with other workers' data, in Figure 22.

Figure 15

Charge dispersion curve at 28 MeV based on independent and cumulative yields

(The right hand side of the curve has been drawn so that the sums of the independent yields give the measured cumulative yields)

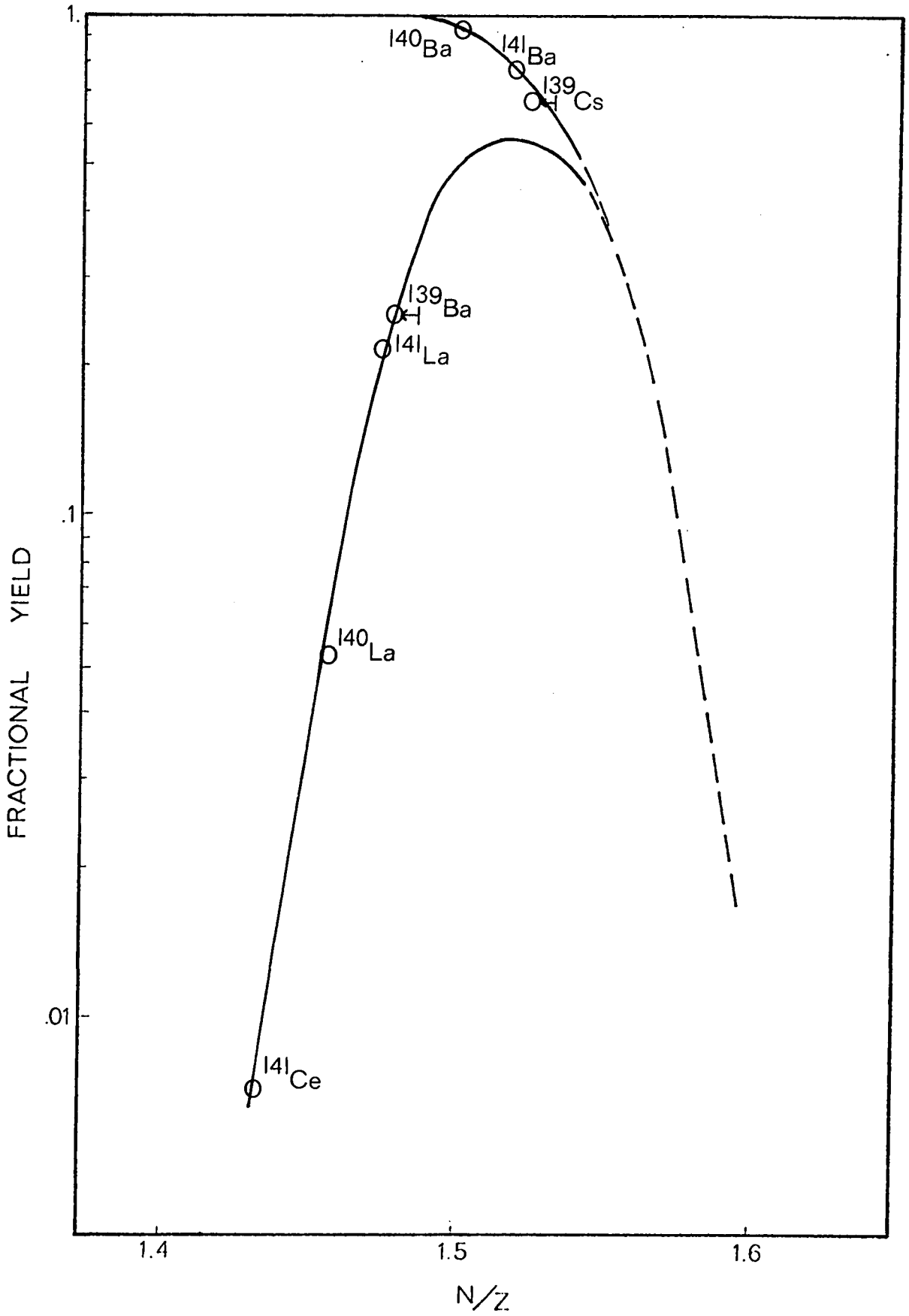
1.
.1
.01
FRACTIONAL YIELD
^{140}Ba
^{141}Ba
^{139}Cs
^{139}Ba
^{141}La
^{140}La
^{141}Ce
1.4
1.5
1.6
N/Z

Figure 16

Charge dispersion curve at 37 MeV based on independent and cumulative yields

(The right hand side of the curve has been drawn so that the sums of the independent yields give the measured cumulative yields)

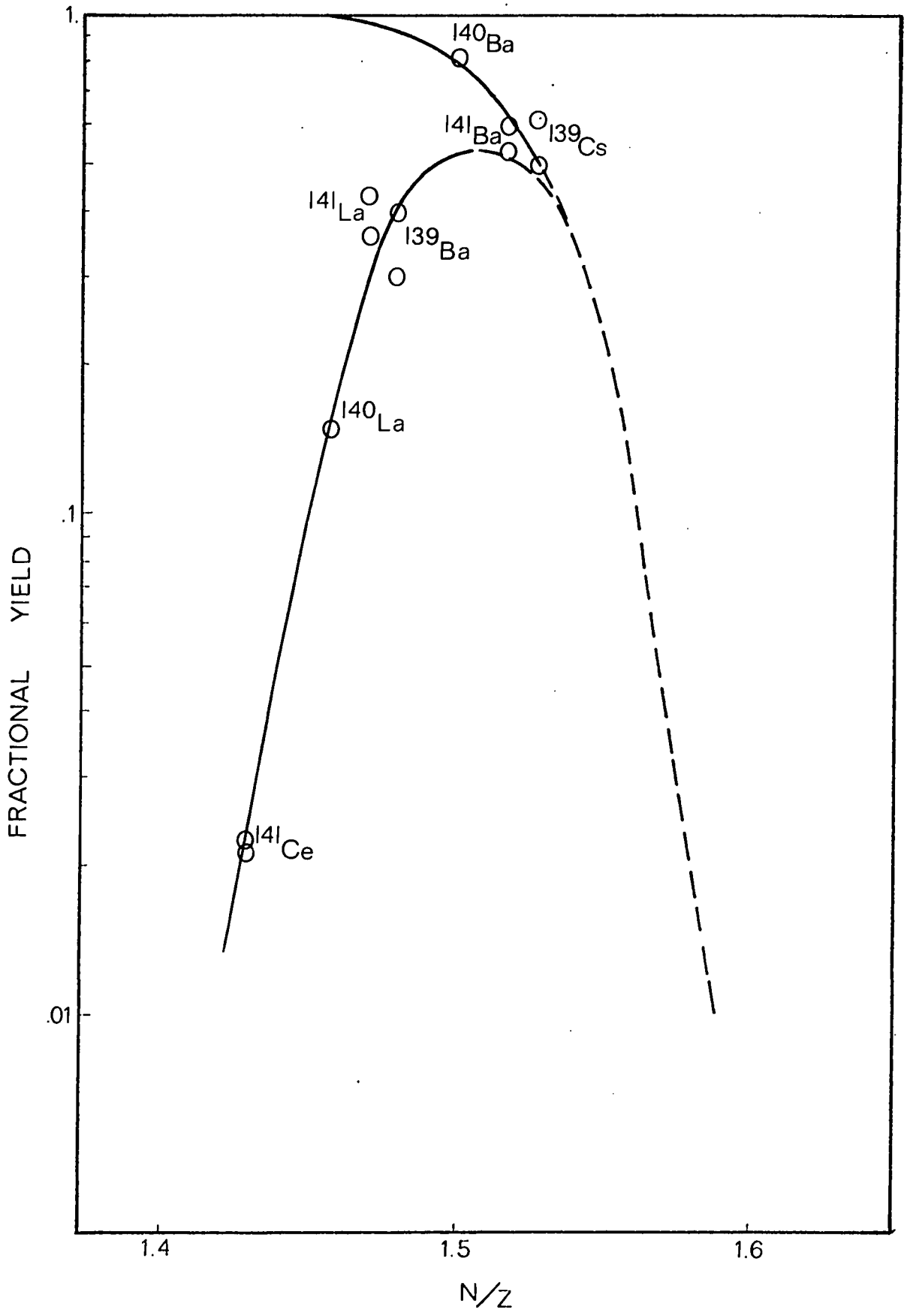
1.
.1
.01
FRACTIONAL YIELD
140Ba
141Ba
139Cs
141La
139Ba
140La
141Ce
1.4
1.5
1.6
N/Z

Figure 17

Charge dispersion curve at 44 MeV based on independent and cumulative yields

(The right hand side of the curve has been drawn so that the sums of the independent yields give the measured cumulative yields)

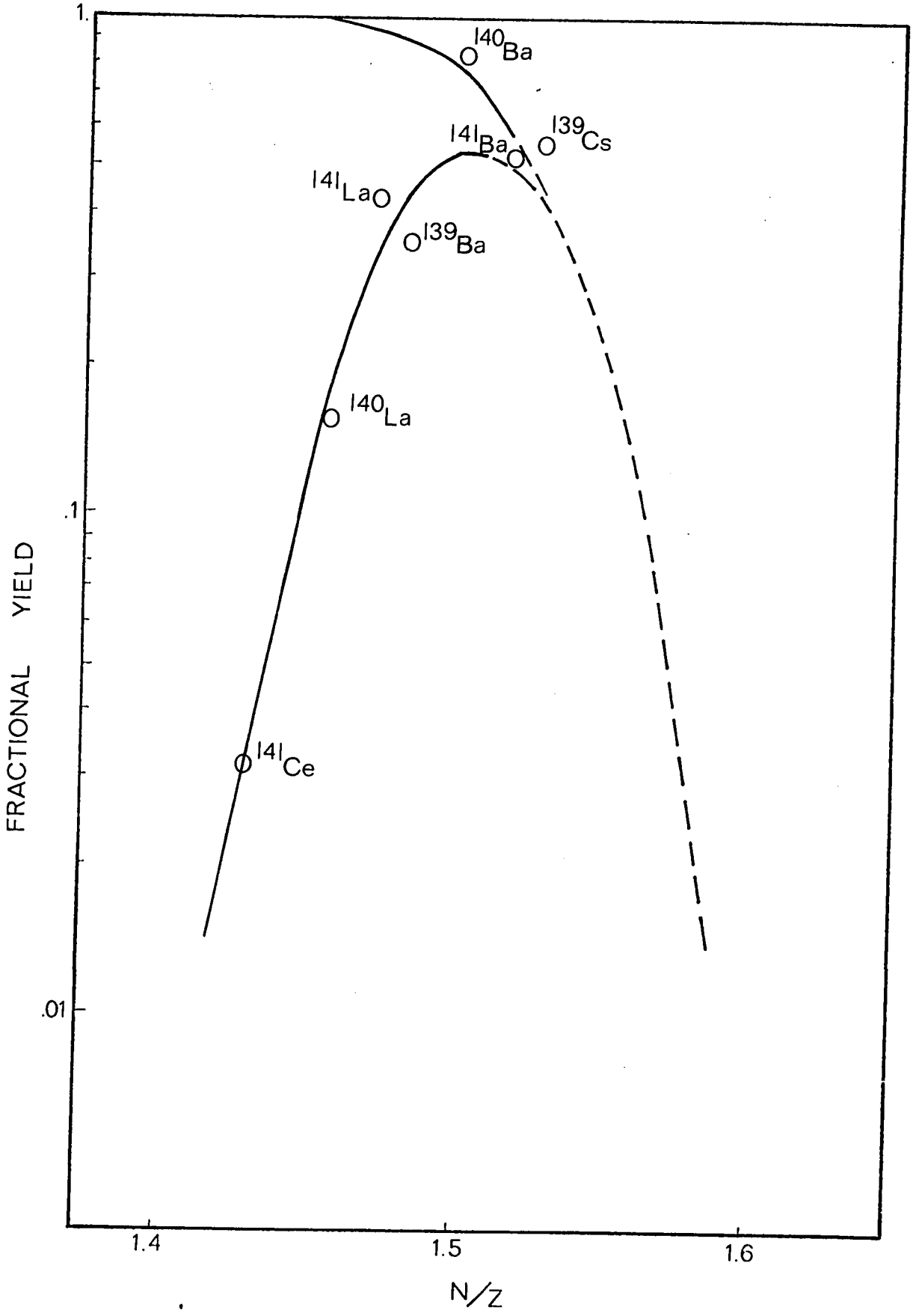
1.
.1
.01
FRACTIONAL YIELD
^{140}Ba
^{141}Ba
^{139}Cs
^{141}La
^{139}Ba
^{140}La
^{141}Ce
1.4
1.5
1.6
N/Z

Figure 18

Charge dispersion curve at 59 MeV based on independent and cumulative yields

(The right hand side of the curve has been drawn so that the sums of the independent yields give the measured cumulative yields)

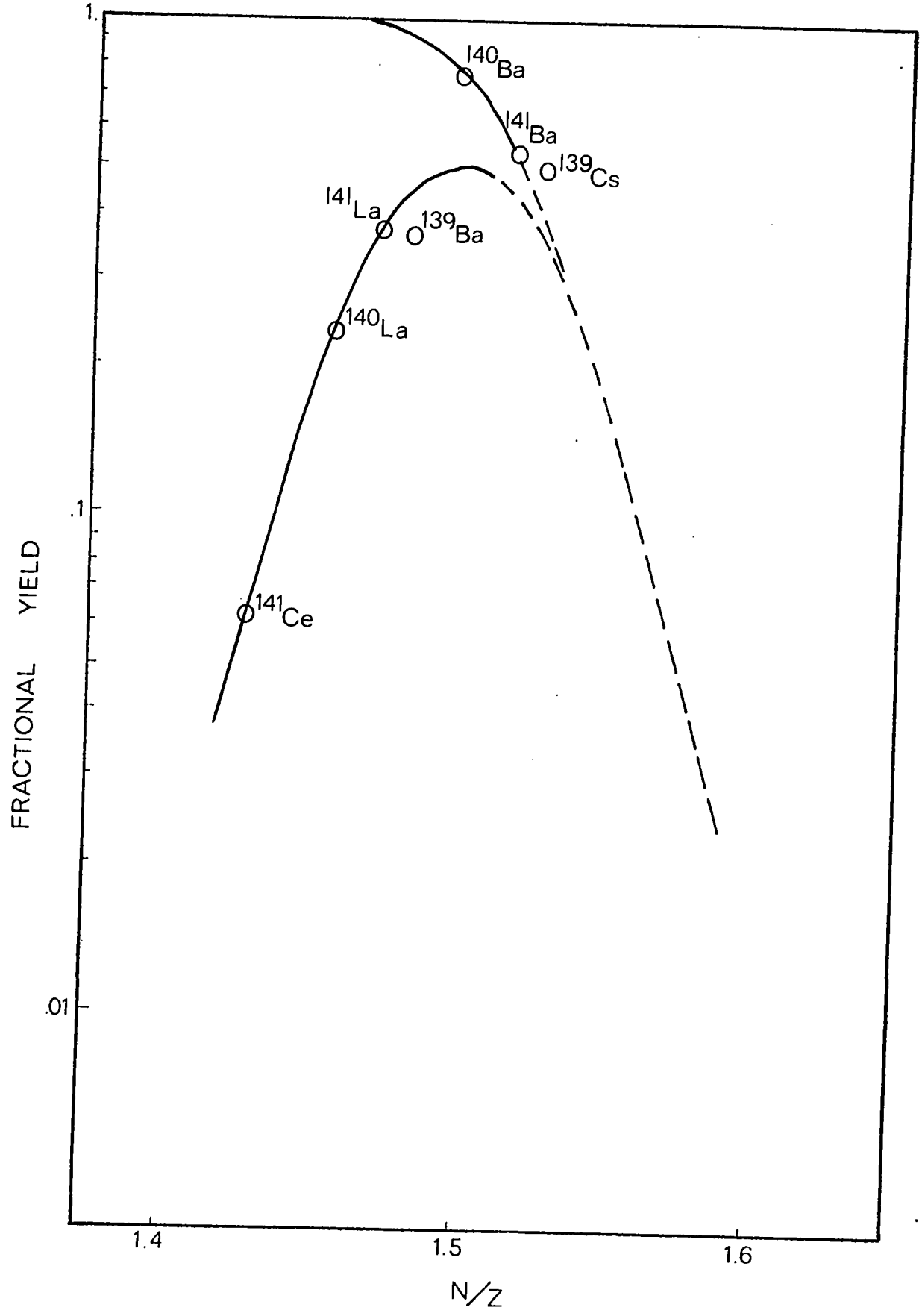
1.
.1
.01
FRACTIONAL YIELD
140Ba
141Ba
139Cs
141La
139Ba
140La
141Ce
1.4
1.5
1.6
N/Z

Figure 19

Charge dispersion curve at 68 MeV based on independent and cumulative yields

(The right hand side of the curve has been drawn so that the sums of the independent yields give the measured cumulative yields)

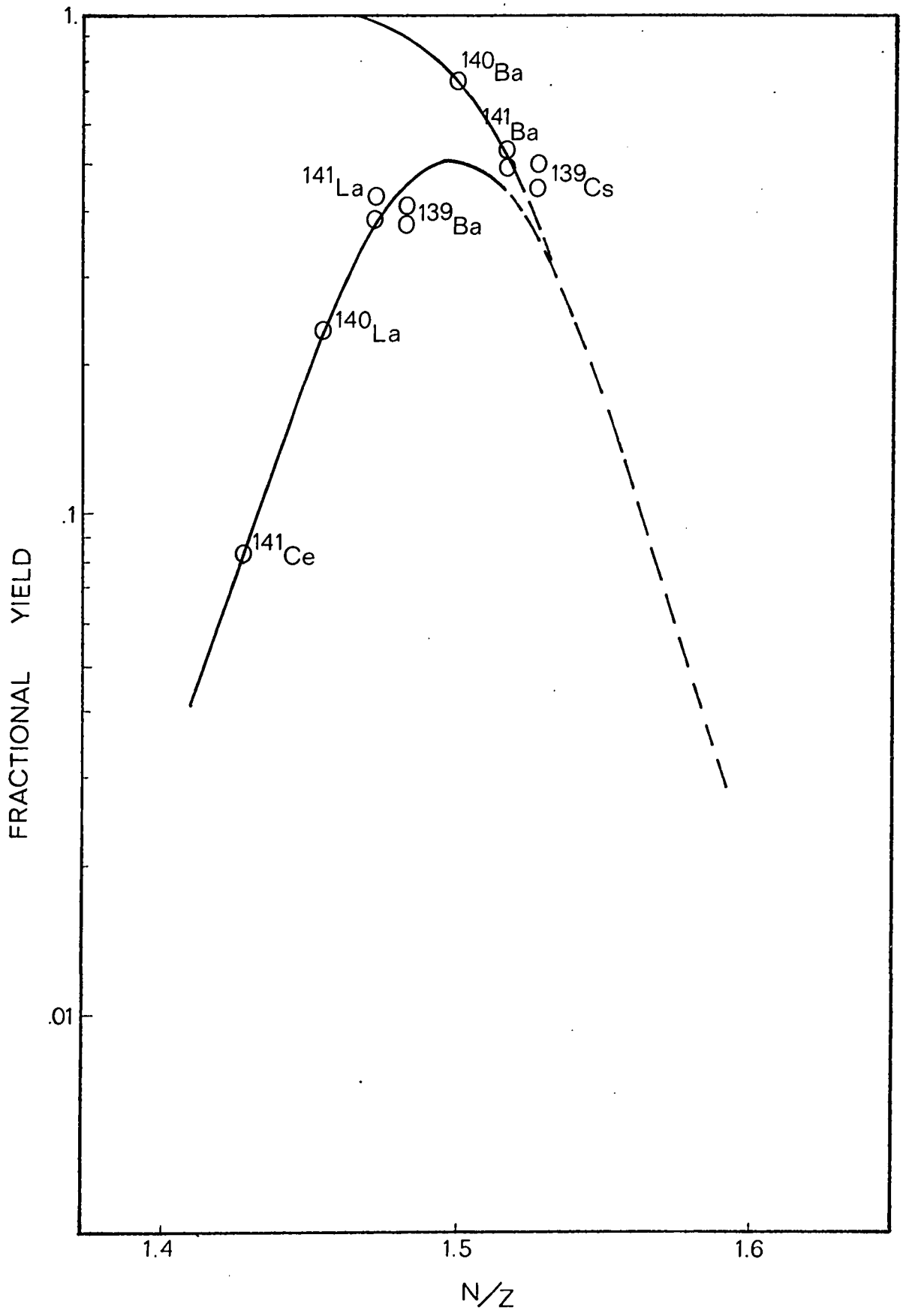
1.
.1
.01
FRACTIONAL YIELD
140Ba
141Ba
139Cs
141La
139Ba
140La
141Ce
1.4
1.5
1.6
N/Z

Figure 20

Charge dispersion curve at 75 MeV based on independent and cumulative yields

(The right hand side of the curve has been drawn so that the sums of the independent yields give the measured cumulative yields)

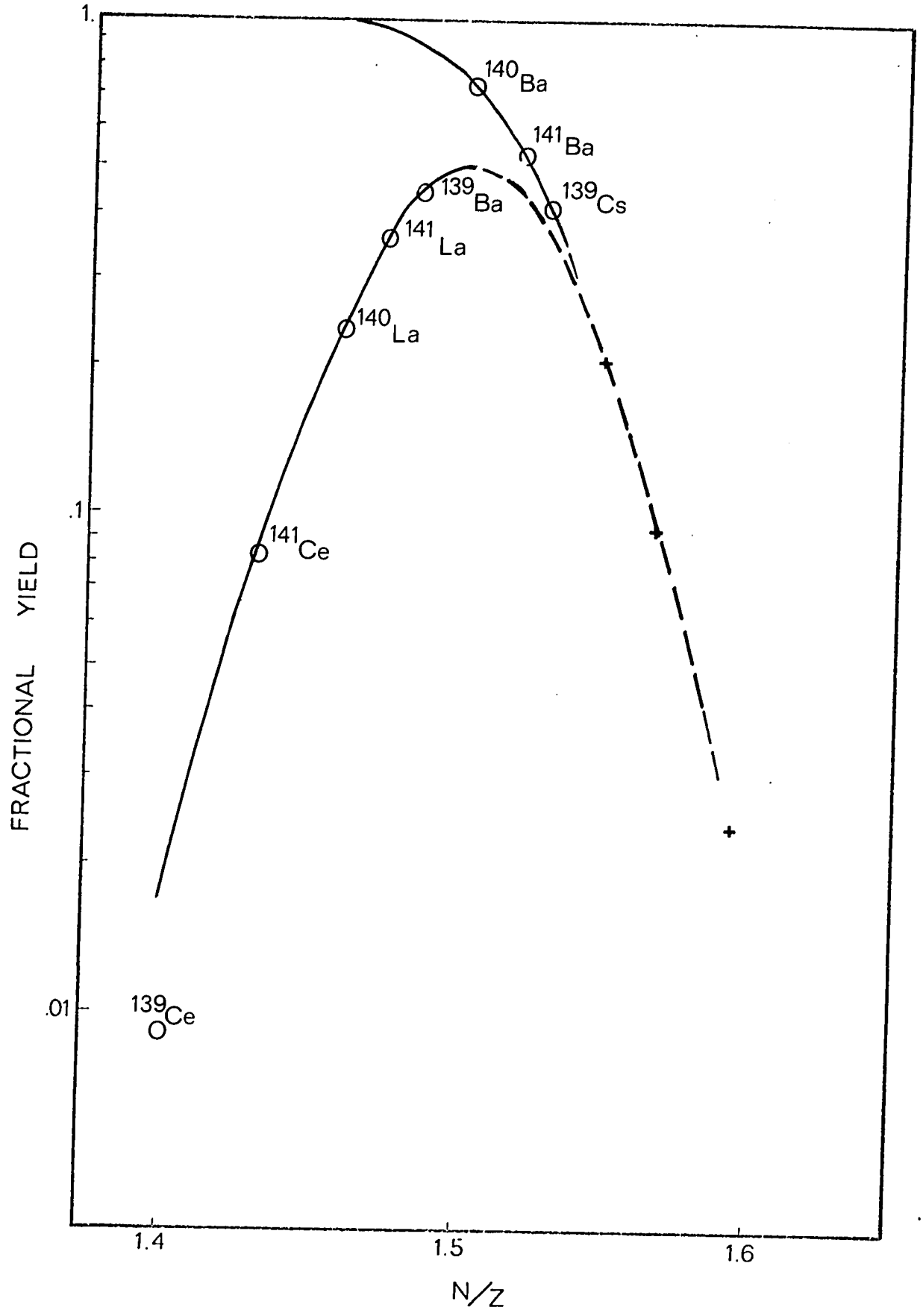
1.
.1
.01
FRACTIONAL YIELD
140Ba
141Ba
139Ba
139Cs
141La
140La
141Ce
139Ce
1.4
1.5
1.6
N/Z

Figure 21

Charge dispersion curve at 83 MeV based on independent and cumulative yields

(The right hand side of the curve has been drawn so that the sums of the independent yields give the measured cumulative yields)

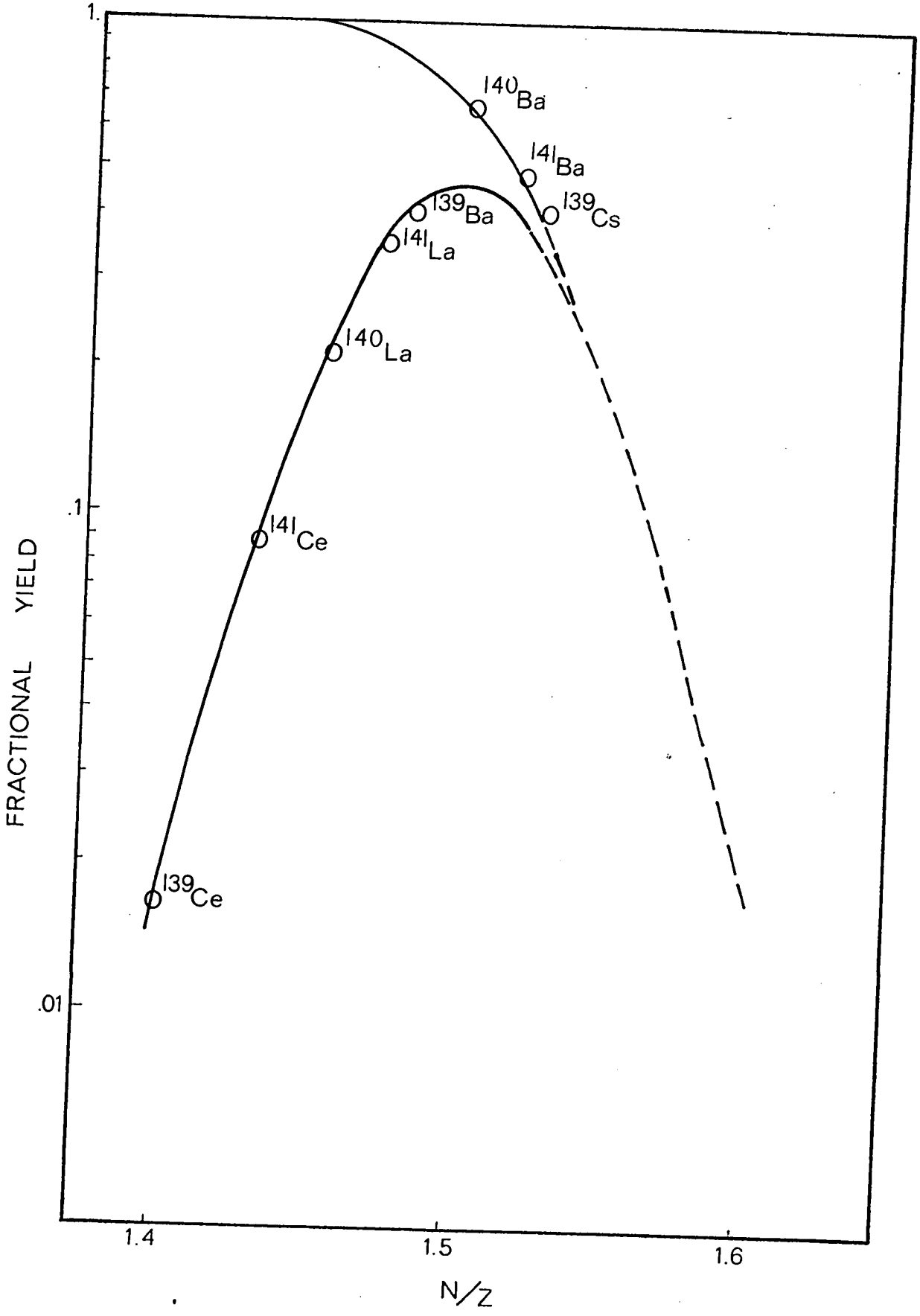
1.
.1
.01
FRACTIONAL YIELD
140Ba
141Ba
139Ba
139Cs
141La
140La
141Ce
139Ce
1.4
1.5
1.6
N/Z

TABLE 10

Parameters of Charge Dispersion Curves

in ^{232}Th Fission

E_p (MeV)	$Z_A - Z_p$	FWHM (Z units)
28	2.55	1.65
37	2.25	1.65
44	2.2	1.67
59	2.15	1.7
68	2.15	1.7
75	2.05	1.8
83	2.05	1.9

Figure 22

Displacement of most probable charge, Z_p towards beta stability, Z_A

o	this work
●	Pate et al.(31)
□	Forster et al.(65)
+	Benjamin et al.(64)

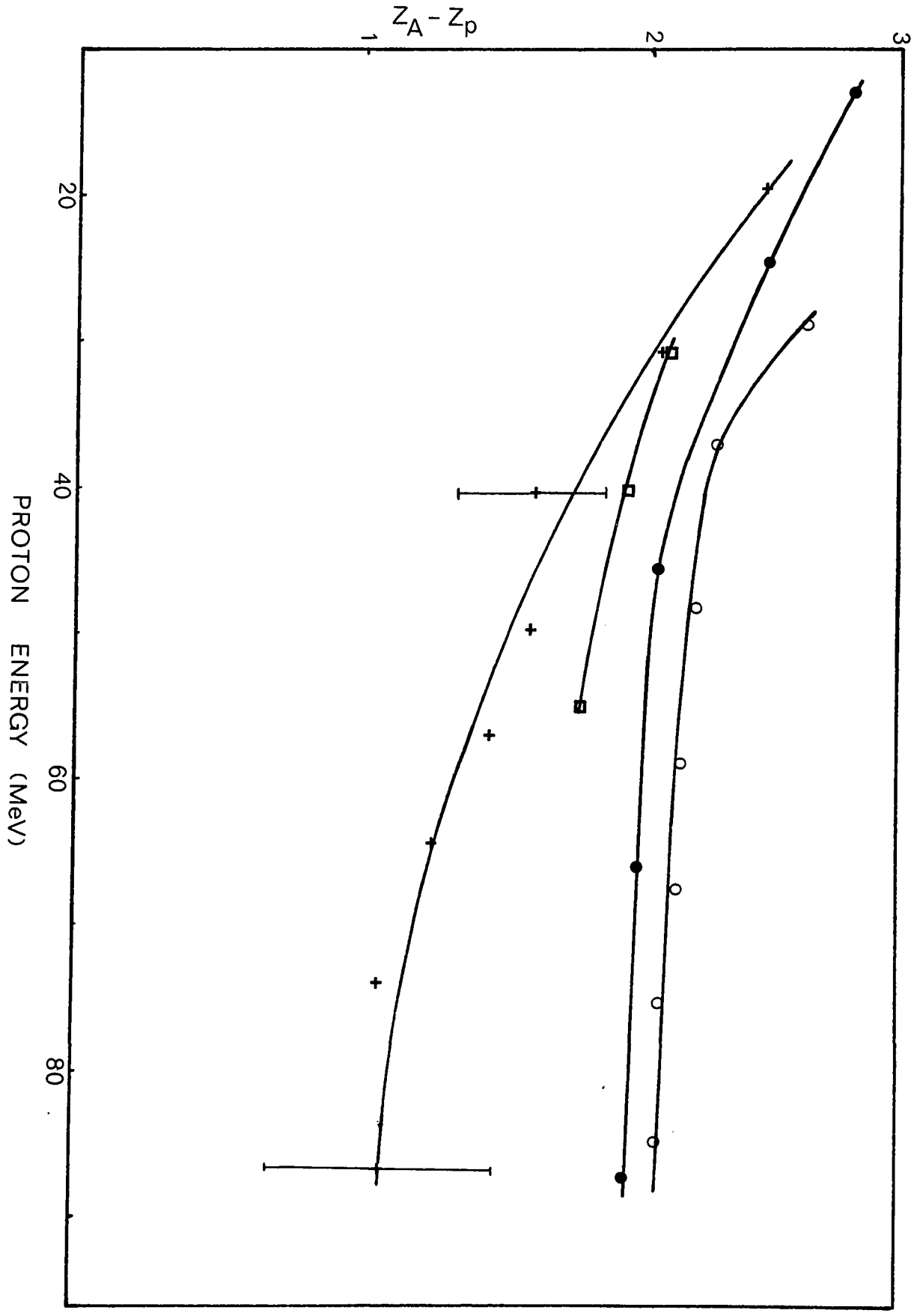
$Z_A - Z_p$
1
2
3
20
40
60
80
PROTON ENERGY (MeV)

Figure 23

Full-width at half-maximum

o this work

● Pate et al.(32)

▫ Forster et al.(65)

+ Benjamin et al.(64)

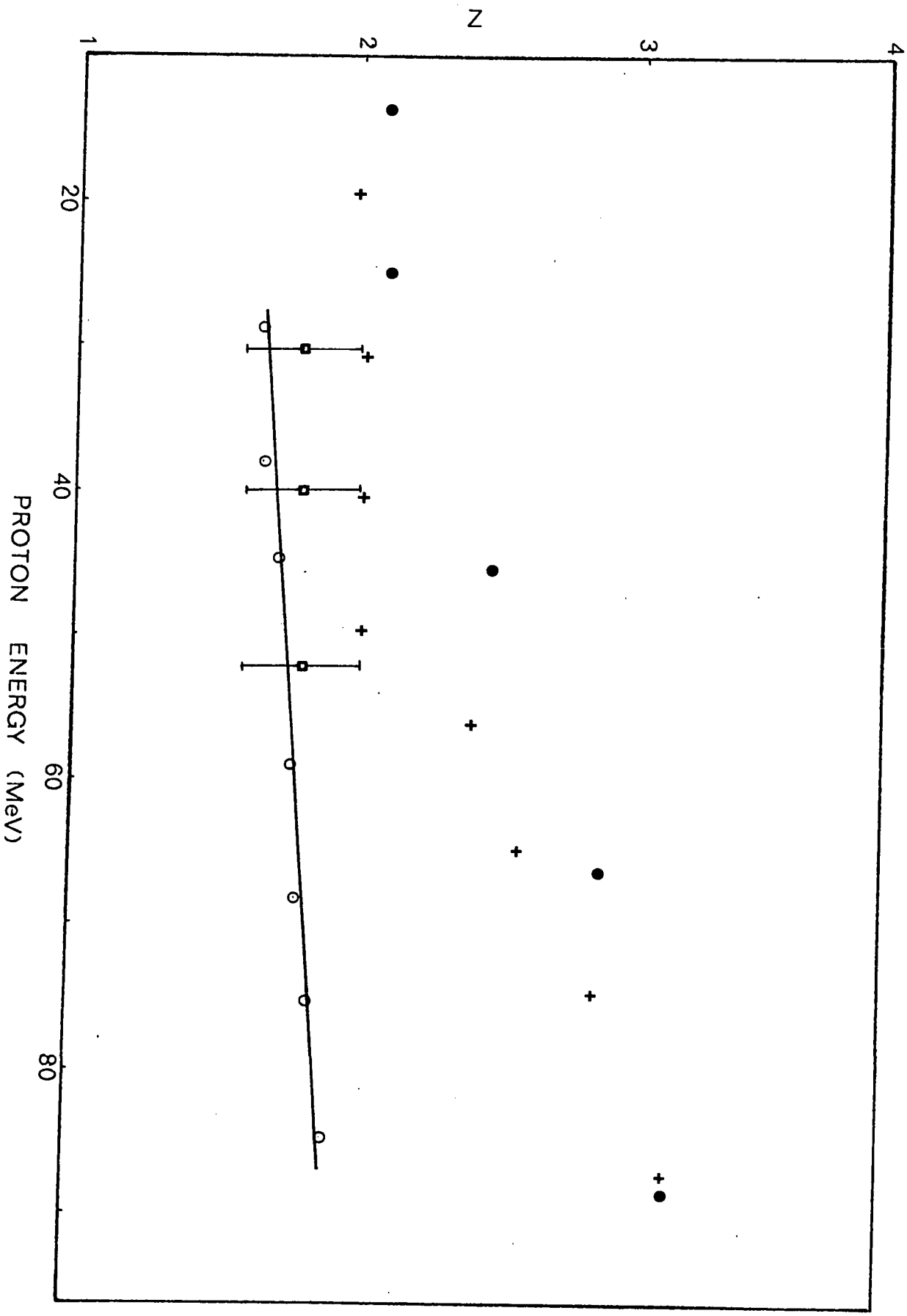
Z
1
2
3
4
20
40
60
80
PROTON ENERGY (MeV)

3. Comparisons with Other Workers' Data

Kjelberg et al. (66) measured ^{140}La in ^{232}Th proton fission in the same energy range as in this work and the agreement both for the independent fractional chain yield for ^{140}La and the cumulative fractional yield for ^{140}Ba is excellent - well within 10%, although different measurement techniques were used.

Croall & Cuninghame (20) give their results in percent yields and the curves in Figure 26 show the mass distribution before neutron emission from the fragments. It is not difficult using values for total fission cross section for ^{232}Th, as given by Pate et al. (32) and McCormick and Cohen (67), to obtain absolute values for the fragments. Croall & Cuninghame (20) report the way they determined the number of neutrons evaporated from the fragments (using the findings of Britt & Whetstone (29) on neutron evaporation) so that finally an approximate fission product mass distribution in absolute numbers can be inferred. With respect to the error quoted for the total ^{232}Th fission cross section (±15%), the agreement is good to within 25% if you compare this with data obtained in this work and by Benjamin et al. (64) The disagreement appears in the slope of the mass distributions. Croall & Cuninghame (20) report less of a slope in the heavy mass side of the mass distribution. The total mass chain yields inferred from charge dispersion curves and from ^{140}La and ^{141}Ce cumulative yields give a slope approximately twice as large. However, this discrepancy is not as serious as Figure 24 suggests. Croall & Cuninghame (20) were much more interested in overall tendencies of the mass distribution than in very accurate details.

Certain small deviations are observed in Figure 22 where

$Z_A - Z_p$, the distance of the most probable charge, Z_p, from the most stable charge for a given mass are given. Forster et al. (65) measured in all cases only one pair of isobars for masses 133 and 135 (obtaining one independent and one cumulative yield) and the value of Z_p depended on the choice of FWHM of Gaussian dispersion used for its determination. Forster does not give data for energies higher than 50 MeV. Benjamin et al. (64), as mentioned previously, quote for higher energies ($E > 50$ MeV) and uncertainty of 0.5 Z so that the deviations are not significant and there is no serious disagreement with their data. It would be helpful if the data of Benjamin et al.(64) were evaluated using Miller's (68) "CURFIT" FORTRAN programme together with more details concerning the N/Z (A) function for ^{232}Th so that more certain information be extracted from those data. It appears likely that for higher energies their values of FWHM will be slightly narrower and Z_ps slightly higher.

In conclusion it is stressed that agreement with the data of Pate et al. (32) is very good as shown in Figure 22.

D. Discussion

1. Introductory Remarks

As argued in the Introduction, nuclear matter, even at excitation energies of the order of 100 MeV with collective and single-particle excitations, is still an assembly of not more than 260 particles subject to an average potential, situation similar to that of the ground state. If one accepts the idea that the single-particle effects are responsible for the asymmetry at low energy fission, then it is natural to assume that the asymmetric portion of the mass distribution (asymmetric fission mode) at moderate energies is caused by the same single-particle effects.

Even at energies higher than 100 MeV where symmetric fission prevails, it has been observed (for instance by Karamian et al. (24)) that the widths of the mass distributions (which are symmetrical), of those nuclei fissioning asymmetrically at low energies, are much wider than those of nuclei that fission symmetrically only ($Z < 84$, as given on page 17). It does not seem unreasonable to assume that this may be some form - unknown yet - of the single-particle effects.

There is no doubt about the uniformizing effect of higher excitation energy. However, there seems to be no reason to expect that this uniformity effect can make, for instance, all higher energy fission distributions describable by just one set of parameters.

This work, along with others' in this laboratory, was undertaken to investigate further the overall trends in fission product formation at moderate bombarding energies and their dependence on the gross characteristics of the target. The data showed

the overall trends behaving in a predictable way (for instance the most probable charge, Z_p, shifts to less neutron-rich nuclides with increasing bombarding energy, the widths of the charge dispersions increase with energy, etc.), so that the basic characteristics were thus determined. Invariably, however, certain small deviations appeared - "fine structures". A comprehensive way of showing these is a graph, such as that first introduced by Friedlander et al.(30), where the proton bombarding energies at which the cross sections of the individual fission products reach their maxima, $E_p(max)$, are plotted against the neutron-to-proton ratio, of these fission products (Figure 14). Other such examples of fine structure may be seen in graphs showing the displacement of the most probable charge from that corresponding to stability, Z_A-Z_p as a function of the ratio of N/Z of the target, for various bombarding energies. One example is shown in Figure 15 in reference (33), for the mass region A = 130 - 140, where the curves deviate from the straight lines quite markedly.

It is very difficult to obtain reliable data on these "fine structures" because they are almost within the experimental error. However, because it is hoped that these might give essential information with respect to single-particle and/or shell effects (including the shell effects in the wider sense of Strutinski (9)) superimposed on the liquid-drop model features, the data collected in this laboratory for several years were investigated in this regard.

In the following discussion the changes of the most probable charge with mass and energy, $Z_p(A)$ and $Z_p(E)$, and of the curvatures of the curves as given on Figure 14, and their fine

structures, are explained using the above expressed ideas together with the notion of symmetric and asymmetric fission competition.

2. Dependence of E_p (max) on N/Z of the Fission Product for Various Targets

The kind of graph shown in Figure 14 is typical of the fine structure which occurs. If there were no fine structures e.g., neutrons would be evaporated in a regular manner depending only on excitation E*, carrying away B_n + 2T energy, where T = nuclear temperature and 2T = kinetic energy. In the energy region of this work this would be approximately 10 MeV. Also if all mass distributions of various fissioning nuclei were the same and kept the same shape with energy, these graphs would appear approximately as a set of parallel straight lines separated by distances depending only on N/Z of the target. Also, consequently, the excitation functions would have approximately the same shape. It is not easy to detect all the reasons leading to the observed variations from the regular pattern outlined above and thus the following argument is therefore going to be qualitative only and confined to our energy region. There is, however, one rather prominent reason, namely the differences in the mass distributions of the targets and their changes with energy. The wider the mass distribution (and the wider it becomes with increasing energy) the more excitation energy is needed in the fissioning act to evaporate one neutron for a particular nuclide because there are more channels available and the excitation energy per channel is correspondingly lower.

For instance it is not surprising that ^{238}U should have a slope in Figure 14 greater than for the other fissioning nuclei because the width of mass distribution as given by Stevenson

et al. (69) (approximately 23 mass units at the half maximum) is distinctly greater than for ^{232}Th at approximately the same excitation energies as given by Croall & Cuninghame (20) (approximately 15 to 18 mass units). So in the case of ^{238}U more excitation energy is needed to accommodate the wider distribution especially with increasing excitation energy - where the valley between the asymmetry peaks is being filled. Unfortunately not enough mass distributions are known in the cases of other targets and excitation energies. For thermal neutron and low-energy fission the full-widths at tenth-maximum were collected by Flynn et al. (70) and these show the same trend, i.e. ^{238}U has somewhat wider distribution than ^{232}Th and ^{233}U.

An equally powerful reason for the changes in Figure 14 is symmetric vs. asymmetric fission, i.e. at what energies symmetric fission sets in and what the shape of the mass distribution curve was. If, as in the case of ^{232}Th, the symmetric fission becomes prominent at energies about 45 MeV (see Figure 26) and few fissioning nuclei fission asymmetrically, the excitation functions as given in Figures 9 - 13 (for the heavy mass region and for the complementary light-mass region) fall off and consequently some peaks are located at lower excitation energies than they would if the mass distribution were widening more "regularly" and, for instance, filling the valley continuously as it is in the case of ^{238}U where the symmetric fission plays a much smaller role. Another consequence of the symmetric vs. asymmetric fission competition in a region where symmetric fission prevails, for instance at energies above 45 MeV in the case of ^{232}Th, is that the excitation functions at energies more than 50 MeV may receive contributions from symmetric fission. The peaks in excitation functions corresponding

to contributions from symmetric fission should occur at higher bombarding energies than those coming from the "regular" situation. In other words the curves in Figure 14 should have small slopes first - with respect to ^{238}U for instance - and at higher energies they should turn up and have a relatively higher slope as is indeed the case with ^{232}Th. For ^{233}U there are no direct data. However, Colby & Cobble (71) claim to have observed, for moderate energy fission ^{233}U (α, f) the characteristic three-humped mass distribution resembling ^{232}Th in Figure 26, so that a similar distribution may occur in proton fission. In any case, the curve in Figure 14 for ^{233}U has a similar trend as that for ^{232}Th, even more curved. ^{235}U shows the same trend, if somewhat less pronounced than that for ^{233}U. ^{239}Pu shows no curvature and upward trend which should indicate very little symmetric fission at these excitation energies and the mass distribution broadens with less speed than that of ^{238}U.

The trends outlined above may reflect the observed tendency for elements of lower neutron number N to fission symmetrically more readily than the elements of the same proton number Z but of higher N. The elements of interest are given in the following Table 11.

TABLE 11

VARIOUS PARAMETERS OF SOME FISSIONING NUCLEI

	Z^2/A	N	Z	A
$^{239}Pu + p$	38.817	145	95	240
$^{238}U + p$	35.81	146	93	239
$^{235}U + p$	36.65	143	93	236
$^{233}U + p$	36.87	141	93	234
$^{232}Th + p$	36.48	142	91	233
$^{237}Np + p$	37.12	144	94	238
$^{232}U + \alpha$	37.28	143	94	237
$^{226}Ra + p$	34.89	138	89	227

The last two fissioning nuclei are those which fission symmetrically at energies as low as 25 MeV and at 13 MeV respectively as reported by Colby & Cobble (71) and Konecny and Schmitt (25).

From Figure 14 and the table above the following may be concluded about the relationship between (E_p) max and N/Z of the fission product:

1. The upward trend shown by some target elements indicates symmetric fission as an important ingredient. This agrees with the observations by Myers & Swiatecki (15) that the ground-state deformation in the heavy-mass region is anomalous and possibly affected more by neutron number and with the observation of Jensen and Fairhall (22) that the tendency to symmetric fission decreases with increasing deformation. It is possible to write for the tendency to symmetric fission (taking the following fissioning nuclei):

$$^{227}Ac > \underbrace{^{234}Np}_{(^{233}U)} > \underbrace{^{233}Pa}_{(^{232}Th)} > \underbrace{^{236}Np}_{(^{235}U)} > ^{237}Pu > ^{240}Am > ^{239}Np$$

One can readily see that indeed the upward trend in Figure 14 has the same order as the underlined isotopes. It is also conceivable that ^{239}Pu and ^{238}U do not have the symmetric peaks growing in at these energies. It is also worth noting that the Z^2/A parameter does not seem to play any significant role.

2. A higher slope corresponds to a broader and also possibly a mass distribution becoming broader more quickly with excitation energy (the valley between the peaks may be being filled from the sides as well as from the middle).

3. Khan et al. (58) found that $(Z_A - Z_p)$ varied with bombarding energy for A $\approx$ 96, in a manner very different from that found by others for A $\approx$ 140 (33). They found that the fission products from ^{235}U acted in a manner indistinguishable from ^{238}U, contrary to the observations of Yaffe (33) for A $\approx$ 140. However the light and heavy peak isotopes would not be expected to fall on the same curve because of the differences in B_n for complementary fragments and because of the irregularities in the mass and proton and neutron distributions with energy. Also if the fragments divide according to the Minimum Potential Energy (MPE), then the light and heavy peaks in the mass distribution have no reason to meet on the same curve. However, as will be dealt with later, even falling on the same curve does not have to mean that the "sudden rupture hypothesis" (sometimes identified with the UCD hypothesis) holds good.

Some of the conclusions are also shown on Figure 14.

According to the ideas presented here the products from $^{237}Np(p, f)$ fission should give a straight line - the intermediate situation between ^{235}U and ^{239}Pu. ^{252}Cf should give a straight line with a slope greater than ^{238}U because it is asymmetrical and

of larger width in thermal fission.

3. Excitation Functions

The excitation functions are given in Figures 9 to 13. The shapes differ substantially from "regular" shapes in the sense introduced in the previous section. They reach maxima "too early" and the cross sections decrease with the onset of the symmetric fission. As mentioned earlier this is in good agreement with the mass distributions as given in Figure 26 where at energies above 45 MeV symmetric fission prevails. On the other hand independent yield of ^{141}Ce as shown in Figure 11 does not show any increase with energy to indicate a peak at 100 MeV if it conformed to the "regular" fashion. Presumably the peak will come at higher energies as the symmetric fission mass distribution widens enough. There is also a possibility that the excitation function will show a broad and rather small peak because the symmetric fission contribution will not be able to offset the low-deposition energy fission which is always present at higher energies.

In the case of the excitation function for independently-formed ^{143}Ce as shown in Figure 12 it is hard to determine any peak. If the peak as suggested on the Figure 12 is plotted in Figure 14 it falls in the expected place with respect to the other peaks.

In the case of ^{140}La and ^{141}La there is no doubt about the location of the peaks, (Figures 10, 11) so that the maximum E_p energy, $E_p(max)$, is determined reliably. This is reasonably correct for the ^{139}Ba peak also.

4. Variation of the Distance of the Most Probable Charge Z_p as a Function of Bombarding Energy

All the pertinent data are given in Figure 25 together with data by Benjamin et al. (64), Forster et al. (65) and Pate

et al. (32). As discussed briefly previously one can see that the agreement with Pate's (32) data is very good; the disagreement with Forster's (65) may be due to the fact that he investigated only two isotopes of masses 133 and 135 and Benjamin's (64) error bars cover the range observed in this work. It should be remembered that the introduction of the Z_A concept introduces shell effects. These are not believed to play a large role in higher energy fission and thus will not be reflected in the Z_p values.

The behaviour observed in this work is again in complete agreement with that found by Croall & Cuninghame (20) Figure 26. When a bombarding energy about 45 MeV is reached the symmetric fission prevails to such a degree that the contributions for the heavy mass peak are minor and consequently the most probable charge Z_p does not change appreciably. The charge dispersion determining Z_p comes mostly from low-deposition energy fission.

The relatively steep beginning up to the energy of 40 MeV might reflect the relative narrowness of the mass distribution and also perhaps low values of neutron binding energies. Any further conclusions would be too speculative because the dependence of fragment neutron evaporation on mass, $\nu(A)$, is not known in sufficient detail, as well as the changes of Z_p, N_p, and widths in charge and neutron distributions with energy. It is not easy to understand the fact that up to 40 MeV bombarding energy the beginnings of the $Z_A - Z_p$ (E) curves for Cs isotopes are the same for all nuclei observed in this laboratory, as shown in Yaffe's paper (33).

5. Charge Dispersion

Charge dispersion is defined by Friedlander et al (30) as changes in formation cross section at a given bombarding energy along an isobaric chain. However one must examine the relation to plots where, instead of Z units along the ordinate, the corresponding N/Z values are plotted. This way of plotting obviously enables one to plot yields from several isobaric chains on one graph. However, there are two assumptions implicitly made:

1. The mass region in question is flat.

2. The N/Z_p ratio ("p" in all cases stands for "most probable") does not change appreciably with the mass of the products.

The correction for the first case is easy to make by taking the fractional chain yields (if known) instead of cross sections. This has been done in this work. For the second the $N/Z_p(A)$ function must be known. To obtain Z_p in a certain mass region most reliably would be to investigate isobars only, however, in most cases $Z_p(A)$ has been determined on the basis of the isotopic charge distributions. Since the value of each of the Z_ps was determined on the basis of one or two isotopic yields closest to the Z_p value (not integer) and not on extrapolations from isotopes of several mass units differing in mass, the determined Z_p values, as will become apparent in the following pages, are within the experimental error. The only quantity which is not negligibly affected by any possible N/Z_p changes with A is the full-width at half-maximum, FWHM. It has been reported by Hogan & Sugarman (35) and partly also by Panontin et al. (34) that corrections have been applied in several cases on FWHM determined from isotopic charge

distribution curves and a good agreement is reported with values determined from isobaric charge dispersion curves (in the heavy-mass region).

It is essential in performing the correction, of course, to have a reliable $N/Z_p(A)$ function. Fortunately, with the accumulation of data from this laboratory it is possible to draw these curves for ^{238}U and partially for ^{232}Th in moderate energy proton fission. (if it is necessary to make interpolations then the N/Z_p functions for all other targets can be inferred from the ^{238}U curve). The functions are given in Figure 24, together with N/Z_As ($Z_{A_{Cor.}}$, as given by Coryell (19) and $Z_{A_{Green}}$ as given by Green (72), the most stable charge for a given mass) and for thermal neutron fission of ^{235}U, as well as for fission of ^{238}U by protons of 150 MeV energy using values given by Coryell et al.(73) and Pappas & Hagebo, (74) respectively. Several features are apparent. The value of N/Z_p is changing considerably with A and with the increasing energy the left and right wings tend to level off, as observed by Pappas & Hagebo (74) and in this work (combined with the data of Benjamin et al. (64) and Pate et al. (32)).

Since with the knowledge of the relations as given in Figure 24 it becomes unjustifiable not to use the corrections, the main rules for applying the corrections for the isotopically observed charge dispersions plotted in N/Z type graphs are set forth below:

1. One isotope is chosen as a reference point (naturally that closest to Z_p for a given mass A.)

2. Values of $N/Z_p(A=\pm1,\pm2,..) - N/Z_p(A)$ are read off the proper curve on Figure 25, (corresponding to the given target and bombarding energy).

Figure 24

Variation of the ratio of the neutron number to the most probable charge, N/Z_p, with mass number A for various energies and targets

Also variation of the ratio of the neutron number to the most stable charge, N/Z_A with A.

—·—··—···—·— ^{235}U (n_{th}, f) Coryell et al. (73)

— — — — — — ^{238}U (p, f) 170 MeV bombarding energy, Pappas & Hagebo (74)

o ^{232}Th (p, f) Pate et al. (32)

\+ ^{232}Th (p, f) Benjamin et al. (64)

□ this work (all bombarding energies for ^{232}Th are 28 MeV and 83 MeV)

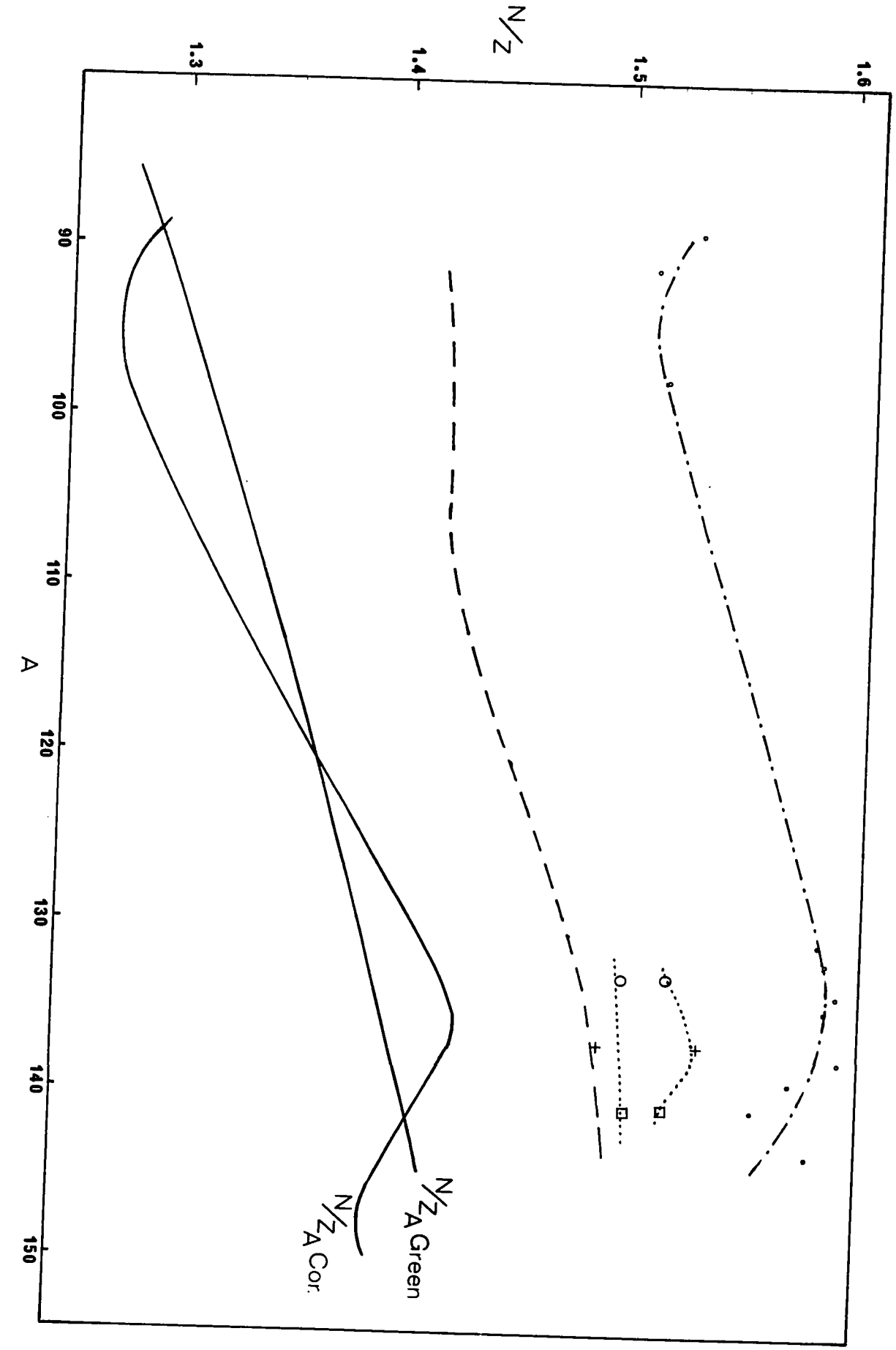
N/Z
1.3
1.4
1.5
1.6
A
90
100
110
120
130
140
150
N/Z A Green
N/Z A Cor.

Figure 25

Detail of Figure 24 in the heavy mass region

o	^{232}Th (p, f)	Pate et al. (32)
■	^{232}Th (p, f)	Forster et al. (65)
+	^{232}Th (p, f)	Benjamin et al. (64)
□	this work	

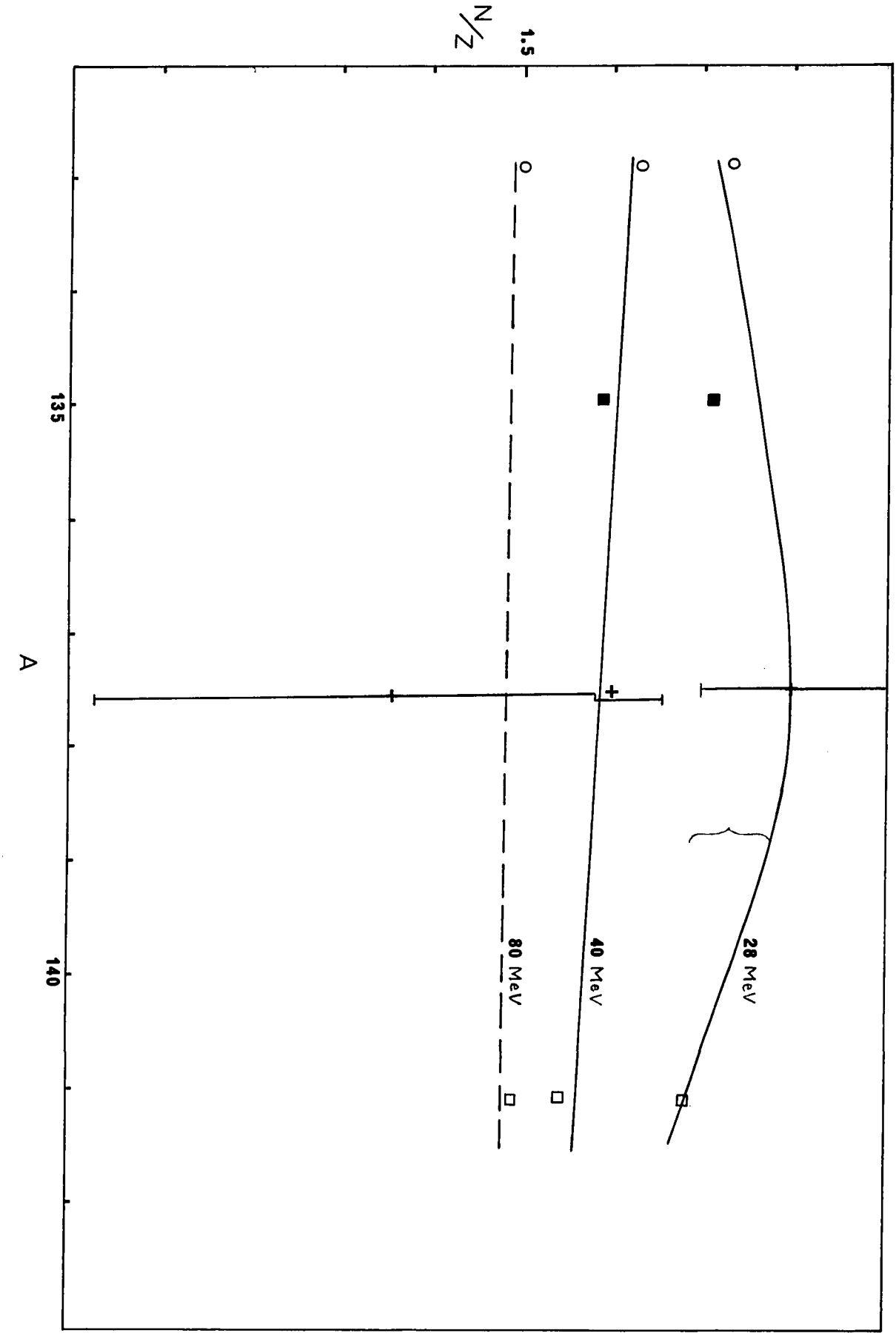
N/Z
1.5
135
140
A
28 MeV
40 MeV
80 MeV

3. If $\frac{d(N/Z_p)}{dA} > 0$, the values read off for isotopes $A < A_{chosen}$ are added to the N/Z values corresponding to the given isotopes. For $A > A_{chosen}$ they are subtracted so that the overall effect on the charge dispersion curve will be to narrow it with respect to that without the correction. A typical example is the charge dispersion of cesium isotopes. ^{136}Cs may be chosen as the reference point (i.e. its N/Z value will not be subject to any addition or subtraction) of N/Z = 1.4727. The value read off (as in point 2 above) for the ^{130}Cs, for example, would typically be .02. This value then is added to ^{130}Cs N/Z = 1.3636 and the measured cross section is plotted against the new value $(N/Z)_{corr}$ = 1.3836.

The same is done for all the measured isotopes of cesium. For those which have a mass higher than 136, the values read off are subtracted. The difference in FWHM, for the isotopic charge dispersions spanning more than 11 mass units,(like, for instance ^{125}Cs to ^{136}Cs in Friedlander et al. (30)), can be up to 20%.

If $\frac{d(N/Z_p)}{dA} < 0$ the same procedure is followed except that the corrections are subtracted instead of added. The overall effect now is to widen the charge dispersion curve. However, as shown in Figure 24, the slope is negative only at low energies and in a narrow region past the closed shell. The detailed figure depicting this situation for ^{232}Th is given in Figure 25, from which it is obvious that only at a bombarding energy of 28 MeV need the correction be made (it is rather small, equal to .003 N/Z only, since the change in the $N/Z_p(A)$ function of mass A = 141 and A = 139 is very small) and at all other bombarding energies the N/Z_p function can be considered constant with mass (especially

with respect to the error of 0.5 Z units quoted by Benjamin et al. (64)).

It should be added that if the charge dispersion curves are constructed in the usual way, i.e. to make the neutron-excessive portion of the charge dispersion curves fit to the observed cumulative yields, the corrective values read off as given under point 2 are related to one particular mass only and the correction is therefore constant for the whole isobaric chain leading to the observed cumulative yield (the $N/Z_p(A)$ value for given mass is constant).

In the case of this work there were no problems with the FWHM determination because the charge dispersion was measured basically isobarically and the mass range was relatively narrow. (The only exception is the case of ^{139}Cs and ^{139}Ba at a bombarding energy of 28 MeV. The correction, equal to .006 N/Z units, is shown in Figure 25). It is very likely that the N/Z_p function for thorium resembles that of ^{238}U in region A = 130 to A = 138 and that corrections applied to the curves of Benjamin et al. (64) would narrow their widths, especially at higher energies. However with respect to Benjamin's quoted errors the corrected values appear to lie within the experimental error. In other words there is no essential disagreement in the FWHMs determined by Benjamin et al. (64) and those determined in this work.

The construction of charge dispersion curves as given in Figures 15 - 21 had to be done using fractional chain yields because, as Figures 6 - 9 show, the mass distribution was not flat. This is also reported by Croall & Cuninghame (20) who investigated the mass distribution in ^{232}Th fission with protons of energy from 13 to 53 MeV. Their mass distribution curves are given in

Figure 26. One can see that at energies around 45 MeV symmetric fission prevails. More will be said about this later. If one plots the fractional chain yields (independent and cumulative), one is dividing one inaccurate number by another one (by the total mass yield). On the other hand, since the total mass yield as well as the individual independent and cumulative yields are in most cases measured by means of the same γ-ray peak of the same isotope, some errors cancel out. This was the case in this work for masses 140 and 141 where it is safe to assume the cumulative yields of ^{141}Ce and ^{140}La represent the total chain yields. (The same was true in the work on ^{140}La by Kjelberg et al. (66)). In any case the charge dispersion curves themselves support this view. For mass 139 it cannot be safely assumed that the cumulative yield of ^{139}Ba represents the total mass 139 yield and more or less accurate extrapolations had to be made (based on the charge dispersion curves as given in Figures 15 - 21). These are given in Tables 6 to 9 where all the measured yields are given. The same holds true for mass 143 with the additional fact that the experimental error was higher due to errors in the determination of the time of separation.

The mass distribution of Croall & Cuninghame (20) could not be used for mass yield determination because the curves were determined using rather crude physical methods and the agreement between the present results and theirs is only approximate and depends on the values used for total fission cross sections.

One more reason for not trying to apply the charge dispersion corrections and perform the extrapolations for determining the total mass yield of A = 139 was the finding of Runnals et al (75) and Wahl (31) about even-odd effects on charge dispersion.

This was not included in this work so that any effort to improve the accuracy beyond a certain limit would have been meaningless.

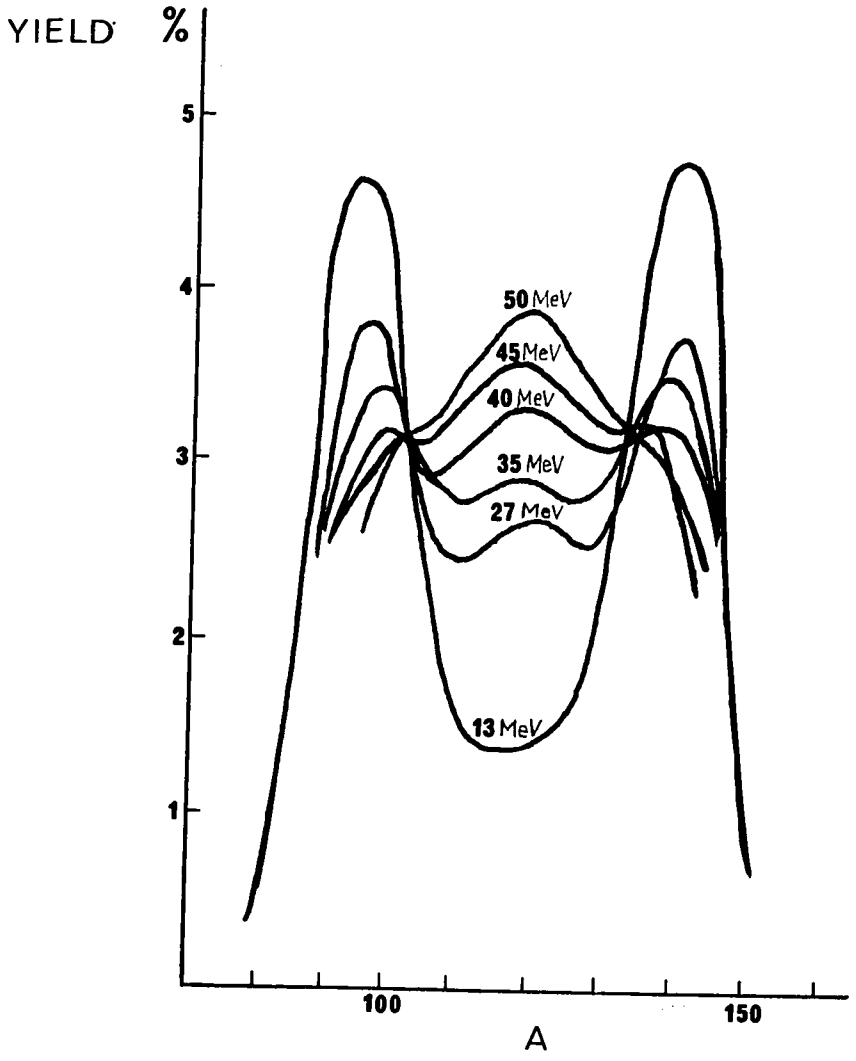

Figure 26

taken from Croall & Cuninghame (20)

After dealing with the problem of corrections for variations of N/Z_p it is still necessary to investigate the effect of energy dependence on the full-width at half-maximum and the shape of the charge dispersion curves.

It may be useful to introduce the notion of "elementary charge dispersion" as that resulting from fission of only one kind of fissioning nucleus, as distinct from that arising from the fission, in competitive manner of a variety of nuclei. Under the former characterization would fall all spontaneous, thermal neutron, and generally low-energy fission (as long as the excitation energy is not sufficient to cause fission after one neutron is evaporated, i.e. second-chance fission). It has been observed in this case that the FWHM is fairly constant for most fissioning nuclei and equals approximately 1.6 Z units (Wahl (76)). This charge dispersion is believed to be preceded by the fragment charge dispersion which is narrower (Glendenin et al. (51) report a FWHM of 1.2 Z units) - the widening is believed to be due to Maxwellian distribution of the neutrons evaporated from the excited fragments. It is also necessary to keep in mind that certain even-odd effects are believed to be responsible for the final charge dispersion (Wahl (31)). Obviously, the broadening of the elementary fragment charge dispersion with the fragment excitation energy occurs, due to the statistical nature of the process of evaporation. However, since these considerations are only qualitative, they will not further be taken into account.

If at moderate energies multichance fission occurs, then it is possible to assume that the resulting charge dispersion is a sum of the elementary charge dispersions. A special case would be the situation described by Friedlander et al. (30) at very high energy fission (0.1 to 6.2 GeV proton bombarding energy) where the charge dispersion is essentially a superposition of low-deposition-energy fission (asymmetric fission) and of high-deposition-energy fission (symmetric fission), namely of their corresponding charge

dispersions. This situation applies only in cases where the fissioning nuclei of wide energy spectrum contribute to the particular region of products. It does not hold, for instance, in the case of ^{197}Au (^{12}C, f) as observed by Blann (23), where low-energy fission does not contribute at all because the fission barrier B_f is high and allows only high-energy fission. In the case described by Blann (23) the charge dispersion width is basically the same as the elementary one.

The elementary charge dispersion can be expressed by

$$\sigma(Z) = \frac{1}{(C\pi)^{\frac{1}{2}}} \ell^{-\frac{(Z-Z_p)^2}{C}} \tag{31}$$

where C is a constant determining the FWHM, C = .92 and Z_p is the most probable charge corresponding to a continuous fractional yield charge dispersion. If more fissioning nuclei of differing compositions and excitation energies are present the resulting charge dispersion can be written as

$$\sigma(Z) = \frac{1}{k(C\pi)^{\frac{1}{2}}} \int_{Z_{p_1}}^{Z_{p_2}} \ell^{-\frac{(Z-Z_p)^2}{C}} \cdot w(Z_p) \cdot dZ_p \tag{32}$$

where k is some normalization constant, Z_{p_1} and Z_{p_2} are charges corresponding to the most probable charges of the lowest and the highest elementary charge dispersions, and $w(Z_p)$ is the weighting factor which includes all irregularities in contributions from various elementary charge dispersions present.

Even though the weighting factor $w(Z_p)$ plays an important role in determining the charge dispersion, it is very difficult to obtain any reliable information concerning this factor. Undoubtedly there are many sources contributing to the value of $w(Z_p)$ of which the most prominent are listed below:

1. The shape of the cascade nuclei excitation energy spectrum generated by the impinging particles. In the energy region in

this work the compound nucleus is formed in most cases.

2. Subsequent competition between fission and neutron evaporation, Γ_n/Γ_f, as given by equation (16). As mentioned previously this ratio is very sensitive to the quantity $B_n - B_f$ where B_n and B_f are the binding energy of the neutron and the fission barrier respectively. This is especially true at low excitation energies, since the neutron binding energy and fission barrier are known only approximately; no conclusion can be made as to the distribution of fissioning nuclei. In the most recent work by Cheifetz et al. (38) it is argued that no combination of parameters as shown in equation (16) gives a satisfactory agreement with the experiment.

3. Symmetric fission vs. asymmetric fission effects, in the sense of the previous sections (in the heavy mass region, for instance, at the energies above 45 MeV there are negligible high-energy contributions).

Without dwelling further on this subject and in the light of this qualitative argument the weighting factor $w(Z_p)$ was set equal to unity.

The question now arises: can anything be inferred about the nature of the contributing elementary charge dispersions from the observed charge dispersions? Can the surprising finding that the widths are relatively narrow up to the excitation energies of 40 - 70 MeV be made more plausible?

An attempt was made to reconstruct the observed charge dispersions by means of equation (31). The approximate values of the integrals according to equation (32) with varying limits were evaluated using probability graph paper where the curves expressing

Figure 27

Area of the Gaussian curve of
$C = 0.92$ ($\sigma = 0.62$)

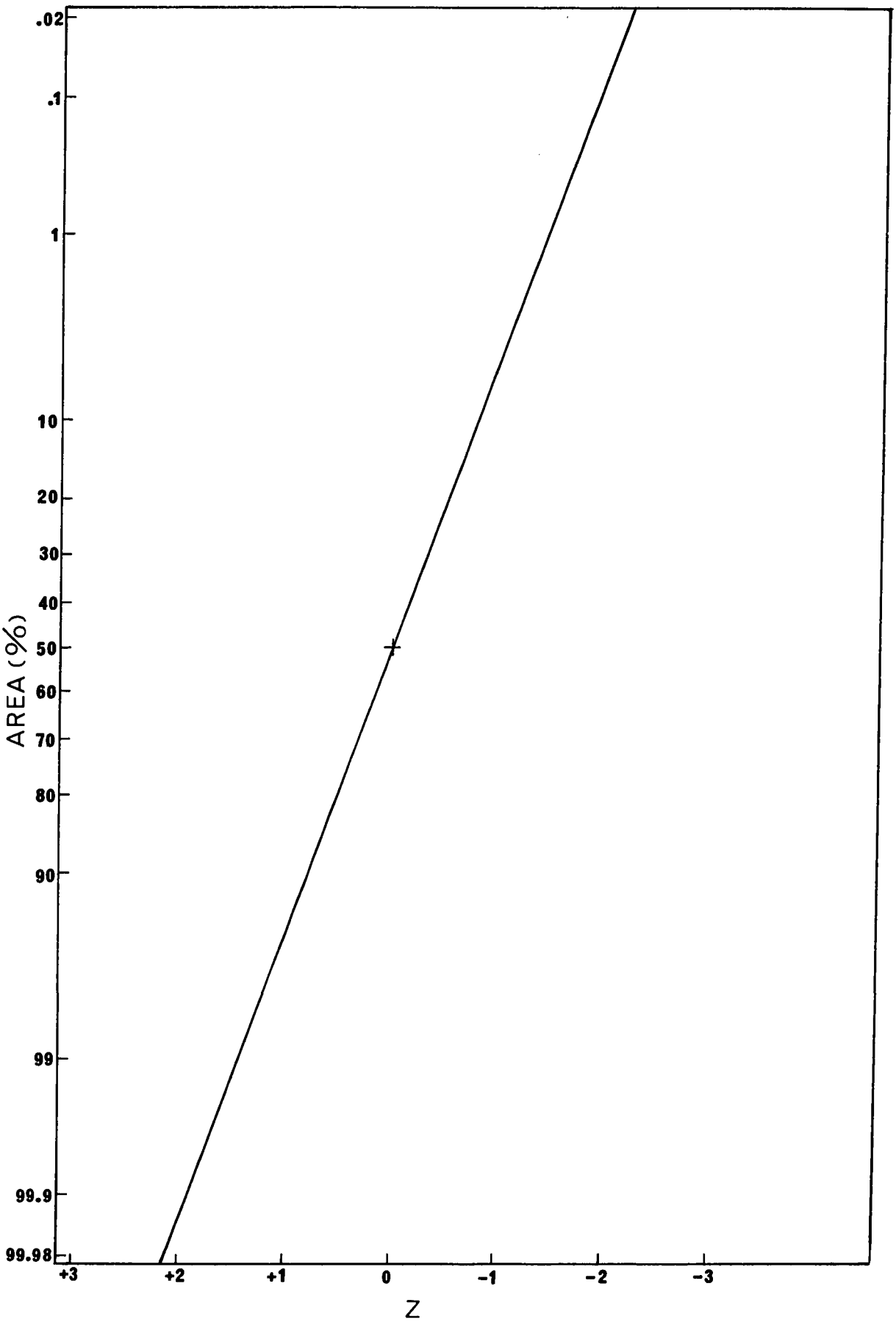
.02
.1
1
10
20
30
40
50
60
70
80
90
99
99.9
99.98
AREA (%)
+3
+2
+1
0
-1
-2
-3
Z

the cumulative Gaussian distribution form straight lines of a slope corresponding to a given width parameter σ . When the cross section from equation (31) was plotted for various ranges of integration as shown in Figure 27, it was found:

1. For the ranges smaller than unity, $Z_{p_1} - Z_{p_2} < 1$, the integrated curves gave approximately the elementary charge dispersion, i.e. the width was unchanged.
2. For the ranges of integration larger than unity, $Z_{p_1} - Z_{p_2} > 1$, the obtained integrated curves reproduced the observed full-width at half-maximum if the range of integration equalled the observed FWHM.

The finding in No. 1 could partially account for the fact that the FWHMs in this work, as well as those given by McHugh & Michel (21) for ^{232}Th (α , f) and ^{238}U (α , f) at the excitation energies of 40 MeV, are so narrow, or in other words, why there one finds practically the elementary charge dispersion widths even though multichance fission occurs.

Finding No. 2 concerns the observed widths from high-energy fission. At high-energy fission the situation is even more complex and the gross simplifications of this argument might be even more inadequate. However, a notion presented by Hogan & Sugarman (35) and Sugarman et al. (77) that along an isobaric charge dispersion each consecutive element of higher Z comes from more excited fissioning nuclei may not hold in the following cases:

1. If the given mass (isobaric chain) is composed of two distinct components from low- and high-energy fission, the former coming from low-energy deposition asymmetric fission, the higher from highly excited fissioning nuclei (the case described by Friedlander et al. (30) as mentioned earlier).

2. If the weighting function $w(Z_p)$ is not some sort of Gaussian curve (i.e. approaching zero very quickly in the limits Z_{p_1} and Z_{p_2} of the integration) then it is not possible to reconstruct the observed Gaussian charge dispersion curve using the above approach. The range of integration must be made narrower, i.e. closer to the observed FWHM. In other words it is possible that two neighboring isobars can arise from the same kind of fissioning nuclei.

The purpose of this lengthy section (and of the previous one too) was to reconcile the findings of this work in the values of FWHMs and $Z_p(E)$ with the works of other workers from this laboratory and also with the interpretations of Hogan & Sugarman (35) with respect to the origins of the individual members in the charge dispersion curves. Another purpose was to try to get a better understanding of the variety of experimental facts in charge dispersion at moderate energies now being accumulated.

6. Interpretation of the Data in a Wider Context

6a. Estimate of the Energies Involved

The belief of many theoreticians that fission can be described by liquid-drop model potential surfaces and liquid-drop dynamics perturbed by single-particle effects is illustrated best in Figure 28 (taken from Vandenbosch (16)) and in Figures 29a, 29b, 29c (taken from Hyde (5)).

In Figure 28 it can be seen that the fission barrier, B_f, is the difference between two large quantities, $E_{surface}$ and $E_{Coulomb}$. Figures 29 give the detailed pictures of the fission barriers for various fissionability parameters "x". The cases in Figures b and c show the relative flatness and length (or better

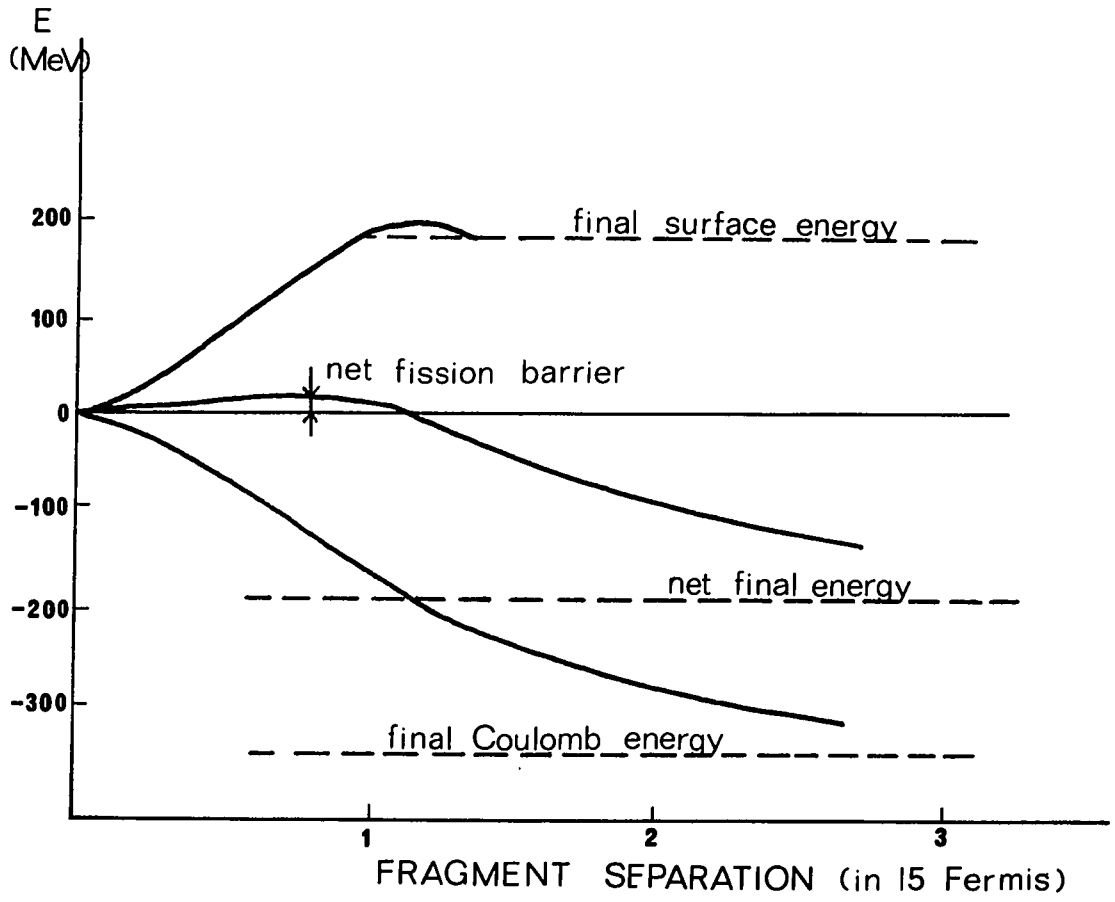

Figure 28

width) of the fission barriers. Under these circumstances it is easy to imagine how the perturbations of single-particle origin, (especially in the cases in Figures 29 b and 29c) imposed on the gross features as the surface energy constant $C_{surface}$ from equation (18) or similarly on the Coulomb energy constant may cause relatively large changes like asymmetry in low-energy fission.

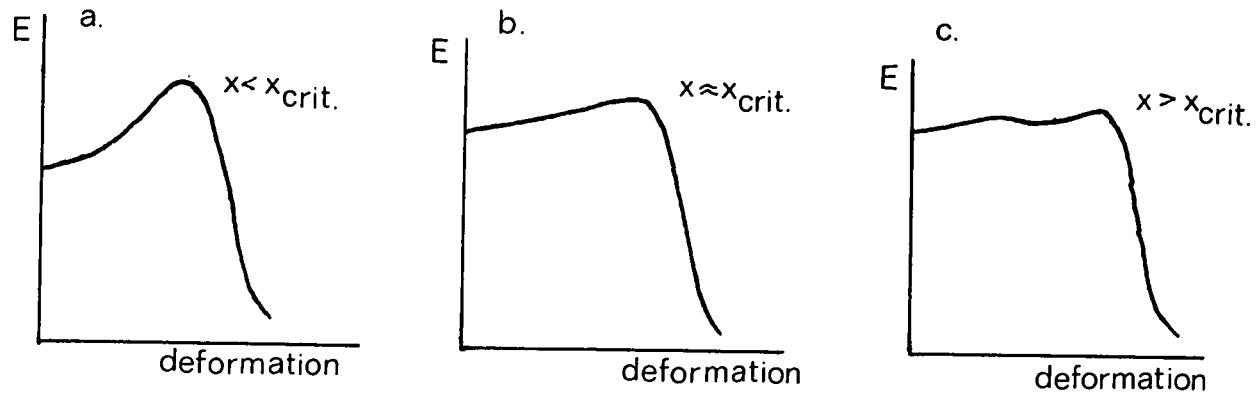

Figure 29

It is natural to add to the above considerations another degree of freedom that is of prime concern in this work, namely polarizability or neutron-proton vibrations of the nuclear matter, i.e. to relieve the requirement of charge uniformity. This case is covered by equation (5) where instead of Z_A determined by Coryell (19) Z_A is substituted as calculated from the liquid-drop mass formula of Green (72) and given by

$$Z_A = \frac{A - \frac{0.4 \times A^2}{200+A}}{2} \qquad (33)$$

The complete treatment is that of the minimum potential energy (MPE) hypothesis, assuming the configuration at scission can be represented by two touching spheres, and that fission will occur in such a manner that the potential energy of the two spheres will be at a minimum. The calculation pertinent to this work will be performed in the last section of this thesis. As mentioned in the Introduction the minimum potential energy treatment was successful in the case of Blann's (20) work and it is easy to see that it represents a liquid-drop model feature. To obtain some feeling for the energies involved two typical cases were chosen, protactinium nuclei of mass A = 232 and of A = 228 and it was assumed that they represent the lower and higher energy fissioning nuclei (within the energy region of this work). The most probable charges for both cases were obtained using the UCD hypothesis (as described in the Introduction) and the energies above those corresponding to the lowest energy charge Z_A were calculated for both values of Z_p using equation (5). Since the elementary charge dispersion spans several units of Z and since the nuclear charge in the energy region of this work is not affected by evaporation (and neglecting all ^{232}Th (p, pxn) reactions) one Z unit was added

for the heavy side of the mass distribution and subtracted for the light side and the energy differences calculated again. All the calculations are given in Table 12 and 13. One can see that the energies involved for certain divisions in the case of ^{232}Pa are quite high (higher than the ordinary fission barriers, for instance). On the other hand in the case of ^{228}Pa the energies are lower. In both cases, however, the argument for MPE seems strong.

In the next subsection an attempt will be made to estimate first and second order perturbations in the liquid-drop feature of MPE with respect to n-z vibrations.

6b. Primary Perturbations in the MPE Model

The source of the primary perturbations in the MPE model is the force responsible for dividing the fissioning nucleus into two unequal parts, whose mass ratio is determined by the number of the antisymmetric states to symmetric states, as stated in the phenomenological rule given by Brandt & Kelson (8). To perform the calculations according to equations (23) and (24) it is necessary to assign the individual states of the single particles properly. For the case of ^{233}Pa (no attempt was made to choose the fissioning nucleus more realistically because all the following considerations are clearly only qualitative) a ground-state deformation of approximately $0.3\,\delta$ was chosen and the states assigned using the Nilsson graph as given in Hyde et al. (52) for the heavy nuclei. Also the Clebsch-Gordan coefficients were calculated and the most probable charge $\langle Z_{\pm} \rangle$ (with respect to charge distribution, not charge dispersion) and the most probable neutron number $\langle N_{+} \rangle$ were determined, together with the appropriate widths, Γ_Z and Γ_N. All the curves obtained are plotted in Figure 30 together with

TABLE 12

Charges and Relative Energies for Given Fission Products

(Fissioning Nucleus ^{232}Pa)

	heavy mass	light mass	
mass split	141	91	
k	0.817	1.21	
$Z_{A_{Coryell}}$	58.55	40.1	
$Z_{A_{Green}}$	58.84	39.8	
Z_p(UCD)	55.3	35.7	total energy
* $E_{(Z_A - Z_p)}$	8.6 MeV	23.4 MeV	32. MeV
$E_{(Z_A - (Z_p \pm 1))}$	14.75 MeV	14. MeV	28.75 MeV
$E_{(Z_A - (Z_p \pm 1))}$	4.1 MeV	35.3 MeV	39.4 MeV
$E_{(Z_A - (Z_p \pm 2))}$	22.5 MeV	7. MeV	29.5 MeV
$E_{(Z_A - (Z_p \pm 2))}$	1.3 MeV	50. MeV	51.3 MeV

* potential energies for complementary fragments for a given mass split. In each of these when 1 (or 2) Z units are added (subtracted) for light (or heavy) mass it must be subtracted (added) from the complementary heavy (or light) fragment because the sum must equal 91 Z units, $Z_l + Z_h = Z_f$ (=91) All Z_A are those given by Coryell (19)

TABLE 13

Charges and Relative Energies for Given Fission Products

(Fissioning Nucleus ^{228}Pa)

	heavy mass	light mass	
mass split	141	87	
Z_A Green	58.84	38.22	
Z_p (UCD)	56.27	34.72	
k	0.805	1.24	
$E\{Z_A - Z_p$ (MeV)$\}$	5.3	15.2	20.5
$E\{Z_A - (Z_p + 1)\}$	10.2		
$E\{Z_A - (Z_p - 1)\}$		7.7	17.9

* potential energies for complementary fragments for a given mass split. In each of these when 1 (or 2) Z units are added (subtracted) for light (or heavy) mass it must be subtracted (added) from the complementary heavy (or light) fragment because the sum must equal 91 Z units, $Z_l + Z_h = Z_f$ (=91)

the experimentally observed data by Croall & Cuninghame (20). If $\vec{l}.\vec{s}$ coupling is not taken into account there is no width in the mass distribution. However in Figure 30 it seems the value of $A_{\pm}$ is closer to the observed most probable mass than to the calculated most probable mass $\langle A_{\pm} \rangle$.

The charge and neutron distributions are plotted in the most convenient way, namely with respect to N/Z of the fissioning nucleus. For instance if the ratio of the most probable charge and most probable neutron number equalled that of the target, all three $\langle A_{+} \rangle$, $\langle N_{+} \rangle$ and $\langle Z_{+} \rangle$ would fall on the same line in Figure 30.

Figure 30 is self-explanatory. It shows clearly that single-particle effects - whatever might be the force behind them - try to form all the nuclides of masses above 128 in a proton-rich manner to quite a great degree. On the other hand those of lower mass should be extremely neutron-rich. This obviously never happens because of the liquid-drop model feature describing the n-z vibrations. The situation depicted in Figure 30 shows the trends of the single-particle perturbations. As mentioned earlier, the shape and location of these distributions depends on the state assignments and the ground-state deformation. For instance that state with the highest possible m_j quantum number for each j does not contribute to the width of the neutron or proton distributions Γ_N and Γ_Z, at all (due to the properties of the Clebsch-Gordan coefficients) while the states close to $m_j = 0$ contribute by a number close to 0.25.

To obtain a better understanding it may be useful to consider three possible cases for the coupling between neutrons and protons. The constant k, the "stiffness" coefficient in the sense of equation (5) can be used.

1. k = 0. There is no connection whatsoever and any neutron number, N, can be connected (associated) with any proton number, Z, and vice versa. The cross section for any nuclide, $\sigma(N, Z)$, (for one complement) can be expressed as

$$\sigma(N,Z) = \frac{1}{2\pi(\Gamma_N \cdot \Gamma_Z)^{\frac{1}{2}}} \ell^{-\frac{(N-N_p)^2}{2\Gamma_N}} \cdot \ell^{-\frac{(Z-Z_p)^2}{2\Gamma_Z}} \qquad (34)$$

where Z_p is the most probable Z and N_p is the most probable N, Γ_N and Γ_Z are the corresponding widths parameters.

2. $k = \infty$. There is no polarizability in the matter, the n-z vibrations are absolutely "stiff" and there would be no charge dispersion and all fragments would have the same N/Z equal to that of the fissioning nucleus. There also would be only one distribution, (N or Z), the one would be just a multiple of the other.

3. $0 < k < \infty$. Intermediate situation which is the real case.

The ideal program would use the constant and single-particle effects described in this section and the liquid-drop model potential surfaces (and dynamics) and arrive at a complete solution for the $Z_p(A)$ function. There is also a possibility to evaluate the single-particle effects quantitatively using the $Z_p(A)$ function.

Very recently, Armbruster (78) published a solution for universal charge dispersion in any fissioning nucleus. It disregards the single-particle effects in the sense of Brandt & Kelson (8) theory. Unfortunately, for the time being there remains a difficulty in the Brandt & Kelson (8) single-particle theory, i.e. the fact that in Figure 30 the most probable masses do not agree with experimental fact. It appears as if the observed mass distribution falls in between the phenomenological rule and the

Figure 30

Mass distribution for ^{232}Th bombarded by protons as calculated on the basis of Brandt & Kelson (8) theory.

Experimental points taken from Croall & Cuninghame (20) at bombarding energy 20 MeV

A_+ , N_+ , Z_+ and

$\langle A_+ \rangle$, $\langle N_+ \rangle$, $\langle Z_+ \rangle$, are given in equations (20), (21) and (24).

A_h is the most probable mass experimentally observed in the heavy mass region

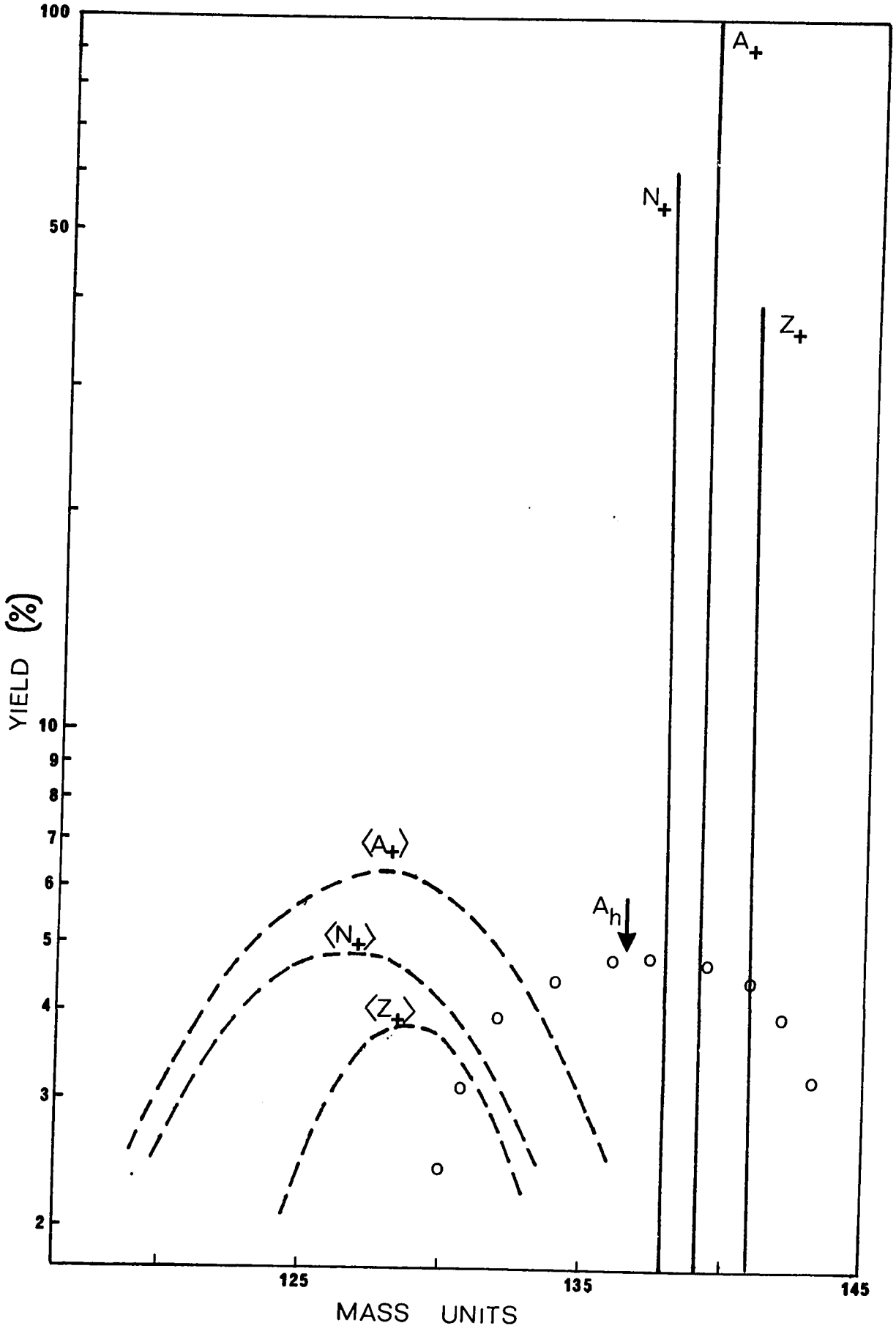
100
50
10
9
8
7
6
5
4
3
2
YIELD (%)
A_+
N_+
Z_+
$\langle A_+ \rangle$
$\langle N_+ \rangle$
$\langle Z_+ \rangle$
A_h
125
135
145
MASS UNITS

mass distribution with the width (with $\vec{l}.\vec{s}$ coupling). Could some other, more deformed ground state, higher energy and with it associated slippage and/or some other single-particle changes in states occupations cause the agreement with the experiment to be complete?

In conclusion of this subsection it should be pointed out that with respect to the smaller energies in the sense of equation (5) for the fissioning nucleus ^{228}Pa (corresponding to higher bombarding energy) as they are given in Table 13, it is conceivable that the single-particle effects - not more than units of MeV in energy - could cause certain nuclides to be formed more easily neutron or proton rich than given by the MPE hypothesis so that the results might become equal to those predicted by the UCD hypothesis, while at lower bombarding energies, where the energies given in Table 12 are much higher, the single-particle perturbation has less chance to affect the MPE formation substantially. More about this will be given at the end of this section.

6c. The Second-Order Perturbation of MPE

In the preceding section it was argued that the fact that the experiments give a more proton-rich $Z_p(A)$ function than predicted by the minimum potential energy hypothesis (liquid-drop model feature) may be explained as basically a first-order perturbation effect. To show this the neutron, proton, and the resulting mass distributions constructed on the basis of Brandt & Kelson (8) theory were plotted in Figure 30 in the most convenient way. From Figure 30 it is obvious that the right-hand side of the heavy-mass distribution is more proton-rich with respect to the left-hand side, so the turn to a more proton-rich $Z_p(A)$ function results. The question of any quantitative evaluation is

clearly beyond the scope of this work. The energies involved must however be lower than the energies involved in the liquid-drop model potential energies. The situation for ^{235}U is shown in Figure 28.

An even more abrupt turn in the observed $Z_p(A)$ function - so that an ECD type of $Z_p(A)$ function results - was observed by many workers in thermal neutron and low-energy fission, for instance by Wahl et al. (76), Fried et al. (79), Anderson et al. (80) and Choppin & Meyer (81) as compiled by Notea (82). Glendenin et al. (51) found in the thermal neutron fission of ^{233}U, ^{235}U and ^{239}Pu that the $Z_p(A)$ functions have three different slopes $(\frac{\Delta Z_p}{\Delta A})_{239_{Pu}} > (\frac{\Delta Z_p}{\Delta A})_{235_U} > (\frac{\Delta Z_p}{\Delta A})_{233_U}$ (all three slopes are lower than the corresponding MPE slopes). At the same time the $Z_p(A)$ functions seem to display similar fine structures in regions close to the closed shells N = 28 and Z = 50. Even though Glendenin et al. (51) prefer not to draw any final conclusion the data seem to suggest that the different slopes reflect three different admixtures of the first-order perturbations (single-particle effects depend primarily on the fissioning nuclei) while the second-order perturbation around closed shells is similar for all three nuclei (depend primarily on the fragments). Similar observations were made by Notea (82) in the case of ^{235}U. These findings are paralleled by the "saw-tooth" shape in the post-fission neutron evaporation reflecting, according to the Vandenbosch (28) hypothesis mentioned in the introduction, the effect of the closed-shell fragments. Another corresponding effect is higher kinetic energy of the fragments with closed shells and smaller distances of separation of the charge centers, due to the fact that one fragment is "harder" and less deformed.

A very important experimental fact observed by many researchers is that at excitation energies as low as 20 MeV, and at all higher energies, all of the effects mentioned previously disappear. For instance, the fine structure in $Z_p(A)$ functions was not observed (its occurrence may be somewhat doubtful because the experimental error is of the same order). Britt & Whetstone (29) and McHugh & Michel (21) report that at 20 MeV the saw-tooth shape is not observed. Also workers in this laboratory (Saha & Yaffe (40)) assume that the excitation energy responsible for the neutron evaporation is divided proportionally to the mass of the fragment. It has also been widely observed that the ECD rule does not hold at higher energies, by Benjamin et al. (64), Yaffe (33), Colby and Cobble (71), McHugh & Michel (21) and in this work. In Figures 24 and 25 the straightening out of the $Z_p(A)$ functions for masses higher than 135 and at energies more than 35 MeV is clearly observable. One can further see that at 170 MeV Pappas & Hagebo (74) observed an almost smoothly increasing function parallel to $Z_A(A)$ as given by Green (72) with no shell effects included. McHugh & Michel (21) in studying the fission of ^{232}Th with alpha particles suggest that the $Z_p(A)$ function is determined by MPE, which does not take into account the shell effects. The same attitude was also adopted by Colby & Cobble (71). Finally the last point concerns the kinetic energies, i.e. the distance of the charge centers at the moment of scission. At this moment it should be mentioned briefly that the triple-peaked mass distribution as, for instance, is shown in Figure 26, was explained by Fairhall et al. (83) as due to two separate symmetric and asymmetric modes. The symmetric mode is characterized by a slightly lower kinetic energy release ($\approx$ 10%) than asymmetric. The nature of the Brandt & Kelson (8)

theory prefers the double-fission mode theory since the moment when the mode is decided is certainly not in the last stages of the fission process, just before scission, as, for instance, the fragment shell theory - the other alternative to the double-fission mode theory - assumes.

Croall & Cuninghame (20) tried to investigate this problem in the fission of ^{232}Th by protons under circumstances similar to this work (only the bombarding energy range was lower, up to 53 MeV). They observed that the mean total kinetic energy as a function of mass split has a peak at A = 132 for 13 MeV energy and moves to A = 138 for 50 MeV. The kinetic energy at the same time decreases by almost 10%. They also presented another kind of kinetic energy distribution as reproduced in Figure 31 (which they call "provisional") showing that while the kinetic energies of 165 MeV and 140 MeV occur in both modes (the 165 MeV curve shows predominance in the asymmetric region, while the 140 MeV is predominant, in a lesser degree, in the symmetric region), the kinetic energy 190 MeV, centered around the closed-shell region with A = 132, persists only in the asymmetric region. The distribution shown in Figure 31 holds for a bombarding energy of 50 MeV where the mass distribution, as shown in Figure 26, is still quite asymmetric.

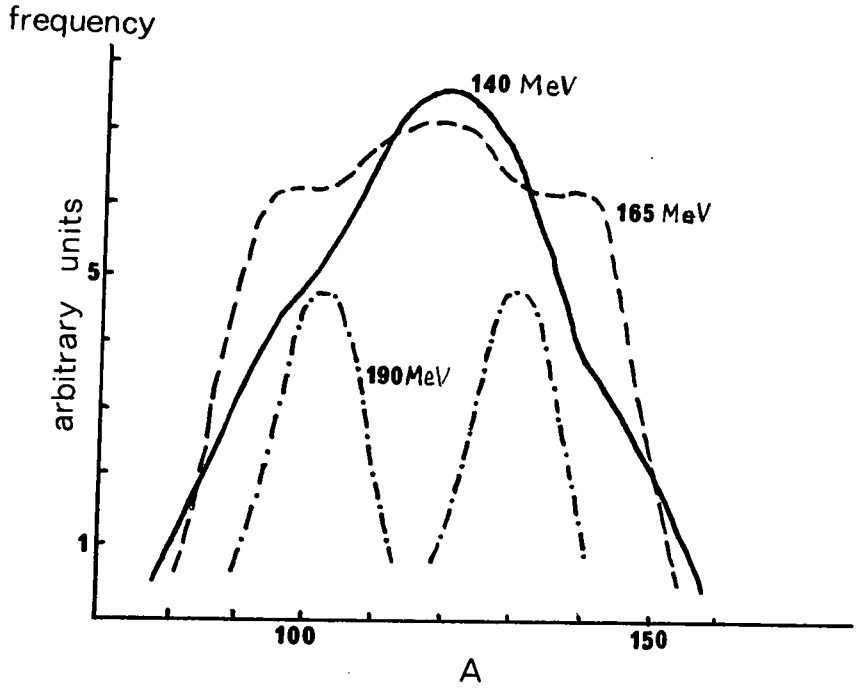

Figure 31

What these data seem to indicate is the possibility of three fissioning "modes":

1a. Asymmetric fission at thermal neutron and low bombarding energies, which behaves as described by the Vandenbosch (28) hypothesis mentioned in the Introduction. This will have an ECD-type $Z_p(A)$ function with a saw-tooth shape neutron distribution and may be viewed as a second-order perturbation due to fragment shell effects superimposed on the first-order perturbation as discussed in the previous section.

1b. Asymmetric fission at higher bombarding energies, where the kinetic energy release is somewhat lower than in the case under 1a., but still higher than for the symmetric case. The saw-tooth shape disappears and the ECD-type $Z_p(A)$ function gradually ceases to hold good. In the case of ^{232}Th proton fission this mode coexists with the symmetric mode, which would explain, as Croall & Cuninghame (20) argue, the shift of the peak of the mean total kinetic energy from A = 132 at 13 MeV to A = 138

at 50 MeV. This case (1b.) may be viewed as the first-order perturbation as discussed in the previous section, with no fragment shell effects.

2. Symmetric mode, prevailing entirely at still higher energies. It also coexists in varying degrees with the asymmetric mode in the energy region up to 80 MeV. It has no first or second-order perturbation in the above mentioned sense and the $Z_p(A)$ function is best approximated by the minimum potential energy hypothesis with no shell effects taken into account, as is argued by Blann (21) in the case of the fission of ^{197}Au with ^{12}C ions.

The implication of these suggestions is, for instance, that the two explanations for the kinetic-energy dip, as given by Vandenbosch (28) and the neutron saw-tooth shape distribution as given by Milton & Fraser (84) who argue that the dip is due primarily to the difference between the symmetric and asymmetric modes, complementing each other satisfactorily. The former holds good for thermal and very low energy fission and the other for higher energies. Both are the result of the same primary perturbation - in terms of Brandt & Kelson (8) theory - leading to the mass asymmetry and to the deviations from MPE (liquid-drop model feature), and one has only the second-order shell effect perturbation.

If the reasoning proposed in this subsection is true it shows how relatively low excitation energy (of tens of MeV in comparison to 1200 MeV of the nucleons' kinetic energy in the potential well) uniformizes (homogenizes) effectively the fissioning matter.

It should be added that the evidence for the early (20 MeV) dissolution of the low-energy (Vandenbosch (28)) pattern and

for the persistence of the asymmetric mode without the above-mentioned pattern at energies from 20 to 60 MeV is not too conclusive. It is quite conceivable that the gradual disappearance of the spherical shell effects of the saw-tooth neutron yield shape and of all the low-energy asymmetric fission features is just an effect of the gradual increase of the symmetric fission component

In the case of the fission of ^{238}U with protons Parikh et al. (85) observed the downward turn of the $Z_p(A)$ function for the dispersion for A = 141 up to a bombarding energy of 85 MeV. On the other hand McHugh & Michel (21) and Britt & Whetstone (29) in ^{233}U, ^{230}Th, ^{235}U and ^{232}Th alpha-fission at energies of approximately 20 - 30 MeV did not observe a similar behavior (not even in the case of $^{235}U + \alpha \Rightarrow {}^{239}Pu^*$ which is very close to Parikh's (85) $^{239}Np^*$). Britt & Whetstone (29) themselves admit that the question of an early disappearance of the saw-tooth shape with energy (at $\approx$ 20 MeV) is not settled yet. Both McHugh & Michel (21) and Britt & Whetstone (29) used physical methods.

It may be that the difficulty of concluding at what energy the spherical shell effects disappear with increasing energy is a reflection of the discrepancies between the radiochemical and physical measurements.

Even though the above section of this subsection is so hypothetical, the basic contention, that the low-energy asymmetric fission is subject to a second-order spherical shell effects perturbation, is not affected, only "mode" 1b. would have to be omitted.

The experimental fact reported, for instance, by Hogan & Sugarman (35) and by Remsberg et al. (39) that the asymmetric mass splits coming from a low-energy deposition events (neutron-rich

fragments) have higher kinetic energy than the same mass splits coming from a high-energy deposition fission (neutron-deficient fragments) justifies the assumption of the excitation energy having a uniformizing effect. Without this uniformizing assumption it would be incomprehensible that in the same mass region and for almost the same fragments one would not get the same spherical shell effects in the region around mass A = 132.

6d. Note on the Brandt & Kelson Phenomenological Rules and on the Double-Fission Mode Hypothesis in the Light of their Theory.

As mentioned previously, there is a weakness in Brandt & Kelson's (8) theory concerning the discrepancy between A_+/A_- ratio obtained from the ground-state spherical configuration disregarding $\vec{l}.\vec{s}$ coupling and $\langle A_+\rangle/\langle A_-\rangle$ obtained from the deformed states where the $\vec{l}.\vec{s}$ coupling is taken into account (as Hyde et al. (52) point out this coupling is responsible for the prolate ground-state deformation for the heavy nuclei). The ratio in the case of ^{233}Pa is higher in the former case than in the latter. As seen in Figure 30 the experimentally-determined A_h/A_l ratio lies in between the two, (closer to the A_+/A_- ratio).

Another difficulty is the existence of symmetric fission for the elements of $Z < 92$ at low bombarding energies, showing itself most clearly in ^{226}Ra fission. Brandt & Kelson (8) explain this as a consequence of the necessity of greater rearrangement of the nuclear matter which, similarly to the effect of the slightly increased excitation energy discussed in the previous section, tends to uniformize it. The resulting "slippage" between the configuration surfaces is interpreted in terms of coupling between the LDM potential (lowest energy states occupied) surfaces and the potential surface where the original spherical states were kept unchanged.

The region where symmetric fission starts to occur is also the region of the critical fissionability parameter, x_{crit}, where, as shown in Figure 29a, the barrier height increases and the saddle-point shape starts to be "necked-in".

Parallel to these changes are the ground-state deformations. As shown in reference (52) on page 123 there is a transition from the spherical shape of the nuclei close to ^{208}Pb to the prolate deformation of nuclei of $A > 224$.

There is no theory yet which would explain satisfactorily the most interesting feature of nuclear fission, the sudden occurrences of the asymmetric- symmetric fission. Brandt & Kelson (8) point out that the question of what shape - whether of the ground state or of the saddle point - should be taken as determining the A_+/A_- (or possibly the $\langle A_+\rangle/\langle A_-\rangle$) is not solved yet at all. Naturally, it could be any state in between, especially if there are some isomer states causing humps in the fission barrier, due to certain shape stabilities in the sense of the Strutinsky (9) and Vandenbosch (16) approaches. The saddle point A_+/A_- ratio is in agreement with the case of symmetric fission but does not explain the asymmetry while the opposite is true about the ground state A_+/A_- ratio.

The situation described in the previous paragraph is shown schematically in Figure 32 (taken partially from Griffin (41)). The curve 1 shows the decrease of the number of symmetric states from the saddle point shape at the fissionability parameter $x = 1$. (it is a sphere) to the saddle point shapes around $x = x_{crit}$ (approximately equal to 0.697) which show the "necking-in". The ratio goes from 1.4 to 1.0, which is what one would intuitively expect realizing that the symmetric states - having crests in the

x-y fissioning plane - are being continuously "squeezed out" by the more and more prolate deformation and finally by "necking-in" of the saddle-point shape. (The calculation is based on Hill & Wheeler (50) article and performed by Griffin (41); it does not take into account the $\vec{l}.\vec{s}$ coupling).

The experimental points in Figure 32 are taken from the review article by Pappas et al. (86) and they show no agreement whatsoever between the curve 1 and the experimentally observed A_h/A_l ratios. Curve 2 shows the A_+/A_- ratio as obtained from the ground-state spherical configuration for nuclei of given fissionability parameter x. No prolate deformation has been taken into account. Curves 1 and 2 meet at $x = x_{crit}$ where the saddle-point shape is spherical. If one superimposes curve 1 on curve 2 from the point where asymmetric fission behavior first appears (the explanation of this is the aim of Brandt & Kelson (8) theory and therefore that is the point where phenomenological rules should be applied). i.e. from the ^{226}Ra region, one gets curve 3 which is in surprisingly good agreement with the experimentally-determined ratios. This superimposition is justified because curve 1 describes the decrease of the symmetric states with prolate deformation - the same deformation known to exist for the heavy nuclei fissioning in that region. (Odd-even effects are neglected).

The remarkable agreement found in Figure 32 shows that Brandt & Kelson (8) phenomenological rules agree well with the observed data (this is in disagreement with Pappas et al. (86) who state that the rules do not agree with the data). The problems arise, however, as mentioned previously, if, for instance, instead of ^{252}Cf, which shows remarkable agreement with the experimental data in all respects (in A_h/A_l ratio and in the width of the mass

distribution) ^{233}Pa is taken. As one can see in Figure 30 the $\langle A_+\rangle/\langle A_-\rangle$ ratio is smaller than A_+/A_- and the observed A_h/A_l falls in between. Fortunately, there is still a great margin for explanations open which hopefully the theoreticians might fill. The main areas of the margin are presented below (in a very sketchy way):-

1. States assignments; sometimes it is not easy to assign the states if two levels of the same quantum number m_j cross (as shown for instance by Bolsterli et al. (87))
2. Impossibility to decide what state configuration to take as determining the A_+/A_- ratio (or $\langle A_+\rangle/\langle A_-\rangle$ ratio).
3. The amount of $\vec{l}.\vec{s}$ coupling needed. It seems reasonable not to take into account in the coupling scheme that determines the width and location of the mass some states of low angular momentum (p, d, f,...). The agreement with the experimental values in the case of ^{233}Pa would be much better and also it seems that the coupling for low-lying states is not so pronounced as in the case of higher lying states.
4. The dependence on the total number of particles. For instance, the surface energy constant as defined in equation (18) (corresponding to the surface energy constant of the Green formula), depends to a considerable degree on the number of particles.
5. The question of the ground-state deformation. Brandt & Kelson(8) chose in the case of ^{232}Cf a ground-state deformation $\delta = 0.4$, while in this work only $\delta = 0.3$ was taken for ^{233}Pa. (Partially because there were no data beyond that point available).

In spite of all the various shortcomings it was considered worthwhile to concentrate heavily on the Brandt & Kelson (8) Single-Particle Theory of Fission and therefore much of the work in this

thesis was devoted to the various aspects of the theory.

7. Calculation of the Most Probable Charges Using UCD, ECD, and MPE Hypotheses

For the sake of completeness the UCD, ECD, and MPE calculations were performed. The product masses chosen were taken as A = 141, the corresponding complementary one depending on the energy available. Fortunately, this quite difficult problem was substantially simplified by using the values for UCD and ECD as calculated by Benjamin et al. (64) with the evaluation of the maximum possible error. Since the accuracy of all the calculations of this kind is not too great, due to the many assumptions introduced for simplification, no attempt was made to develop an independent approach to this problem.

The error estimate was based on the following consideration. The relation used by Benjamin et al. (64) for finding the corresponding fragment mass for a chosen mass A = 136 of a product is given by

$$A_h = 136 + 1 + \left(\frac{E_f^*}{9} \times \frac{A_h}{A_f}\right) \qquad n = 1 + \frac{E_f^* \cdot 137}{9A_f - E_f^*}$$

where E_f^* = excitation energy of the fissioning nucleus and A_f = mass of the fissioning nucleus.

The the case of mass 141 it is

$$A_h = 141 + 1 + \left(\frac{E_f^*}{9} \times \frac{A_h}{A_f}\right) \qquad n' = 1 + \frac{E_f^* \cdot 142}{9A_f - E_f^*} \qquad (35)$$

The difference between the number of neutrons evaporated, which is the main source of error in this procedure, is simply

$$n - n' = \frac{E_f^* \cdot 5}{9A_f - E_f^*} \approx .1 \qquad (36)$$

This error is negligible. The additional error arising from the difference in Z for Cs and Ba is also negligible. The values of N/Z_p(UCD) and N/Z_p(ECD) for energies 28 MeV, 44 MeV, and 57 MeV

Figure 32

The ratios of symmetric to antisymmetric states, $\frac{A_+}{A_-}$, for various fissionability parameters, χ.

o o — — — — o o — — experimental points showing the ratios of most probable mass of the heavy mass peak to that of the light mass peak, $\frac{A_h}{A_I}$, taken from Pappas et al. (86).

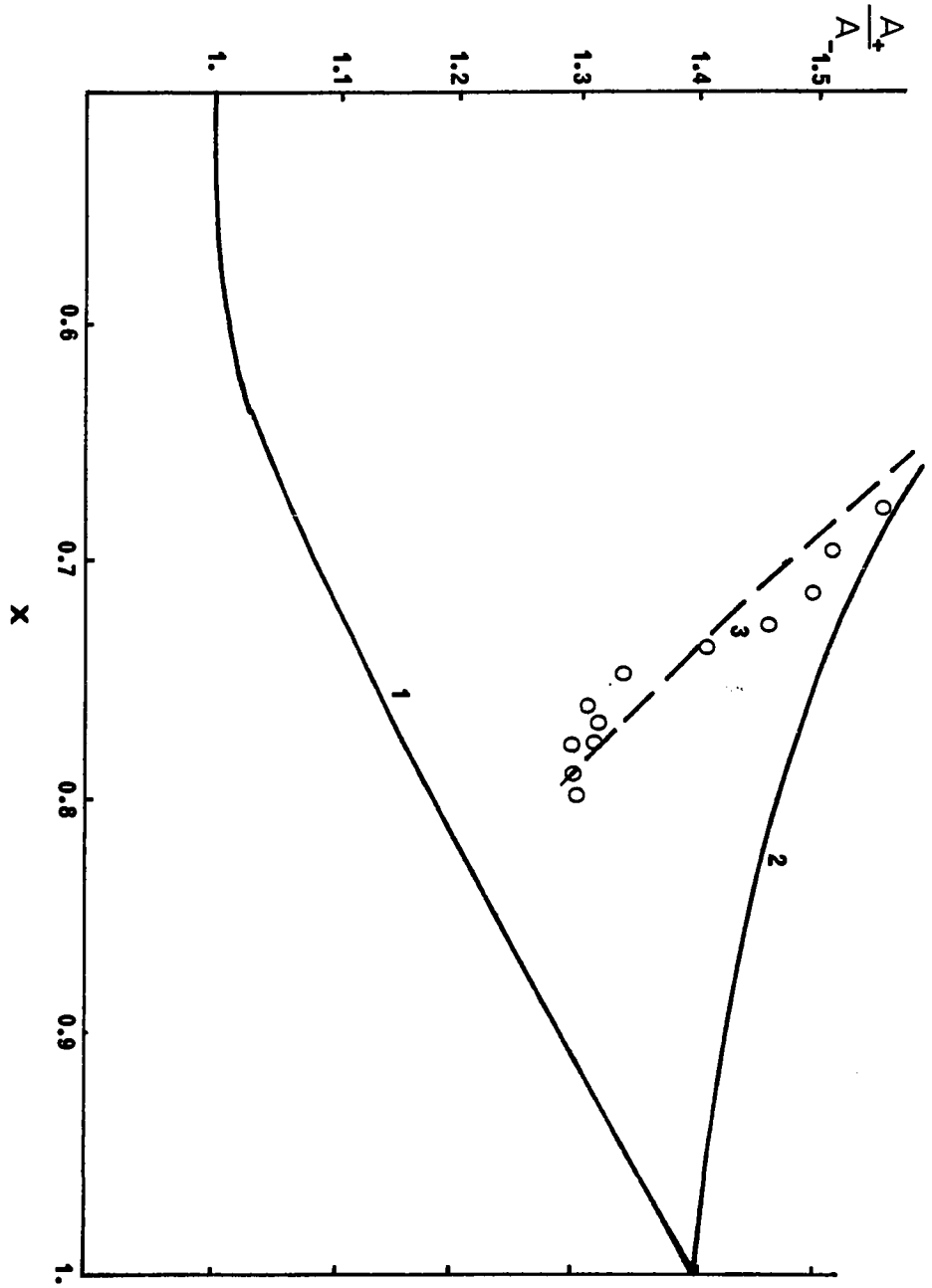
$\frac{A_+}{A_-}$
1.
1.1
1.2
1.3
1.4
1.5
x
0.6
0.7
0.8
0.9
1.
1
2
3

are given in Table 14. The corrections for the $Z_A(A)$ function in the case of the most probable charge determination via ECD were done simply by subtracting the difference between the N/Z_A ratio corresponding to the mass A = 136 region and the N/Z_A ratio corresponding to the mass of region A = 141. This method is not rigorous because the shell-affected $Z_A(A)$ function is inserted after the calculation. However, it is believed that the difference is very small.

The minimum potential energy calculation was performed using the formula as given by McHugh & Michel (21). (the units used were ergs for the mass formula constants, centimeters for the distance of separation of the charge centers and e.s.u. for charge) The average fissioning nucleus was taken from Croall & Cuninghame (20) who obtained the values using Huizenga & Vandenbosch (36) formula (schematically presented in the Introduction as equation 16)). The corresponding values for the average fissioning nucleus, the estimated excitation energy of the fragment and assumed number of neutrons evaporated are given in Table 14. The same reasoning used by Benjamin et al. (64) was used here.

It should be pointed out that the assumption made by Benjamin et al. (64) and in this calculation, i.e. that the amount of energy taken away by the gamma radiation and by one additional neutron for each fragment as given in equation (35) approximately equals the energy of the mass deficit of the fragments after subtracting the kinetic energy, seems to be acceptable even though, for instance, Hogan & Sugarman (35) take both quantities into account. It is expected that the error generated by such a simplification is not larger than the error of the experimental points.

In conclusion it can be seen from Table 14 that the

experimental values lie, as observed many times in this laboratory, in between the results predicted by UCD and ECD hypotheses. Under the assumption of regular division of the excitation energy between the fragments (i.e. proportional to the mass of the fragment) the MPE energy calculations give, as expected, values slightly more neutron-rich than the experimental points at low energies. The first-order perturbation, due to the single-particle mechanism as discussed in the previous sections, would be expected to produce more proton-rich most probable charges than predicted by the MPE hypothesis (without shell effects).

No attempt was made to calculate any $Z_p(A)$ values in the case of higher energies, since there was very little change in the Z_p experimental values and since there was an increasingly low probability of compound nucleus formation.

TABLE 14

The Most Probable Charge Calculations

Proton energy (MeV)	Approximate excitation energy E* (MeV)	Average Fissioning Nucleus	No. of Neutrons assumed evaporated from fragment in the case of MPE calculation	MPE N/Z_p	UCD N/Z_p	ECD N/Z_p	Experimental N/Z_p
28	33	231.5	2.	1.538	1.513	1.548	1.52
44	49	231.4	3.	1.52	1.493	1.532	1.502
57	62	231.3	4.	1.50	1.481	1.522	1.498

E. SUMMARY AND CONTRIBUTION TO KNOWLEDGE

In this work the independent formation cross sections of ^{139}Ba, ^{140}La, ^{141}La, ^{141}Ce, ^{143}Ce, ^{139}Ce and the cumulative cross sections of ^{139}Cs, ^{140}Ba, ^{141}Ba, ^{143}La, ^{141}Ce, and ^{144}Ce produced in the proton-induced fission of ^{232}Th at energies 28 - 83 MeV have been measured by radiochemical methods.

The excitation functions of the independently-formed nuclides ^{140}La, ^{141}La, ^{139}Ba, and ^{143}Ce have been found to reach their maxima at lower bombarding energies than expected on the basis of earlier results. The excitation function maxima plotted vs. the corresponding N/Z ratio gave a curve whose shape may reflect the increased contribution of symmetric fission. The charge dispersion parameters, the shift of the most probable charge, Z_p, towards the β-stability line and the full-width at half-maximum have been found not to change appreciably for energies higher than 45 MeV. Again, this has been explained by the increased contribution from symmetric fission which, being concentrated around its most probable mass $A \approx 115$, leaves the asymmetric region around mass $A \approx 141$ relatively unchanged and with relatively lower cross sections.

In a wider context the variations of Z_p with mass have been explained by the minimum potential energy, MPE, mechanism - a liquid-drop model feature - perturbed by the single-particle effects based on Brandt & Kelson (8) theory. It was suggested that if proton and neutron distributions are taken as two separate distributions tied together by nuclear forces that allow certain N-Z vibrations, then, for instance, a higher most probable charge than that corresponding to the fissioning nucleus could produce

more proton-rich products than predicted by the MPE hypothesis. It was also suggested that additional finer "ripples" on the $Z_p(A)$ function may be caused by secondary perturbations due to spherical shell effects, as described for instance, by Vandenbosch (28).

It has been shown that if the phenomenological rules suggested by Brandt & Kelson (8) are complemented by considerations of changes of ratio in symmetric to antisymmetric states due to the increased ground-state deformation, then the ratios of symmetrical to antisymmetric states, A_+/A_-, agree with the experimentally-found ratios of the most probable mass of the heavy-mass region to the most probable mass of the light-mass region, A_h/A_l.

In conclusion, the most probable charges based on the ECD, UCD, and MPE hypotheses have been calculated.

F. APPENDICES

1. Appendix A

In the case of ^{140}Ba - ^{140}La parent-daughter system the counts per minute for ^{140}La, CPM_2, at time t, can be written as

$$CPM_2 = CPM_1^o \frac{\lambda_2}{\lambda_2-\lambda_1}\left(\ell^{-\lambda_2 t} - \ell^{-\lambda_1 t}\right) + CPM_2^o\, \ell^{-\lambda_2 t} \qquad (37)$$

where CPM_1^o and CPM_2^o are the counts per minute for ^{140}Ba and ^{140}La respectively, at time $t = t_o$, which are to be determined; and are the decay constants.

Since $\lambda_2 > \lambda_1$, a transient equilibrium is reached in approximately 10 days. The equation (37) can be written then as

$$CPM_2' = CPM_1^o \frac{\lambda_2}{\lambda_1-\lambda_2}\, \ell^{-\lambda_1 t'} \qquad (38)$$

where $'$, $''$ indicates the measurements in the equilibrium cycle. From equation (38) CPM_1^o can be obtained, substituted into equation (37) and CPM_2^o obtained using the following equation

$$CPM_2^o = CPM_2\, \ell^{\lambda_2 t} - CPM_1^o \frac{\lambda_2}{\lambda_2-\lambda_1}\left(1-\ell^{(\lambda_2-\lambda_1)t}\right). \qquad (39)$$

CPM_1^o from equation (38) gives the cumulatively-formed ^{140}Ba cross section and CPM_2^o from equation (39) gives the independently-formed ^{140}La cross section.

2. Appendix B

In the case of ^{141}Ba - ^{141}La - ^{141}Ce grandparent-parent-daughter system where all members are genetically connected and formed independently, the most convenient way of treating the problem is to divide the time sequence into two sections, (a) during the bombardment and (b) after the bombardment.

1. Formation of the first isobar - ^{141}Ba - during the bombardment is described by

$$\frac{dN_1}{dt} = k_1 - N_1\lambda_1 \tag{40}$$

where N_1 is the number of atoms of the species and λ_1 is the decay constant, k_1 is a constant including numbers of atoms of the target n, the flux of protons I, and the function cross section σ_1. Using the method of separation of variables one gets for the number of atoms at the end of bombardment, N^{EOB},

$$N_1^{EOB} = \frac{k_1}{\lambda_1}\left(1 - e^{-\lambda_1 t_0}\right) \tag{41}$$

where t_0 is the time of the end of bombardment, EOB.

Formation of the second isobar - ^{141}La - is described by

$$\frac{dN_2}{dt} = k_2 + N_1\lambda_1 - N_2\lambda_2 \tag{42}$$

and at the end of bombardment

$$N_2^{EOB} = \frac{k_2 + k_1}{\lambda_2}\left(1 - e^{-\lambda_2 t_0}\right) - \frac{k_1}{\lambda_2 - \lambda_1}\left(e^{-\lambda_1 t_0} - e^{-\lambda_2 t_0}\right) \tag{43}$$

where the symbols are as in equation (40) and (41).

For the case of the third isobar - ^{141}Ce -

$$\frac{dN_3}{dt} = k_3 + N_2\lambda_2 - N_3\lambda_3 \tag{44}$$

and at the end of bombardment

$$N_3^{EOB} = \frac{k_3+k_2+k_1}{\lambda_3}\left(1-e^{-\lambda_3 t_0}\right) - \frac{k_2+k_1}{\lambda_3-\lambda_2}\left(e^{-\lambda_2 t_0} - e^{-\lambda_3 t_0}\right) -$$

$$- k_1\lambda_2\left[\frac{e^{-\lambda_1 t_0}}{(\lambda_3-\lambda_1)(\lambda_2-\lambda_1)} - \frac{e^{-\lambda_2 t_0}}{(\lambda_3-\lambda_2)(\lambda_2-\lambda_1)} - \frac{e^{-\lambda_3 t_0}}{(\lambda_3-\lambda_1)(\lambda_3-\lambda_2)}\right] \quad (45)$$

The development from time $t = t_0$ to the time of separation at time t is a situation described by Bateman's formula as given in reference (14)

$$N_3^{SEP} = \lambda_1\lambda_2 N_1^{EOB}\left[\frac{e^{-\lambda_1 t}}{(\lambda_2-\lambda_1)(\lambda_3-\lambda_1)} - \frac{e^{-\lambda_2 t}}{(\lambda_2-\lambda_1)(\lambda_3-\lambda_2)} - \frac{e^{-\lambda_3 t}}{(\lambda_3-\lambda_1)(\lambda_3-\lambda_2)}\right] +$$

$$+ \frac{\lambda_2}{\lambda_3-\lambda_2} N_2^{EOB}\left(e^{-\lambda_2 t} - e^{-\lambda_3 t}\right) + N_3^{EOB}\, e^{-\lambda_3 t} \quad (46)$$

where N_1^{EOB}, N_2^{EOB} and N_3^{EOB} are given in equations (41), (43) and (45)

The program based on equations (46) is shown on the following page.

```
0001  /JOB
0002  /FTC
0003        READ(5,10)GM,G3,G2,G1
0004     40 READ(5,20)C,E,T0,T11,T12,T13,ST,S11,SM
0005        READ(5,30)D11,D12,D13,DM
0006        S1=S11
0007        K=0
0008        T1=T11
0009        D1=D11
0010        B3=ALOG(2.)/G3
0011        B2=ALOG(2.)/G2
0012        B1=ALOG(2.)/G1
0013        BM=ALOG(2.)/GM
0014        DMI=DM/(1.-EXP(-BM*T0))
0015        F=C*SM/DMI
0016      4 D3=D1*EXP(-B3*T1)
0017        C11=EXP(-B1*T1)/((B3-B1)*(B2-B1))
0018        C12=EXP(-B2*T1)/((B3-B2)*(B2-B1))
0019        C13=EXP(-B3*T1)/((B3-B2)*(B3-B1))
0020        C1=B3*B2*(1.-EXP(-B1*T0))*(C11-C12+C13)
0021        C31=EXP(-B2*T1)-EXP(-B3*T1)
0022        C3=B3/(B3-B2)*(1.-EXP(-B2*T0))*C31
0023        C4=B2*B3/((B3-B2)*(B2-B1))*(EXP(-B1*T0)-EXP(-B2*T0))*C31
0024        C5=(1.-EXP(-B3*T0))*EXP(-B3*T1)
0025        C6=B3/(B3-B2)*(EXP(-B2*T0)-EXP(-B3*T0))*EXP(-B3*T1)
0026        C71=EXP(-B1*T0)/((B3-B1)*(B2-B1))
0027        C72=EXP(-B2*T0)/((B3-B2)*(B2-B1))
0028        C73=EXP(-B3*T0)/((B3-B2)*(B3-B1))
0029        C7=B2*B3*(C71-C72+C73)*EXP(-B3*T1)
0030        S3=(F*D3+S1*(C7+C4-C1)+ST*(C6-C5-C3))/(C6-C3)
0031        S2=ST-S3-S1
0032        WRITE(6,50)E,S1,S2,S3
0033        K=K+1
0034        IF(K-2)1,2,3
0035      1 T1=T12
0036        D1=D12
0037        GO TO 4
0038      2 T1=T13
0039        D1=D13
0040        GO TO 4
0041      3 GO TO 40
0042     10 FORMAT(4F10.1)
0043     20 FORMAT(F6.4,3F7.2)
0044     30 FORMAT(4E10.4)
0045     50 FORMAT(F10.1,3F10.3)
0046        END
*END

*GO
```

REFERENCES

1. O. Hahn and F. Strassmann, Naturwiss, 27, 11 (1939)
2. N. Bohr and J. A. Wheeler, Phys. Rev., 56, 426 (1939)
3. W. J. Swiatecki, Phys. Rev., 101, 651 (1956) and Phys. Rev., 104, 993 (1956)
4. L. Wilets, "Theories of Nuclear Fission", Oxford Univ. Press, London and New York (1964)
5. E. K. Hyde, "A Review of Nuclear Fission", University of California Radiation Laboratory Report UCRL-9036, 1960
6. J. S. Fraser and J. C. D. Milton, "Nuclear Fission", An. Rev. Nucl. Sc., 16 (1966)
7. J. E. Gindler and J. R. Huizenga, "Nuclear Chemistry": Nuclear Fission, edited by Leo Yaffe, Academic Press Inc., New York, Vol. II, I (1968)
8. A. Brandt and I. Kelson, Phys. Rev., 183, 1025 (1969)
9. V. M. Strutinski and H. C. Pauli, Proc. Symp. Phys. Chem. Fission, Vienna, Austria Paper SM-122/203,IAEA (1969)
10. "Nuclear Chemistry", Vol.I and II, edited by Leo Yaffe, Academic Press Inc., New York and London (1968)
11. M. A. Preston", Physics of the Nucleus", Addison-Wesley Inc., Reading, Massachusetts (1962)
12. J. M. Blatt and V. F. Weisskopf, "Theoretical Nuclear Physics, John Wiley and Sons, New York (1952)
13. A. Messiah, "Quantum Mechanics", John Wiley and Sons, New York (1961)
14. G. Friedlander, J. W. Kennedy and J. M. Miller "Nuclear and Radiochemistry", John Wiley and Sons, New York (1961)
15. W. D. Myers and W. J. Swiatecki, University of California Radiation Laboratory Report, UCRL-11980 (1965)
16. R. Vandenbosch, "Nuclear Models and Nuclear Fission", paper presented at Am. Nucl. Soc. Meeting, 6/10/1969
17. T. Ericson, Phil. Mag. Suppl., 9, No. 36, 425 (1960)
18. A. E. S. Green, Rev. Mod. Phys., 30, 569 (1958)
19. C. D. Coryell, Ann. Rev. Nucl., 2, 305 (1953)

20. I. F. Croall and J. G. Cuninghame, Nucl. Phys., A125, 402 (1969)

21. J. A. McHugh and M. C. Michel, Phys. Rev., 172, 1160 (1968)

22. R. C. Jensen and A. W. Fairhall, Phys. Rev., 109, 942 (1958)

23. H. M. Blann, University of California Radiation Laboratory Report, UCRL-9190 (1960)

24. S. A. Karamian, J. C. Oganesian, B. J. Pustylnik and G. N. Flerov, Proc. Symp. Phys. Chem. Fission, Vienna, Austria, Paper SM-122/130, IAEA (1969)

25. E. Konecny and W. H. Schmitt, Phys. Rev., 172, 1213 (1968)

26. J. C. D. Milton and J. S. Fraser, Can. J. Phys., 40, 1626 (1962)

27. J. Terrell, Phys. Rev., 127, 880 (1962)

28. R. Vandenbosch, Nucl. Phys., 46, 129 (1963)

29. H. C. Britt and L. Whetstone, Phys. Rev., 133, B603 (1964)

30. G. Friedlander, L. Friedman, B. Gordon and L. Yaffe, Phys. Rev., 129, 1809 (1963)

31. A. C. Wahl, A. E. Norris, R. A. Rouse and J. C. Williams, Proc. Symp. Phys. Chem. Fission, Vienna, Austria, Paper SM-122/116, IAEA (1969)

32. B. D. Pate, J. S. Foster and L. Yaffe, Can. J. Chem., 36, 1691 (1958)

33. L. Yaffe, Proc. Symp. Phys. Chem. Fission, Vienna, Austria, Paper SM-122/3, IAEA (1969)

34. J. A. Panontin and N. T. Porile, J. inorg. nucl. Chem., 30, 2891 (1968)

35. J. J. Hogan and N. Sugarman, Phys. Rev., 182, 1210 (1969)

36. J. R. Huizenga and R. Vandenbosch, "Nuclear Reactions" (Edited by P. M. Endt and P. B. Smith), Vol. II, North Holland, Amsterdam (1962)

37. G. N. Harding and H. J. M. Farley, Proc. Phys. Soc., A69, 853 (1956)

38. E. Cheifetz, Z. Fraenkel, J. Galin, N. Lefort, J. Péter and X. Tarrago, Private Communication

39. L. Remsberg, F. Plasil, J. B. Cumming and M. L. Perlman, Phys. Rev., 187, 1597 (1919)

40. G. B. Saha and L. Yaffe, J. inorg. nucl. Chem., 32, 745 (1970)

41. J. J. Griffin, Spec. Publications N.B.S., 299 (Vol. II), Conf. 680307 (1968)

42. J. J. Griffin, Proc. Symp. Phys. Chem. Fission, Vienna, Austria, Paper SM-122/200, IAEA (1969)

43. P. Fong, Phys. Rev., 102, 434 (1956)

44. H. J. Krappe and V. Wille, Proc. Symp. Phys. Chem. Fission, Vienna, Austria, Paper SM-122/96, IAEA (1969)

45. J. R. Nix, Discussion, Proc. Symp. Phys. Chem. Fission, Vienna, Austria, Paper SM-122/96, IAEA (1969)

46. L. Wilets, Discussion, Proc. Symp. Phys. Chem. Fission, Vienna, Austria, after paper SM-122/203, IAEA (1969)

47. W. Kauzman, "Quantum Chemistry", Academic Press, New York (1957)

48. Proc. Symp. Phys. Chem. Fission, Vienna, Austria, IAEA (1969)

49. L. Pauling and E. B. Wilson, "Introduction to Quantum Mechanics", McGraw-Hill, New York (1935)

50. D. L. Hill and J. A. Wheeler, Phys. Rev., 89, 1102 (1953)

51. L. E. Glendenin, H. C. Griffin, W. Reisdorf and J. P. Unik, Proc. Symp. Phys. Chem. Fission, Vienna, Austria, Paper SM-122/114, IAEA (1969)

52. E. K. Hyde, I. Perlman and G. T. Seaborg, "The Nuclear Properties of the Heavy Elements, Prentice Hall, New Jersey (1964)

53. P. Armbruster, D. Hovestadt, H. Meister and J. H. Specht, Nucl. Phys., 54, 586 (1964)

54. L. E. Glendenin, J. P. Unik and H. C. Griffin, Proc. Symp. Phys. Chem. Fission, Salzburg, Austria, Paper SM-60/31, IAEA (1965)

55. G. C. Carlson and E. Schick, Nucl. Phys. A125, 267 (1969)

56. Collected Radiochemical Procedures, Los Alamos Scientific Laboratory of the University of California, La 17211 (1958)

57. Y. Kusaka and W. W. Meinke, "Rapid Radiochemical Separations, NAS-NS3104, Washington (1961)

58. A. H. Khan, G. B. Saha and L. Yaffe, Can. J. Chem., 48, 1924 (1970)

59. J. B. Cumming, "Application of Computers to Nuclear and Radiochemistry", National Academy of Sciences, National Research Council, Nucl. Sci. Series, NAS - NS 3107, 25 (1962)

60. C. M. Lederer, J. M. Hollander and I. Perlman, "Table of Isotopes", Sixth Edition, John Wiley and Sons, New York (1967)

61. G. B. Saha, Ph. D. thesis, McGill University (196)

62. S. Meghir, Ph. D. thesis, McGill University (1962)

63. I. Tomita and L. Yaffe, Can. J. Chem., 47, 2921 (1969)

64. P. P. Benjamin, D. A. Marsden, N. T. Porile and L. Yaffe, Can. J. Chem., 47, 301 (1969)

65. J. H. Forster, N. T. Porile and L. Yaffe, Can. J. Chem., 44, 295 (1966)

66. A. Kjelberg, H. Taniguchi and L. Yaffe, Can. J. Chem., 39, 635 (1961)

67. G. H. McCormick and B. L. Cohen, Phys. Rev., 96, 722 (1954)

68. L. Miller, Private Communication

69. P. C. Stevenson, H. G. Hicks, W. E. Nervik and D. R. Nethaway, Phys. Rev., 111, 886 (1958)

70. K. H. Flynn and H. R. Von Gunten, Proc. Symp. Phys. Chem. Fission, Vienna, Austria, Paper SM-122/1, IAEA (1969)

71. L. J. Colby and J. W. Cobble, Phys. Rev., 121, 1410 (1961)

72. A. E. S. Green, "Nuclear Physics", McGraw-Hill, New York (1955)

73. C. D. Coryell, M. Kaplan and R. D. Fink, Can. J. Chem., 39, 646 (1961)

74. A. C. Pappas and E. Hagebo, J. inorg. nucl. Chem., 28, 1769 (1966)

75. N. G. Runnals and D. E. Troutner, Phys. Rev., 179, 1188 (1969)

76. A. C. Wahl, L. C. Ferguson, D. R. Nethaway, E. Troutner and K. Wolfsberg, Phys. Rev., 126, 1112 (1962)

77. N. Sugarman, H. Munzel, J. A. Panontin, K. Wielgoz, M. V. Ramaniah, G. Lange and E. Lopez-Menchero, Phys. Rev., 143, 952 (1966)

78. P. Armbruster, Nucl. Phys., A140, 385 (1970)

79. S. H. Fried, J. L. Anderson and G. R. Choppin, J. inorg. nucl. Chem. 30, 3155 (1968)

80. J. L. Anderson, S. H. Fried and G. R. Choppin, J. inorg. nucl. Chem., 30, 3167 (1968)

81. G. R. Choppin and E. F. Meyer Jr., J. inorg. nucl. Chem. 28, 1509 (1966)

82. A. Notea, Phys. Rev., 182, 1331 (1969)

83. A. W. Fairhall, R. C. Jensen and E. F. Neuzil, Proc. U. N. Intern. Conf. Peaceful Uses at Energy, 2nd, Geneva, 15, 452, P/677, UN New York (1958)

84. J. C. D. Milton and J. S. Fraser, Phys. Rev. Letters 7, 67 (1961)

85. S. S. Parikh, D. A. Marsden, N. T. Porile and L. Yaffe, Can. J. Chem., 45, 1863 (1967)

86. A. C. Pappas, J. Alstad and E. Hagebo, Proc. Symp. Phys. Chem. Fission, Vienna, Austria, Paper SM-122/2061 IAEA (1969)

87. M. Bolsterli, E. O. Fiset and J. A. Nix, Proc. Symp. Phys. Chem. Fission, Vienna, Austria, Paper SM-122/109, IAEA (1969)